Refining Adverse Outcome Pathways using Japanese Medaka Embryos *(Oryzias latipes)* Exposed to 2,3,7,8-Tetrachlorodibenzodioxin

by

Shreya Jain

A thesis submitted to the
School of Graduate and Postdoctoral Studies in partial
fulfillment of the requirements for the degree of

Master of Science in Applied Bioscience

Faculty of Science

University of Ontario Institute of Technology (Ontario Tech University)

Oshawa, Ontario, Canada

August 2021

THESIS EXAMINATION INFORMATION
Submitted by: **Shreya Jain**

Master of Science in Applied Bioscience

Thesis title: Refining Adverse Outcome Pathways using Japanese Medaka Embryos *(Oryzias latipes)* Exposed to 2,3,7,8-Tetrachlorodibenzodioxin

An oral defense of this thesis took place on August 19, 2021, in front of the following examining committee:

Examining Committee:

Chair of Examining Committee	Dr. Janice Strap
Research Supervisor	Dr. Denina Simmons
Examining Committee Member	Dr. Jean-Paul Desaulniers
Thesis Examiner	Dr. Sean Forrester, Ontario Tech University

The above committee determined that the thesis is acceptable in form and content and that a satisfactory knowledge of the field covered by the thesis was demonstrated by the candidate during an oral examination. A signed copy of the Certificate of Approval is available from the School of Graduate and Postdoctoral Studies.

ABSTRACT

Adverse outcome pathways (AOPs) are a framework that categorizes the impact of chemicals biologically from the initial molecular interaction through to the ecosystem level. This research aims to refine two existing AOPs that are initiated when dioxins and dioxin-like chemicals bind to molecular receptors. When embryonic development is adversely impacted by dioxins, we hypothesize that there are differences in gene and protein expression, which will distinguish the molecular level key events in these two AOPs. To test this, we performed qPCR on AOP key event genes, and also non-targeted proteomics on teleost embryos from different stages of development after exposure to dioxins and linked these to higher-level adverse effects, specifically cardiac impairment, and malformations. Refining these AOPs will benefit society by improving our ability to respond to chemical contaminants more effectively to prevent adverse outcomes in humans and their environment.

Keywords: adverse outcome pathways; toxicology; key events; genetic markers; aryl hydrocarbon receptor

AUTHOR'S DECLARATION

I hereby declare that this thesis consists of original work of which I have authored. This is a true copy of the thesis, including any required final revisions, as accepted by my examiners.

I authorize the University of Ontario Institute of Technology (Ontario Tech University) to lend this thesis to other institutions or individuals for the purpose of scholarly research. I further authorize University of Ontario Institute of Technology (Ontario Tech University) to reproduce this thesis by photocopying or by other means, in total or in part, at the request of other institutions or individuals for the purpose of scholarly research. I understand that my thesis will be made electronically available to the public.

_____ SHREYA JAIN

STATEMENT OF CONTRIBUTIONS

I hereby certify that I am the sole author of this thesis and that no part of this thesis has been published or submitted for publication. I have used standard referencing practices to acknowledge ideas, research techniques, or other materials that belong to others. Furthermore, I hereby certify that I am the sole source of the creative works and/or inventive knowledge described in this thesis.

ACKNOWLEDGEMENTS

I would like to express my gratitude towards Professor Denina Simmons for giving me an opportunity to grow independently as a scientist in her aquatic facility. It is her guidance and support that has trained me to become a resilient researcher during this research project. Not only was she an encouraging supervisor but an empathetic friend which was a necessity to survive as a graduate student during the pandemic. I am grateful to have shared these wonderful two years in this lab to learn all the skills that I have. Thank you for always believing in your students, Nina.

Furthermore, I would like to extend my appreciation towards Dr. Linda Lara-Jacobo for being the best mentor anyone could ask for. I cannot thank you enough for joining the lab and encouraging me from the start. You never hesitated to offer your help and I am grateful to have had your support through my masters. You shared so many skills and valuable experiences with me and you were also the friend that I needed during the thick of it. Thank you for all that you have taught me with patience and understanding during this experience. You have given me the confidence a scientist needs!

I am also very thankful for having Urvi Pajankar as a supporting member of the lab who never failed to volunteer to help me out. She gave me her precious time on weekends and early mornings which I will remember forever. Her support was vital toward my resilience which was tested during this project. Her attention to detail, patience and kindness are unmatched even on the most stressful days. Thank you for always being there for me.

Additionally, I would also like to thank all my fellow lab mates for being friendly, encouraging, and supporting and I especially want to thank those who helped keep my

medaka alive! I am grateful for all the time everyone provided me. Thank you for always reminding me that we are all in this together.

Finally, I would like to thank the undergraduate lab members: Almira Khan, Aleen Zhera and Mohammed Faiz Chauhan for assisting during my busiest times in the lab and completing the tasks I needed in a timely manner. I couldn't have done it without you guys, thank you.

My biggest thanks go to my family and my loving partner, Phil Snache, for always being the rock that I needed to listen to all my problems (scientific or not) to help keep me sane as a researcher. I am especially thankful for the sustenance you provided during my vigorous sample collection month. Thank you for coming into my life and becoming the support that has brought us to this achievement.

TABLE OF CONTENTS

Appendices

LIST OF TABLES

CHAPTER 2

CHAPTER 3

CHAPTER 3 (Continued)

CHAPTER 3 (Continued)

LIST OF FIGURES

CHAPTER 1

CHAPTER 2

CHAPTER 3

CHAPTER 3 (Continued)

LIST OF ABBREVIATIONS AND SYMBOLS

AOPs	Adverse Outcome Pathways
AOP-Wiki	Adverse Outcome Pathway Wiki
MIE	molecular initiating event
AO	adverse outcome
KE	key event
AhR	aryl hydrocarbon receptor
HSP90	90-kDa heat shock protein
AIP, also known as XAP2 or Ara9	AhR-interacting protein
c-SRC	Proto-oncogene tyrosine-protein kinase Src
ARNT	AhR nuclear translocator
DRE	dioxin-responsive elements
COX-2	cyclooxygenase-2
HIF-1α	hypoxia-inducible factor-1α
VEGF	Vascular endothelial growth factor
PCBs	polychlorinated biphenyls
PAHs	polycyclic aromatic hydrocarbons
TCDD	2,3,7,8-Tetrachlorodibenzodioxin
CV	cardiovascular
PE	pericardial edema
dpf	days post fertilization
RNA	Ribonucleic acid
rpm	Rotations per minute
rpl7	Ribosomal Protein L7
qPCR	quantitative polymerase chain reaction
IAA	Iodoacetamide
ppb	parts per billion
DNA	Deoxyribonucleic acid
NoRT	no reverse-transcriptase
NTC	no template control
TECP	Tris(2-carboxyethyl) phosphine hydrochloride
RPLC	reverse-phase liquid chromatography
Q-TOF	Quadrupole Time-of-Flight
MPP	Mass Profiler Professional
FDR	false-discovery-rate
EGFR	Epidermal growth factor receptor

Chapter 1. Introduction

In 2012, the Organization for Economic Co-operation and Development (OECD) launched a new program on the development of adverse outcome pathways (AOPs) (Bolt, 2017). AOPs are a collaborative scientific framework that presents the effects of various chemicals in increasing levels of biological organization (Bolt, 2017). This framework encompasses the impact of a chemical from the molecular level up to the ecosystem level. AOPs allow scientists to collaborate effectively to gauge the biological effect of various chemicals in the environment. This ultimately assists with setting environmental regulation policies for emerging chemicals of concern. Clarifying the active online 296 AOPs available on the Collaborative Adverse Outcome Pathway Wiki (AOP-Wiki) database will also assist in understanding the various mechanisms of action and possible mitigation strategies to combat the effects of harmful chemicals (Jeong & Choi, 2017).

AOPs are similar to a domino sequence; once a threshold of a level (similar to pushing the first domino) has been achieved, the next step in the adverse outcome pathway is inevitable. Due to this design, a "strong" AOP is where the molecular initiating event (MIE), or the first step of the AOP, is very strongly linked to the ultimate adverse outcome (AO) through well-defined key events (KE) (Bolt, 2017). A single MIE can activate many AOPs, and these can be conserved across various species, such as from fish to humans. Current knowledge suggests that some pathways work in conjunction with each other, and others are contradictory to one another - and there are many more that require additional data for validation.

In particular, one MIE in the AOPwiki database is connected to multiple AOs: [Key Event: 18- Activation, AhR] or activation of the aryl hydrocarbon receptor (AhR). This nuclear receptor is a transcription factor found in the cytoplasm as a complex that senses various changes in the environment related to circadian rhythm, oxygen tension, and redox potential (Denison & Nagy, 2003; Gutierrez-Vazquez & Quintana, 2018; Kawajiri, 2017; Rowlands & Gustafsson, 1997). It responds to these changes by controlling the transcription of a wide variety of target genes (Kawajiri, 2017). The inactive form of the AhR receptor consists of the AhR itself, 90-kDa heat shock protein (HSP90), co-chaperone p23, AhR-interacting protein (AIP, also known as XAP2 or Ara9), and Proto-oncogene tyrosine-protein kinase Src (c-SRC) (Figure 1.1). While HSP90 stabilizes the AhR conformation to have a high affinity for ligands (Grenert et al., 1997), its associated co-chaperone p23 facilitates the adenosine triphosphate–driven cycle of HSP90 (Young & Hartl, 2000). Meanwhile, AIP prevents ubiquitination and degradation of AhR, maintaining it at steady levels (Denison & Nagy, 2003). c-SRC is regulated by the AhR which controls its activity by phosphorylation and dephosphorylation (B. Dong et al., 2011; Xie, Peng, & Raufman, 2012). Upon phosphorylation, the c-SRC protein is released from the AhR complex and can phosphorylate multiple target proteins associated with cell differentiation, proliferation, survival, cell adhesion, cell morphology, and motility (B. Dong et al., 2011; Xie et al., 2012).

The AhR has undergone genome duplication and diversification in vertebrates which has resulted in various isoforms of the AhR protein. The main clades are AhR1, AhR2, and AhR3, which are often encoded on different chromosomes (J. A. Doering, Giesy, Wiseman,

& Hecker, 2013). Mammals express a single AhR that is homologous to the AhR1. Meanwhile, fishes and birds express AhR1s and AhR2s. AhR3 is poorly understood and only found in some cartilaginous fishes (J. A. Doering et al., 2013). In some taxa, such as in the case of Japanese Ricefish (Oryzias latipes), genome duplication events have created multiple isoforms. Japanese Ricefish *(Oryzias latipes)* have four isoforms (AhR1b-1, AhR1b-2, AhR2a, and AhR2b) (Hanno, Oda, & Mitani, 2010). Isoform AhR2a is the most active towards dioxin ligands and is relevant to any AOPs initiated by key event 18 (Activation, AhR) (Hanno et al., 2010).

Upon activation of AhR by a ligand, the complex translocates to the nucleus. Once this happens, the accessory proteins release from AhR, making it active and available to bind with the AhR nuclear translocator (ARNT) (Vorrink & Domann, 2014). The AhR/ARNT complex then responds to regions in the DNA referred to as dioxin-responsive elements (DRE) which are genes vital for survival that are involved in regulatory processes anywhere from cell proliferation to apoptosis (Vorrink & Domann, 2014). Concurrently, dimerization with ARNT is also required by hypoxia-inducible factor-1α (HIF-1α), which is a key transcription factor that regulates responses to reduced oxygen and stimulates angiogenesis, which is the formation of new blood vessels, via regulation of vascular endothelial growth factor (VEGF) (Gabriely, Wheeler, Takenaka, & Quintana, 2017; Pillai & W, 2012). VEGF is a signalling protein essential for normal vasculogenesis and therefore cardiogenesis (Ivnitski-Steele, Friggens, Chavez, & Walker, 2005). Vasculogenesis is the process by which an embryo forms a network of blood vessels by stimulating precursor cells called angioblasts to proliferate and differentiate into endothelial cells which then

develop into the cardiovascular system. Due to the dual function of ARNT, both the AhR and HIF-1α signalling pathways are hypothesized to have significant crosstalk which is worth further exploration. Crosstalk among nuclear receptors is common and thus downstream effects are complex and diverse, making deciphering the effect of each receptor individually difficult (Ordonez-Moran & Munoz, 2009).

Ligands of the AhR are found naturally through diet, free radical formation, and enzymatic activities (Denison & Nagy, 2003; Gutierrez-Vazquez & Quintana, 2018; Kawajiri, 2017). The largest group of naturally occurring dietary AhR ligands are flavonoids, including flavones, flavanols, flavanones, and isoflavones (Denison & Nagy, 2003) (Figure 1.3). These chemicals are widely distributed in dietary vegetables, fruits, and teas (Denison & Nagy, 2003). Flavonoid levels in human blood have been reported to be in the low μM range (Denison & Nagy, 2003), and these concentrations of ligands are sufficient to activate AhR. Thus, plant-derived materials appear to commonly contain AhR ligands or precursors that are readily converted into AhR ligands. Additionally, chemical contaminants such as dioxins, polychlorinated biphenyls (PCBs), hexachlorobenzene (fungicide), and polycyclic aromatic hydrocarbons (PAHs) may act as ligands, as well, where binding can result in adverse outcomes such as reduced blood flow, pericardial edema, and impaired angiogenesis (J. A. Doering, Wiseman, Beitel, Giesy, & Hecker, 2014).

Dioxins are a particularly notorious activator of the AhR and can also be produced from natural processes, such as forest fires and volcanic eruptions (Tuomisto, 2019). Most

dioxins are introduced to the environment through the air and can travel long distances across the atmosphere (Tuomisto, 2019). Dioxins bioaccumulate and most people are exposed through their diet most often rather than through air, water or soil (Tuomisto, 2019). Meat, dairy and fish have higher levels of dioxins than fruit, vegetables and grains (Thompson & Darwish, 2019). Other pathways of exposure include inhalation from waste incinerators or other combustion processes. Additional sources include emissions from iron and steel production, various types of fuel-burning, electric power generation, and tobacco smoke (Tuomisto, 2019). The most potent and toxic dioxin remains 2,3,7,8-Tetrachlorodibenzodioxin (TCDD) which is a persistent organic pollutant (POP) meaning it is resistant to environmental degradation by chemical, biological, and photolytic processes (Tuomisto, 2019) (Figure 1.4 and 1.5).

Exposure to dioxins in humans is known to cause a multitude of adverse effects such as skin disorders (ex. chloracne), liver problems, impairment of the immune, endocrine, developing nervous and/or reproductive systems including certain types of cancers (Tuomisto, 2019). Effects of exposure are dependent on the concentration of the contaminant, mode of exposure and duration of exposure. In fish, mice, and chickens, dioxins have been shown to cause altered cardiovascular development due to early life stage exposure which is expressed in two AOPs: AOP 150 and 21 (J. H. Doering, Markus; Villeneuve, Dan; Zhang, Xiaowei, 2019; Farhat & Kennedy, 2019).

AOP 150 (Farhat & Kennedy, 2019) is a pathway that is initiated by key event 18. In AOP 150, the quantitative understanding regarding the relationship of individual key events is

weak; however, the link between the MIE [Key Event: 18 - Activation, AhR] and AO (mortality) is strong (W. Dong, Matsumura, & Kullman, 2010; Elonen et al., 1998; Hanno et al., 2010; Lanham, Plavicki, Peterson, & Heideman, 2014; Plavicki, Hofsteen, Peterson, & Heideman, 2013; Wisk & Cooper, 1990). Mortality is caused due to altered development of the cardiovascular system which leads to reduced blood flow, pericardial edema, and impaired angiogenesis when the organism is exposed to various chemicals including dioxins. In AOP 150, the theory is that increased activation of AhR results in sustained AhR/ARNT dimerization, resulting in insufficient levels of ARNT remaining for dimerizing with HIF-1α. ARNT/HIF-1α dimerization is essential for the production of Vascular endothelial growth factor (VEGF), which is required for vasculogenesis. Thus, when AhR competes with HIF-1α for ARNT, the adverse outcome of impaired cardiovascular development and mortality results due to lack of VEGF production. There is strong evidence supporting this AOP (W. Dong et al., 2010; Elonen et al., 1998; Hanno et al., 2010; Lanham et al., 2014; Plavicki et al., 2013; Wisk & Cooper, 1990); however, some contradictory data regarding the effect of AhR on VEGF still exists as this relationship seems highly dependent on tissue type and life stage. Moreover, AhR is an essential target for various pathways, making it plausible that many pathways interact with one another.

Another AOP with AhR activation as the MIE and cardiovascular development issues leading to mortality as the AO is AOP 21 (J. H. Doering, Markus; Villeneuve, Dan; Zhang, Xiaowei, 2019). This AOP may overlap with AOP 150 (Farhat & Kennedy, 2019) in that it suggests an alternative pathway of cardiotoxicity through AhR/ARNT dimerization.

AOP 21 suggests that this dimerization leads to the activation of a specific dioxin response element (DRE) found in the DNA with known inflammatory properties, COX-2, which may play a new role in vasculogenesis not previously established. Since AOP 21 has the same MIE and AO, it is as "strong" as AOP 150; therefore, these pathways require more data to clarify the relationships between them.

Past research under both AOPs (Figure 1.6) (J. H. Doering, Markus; Villeneuve, Dan; Zhang, Xiaowei, 2019; Farhat & Kennedy, 2019) have explored these pathways in zebrafish, chicken, and mice. Studies of knock-out and knock-down of several genes have been conducted including exploring the rescuing effect caused by several genes when induced exogenously. Research on the MIE of AHR activation by TCDD includes, Ahr2 knockout zebrafish mutants that were protected against TCDD toxicity, including pericardial edema and epicardium development (Goodale et al., 2012; Plavicki et al., 2013); as well as AHR-null mice have impaired angiogenesis in vivo where endothelial cells failed to branch and form tube-like structures (Roman, Carvajal-Gonzalez, Rico-Leo, & Fernandez-Salguero, 2009) which shows the necessity of AhR in angiogenesis. In relation, Arnt1 morpholino knockdown in zebrafish protected against pericardial edema and reduced blood flow (Prasch, Tanguay, Mehta, Heideman, & Peterson, 2006). ARNT knockout and HIF1α knockout mice, both, displayed blocks in developmental angiogenesis and cardiovascular malformations (Kozak, Abbott, & Hankinson, 1997; Maltepe, Schmidt, Baunoch, Bradfield, & Simon, 1997; Ryan, Lo, & Johnson, 1998) which indicates the necessity of the HIF1α pathway for angiogenesis. Further, mice lacking VEGF displayed defective vascularization, early embryonic lethality (Carmeliet et al., 1996; Ferrara et al.,

1996), impaired myocardial angiogenesis and reduced contractility leading to ischemic cardiomyopathy (Carmeliet et al., 1999). Interestingly, injection of exogenous VEGF rescues the inhibitory effect of TCDD on vasculogenesis (Ivnitski-Steele & Walker, 2003). COX-2 is another gene known to have a role in heart development in vertebrates (Dong et al 2010; Teraoka et al 2008; 2014). Dysregulation of COX-2 occurs by AhR which is associated with altered cardiovascular development, decreased blood flow, and cardiac failure causing mortality in early life stages of fish and birds (W. Dong et al., 2010). COX-2 knockdown and selective antagonists of COX-2 prevent TCDD induced alteration in cardiovascular development and function (W. Dong et al., 2010). COX-2 inducers, known to not be agonists of the AhR, cause altered cardiovascular development that is consistent with activation of the AhR (Huang, Chen, Huang, & Yu, 2007).

This research aims to provide additional data that aids in differentiating between these two AOPs. Using embryos from Japanese Ricefish, qPCR, proteomics, heartbeat, and malformation analysis, we will create a platform to compare differences in molecular key events through to the whole organism effect level. The goal of this approach is to generate a more accurate AOP framework.

1.2 Objectives

The goal of this research is to provide sufficient evidence to distinguish between AOP 21 and 150. To achieve this aim, we chose to apply what we know about dioxins to create an experimental design that would result in an adverse effect in Japanese Ricefish (*Oryzias latipes*). We hypothesized that an acute exposure at an early stage of embryonic development would cause a chain of interconnected key events, which we could measure using molecular tools, and that these key events would allow us to distinguish the mechanistic differences occurring between the two AOPs. Ultimately, this research will address knowledge gaps in the AOP framework and contribute towards understanding which AOP, 150 or 21 (Figure 1.6), more greatly influences adverse cardiac development when the aryl hydrocarbon receptor is activated.

Figures

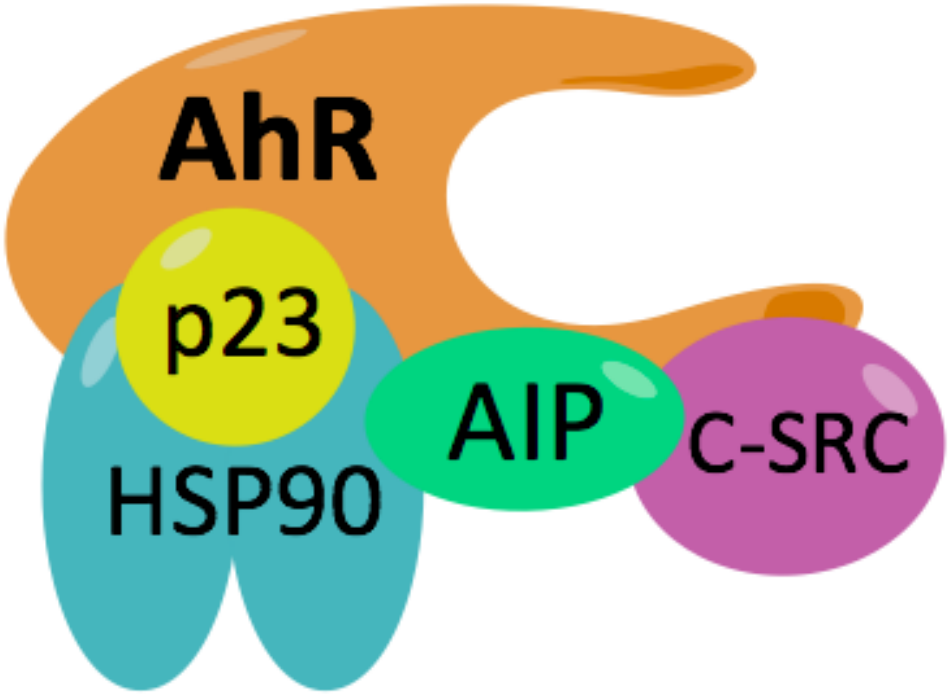

Figure 1.1: Visual representation of the AhR complex in its inactive state found in the cytoplasm.

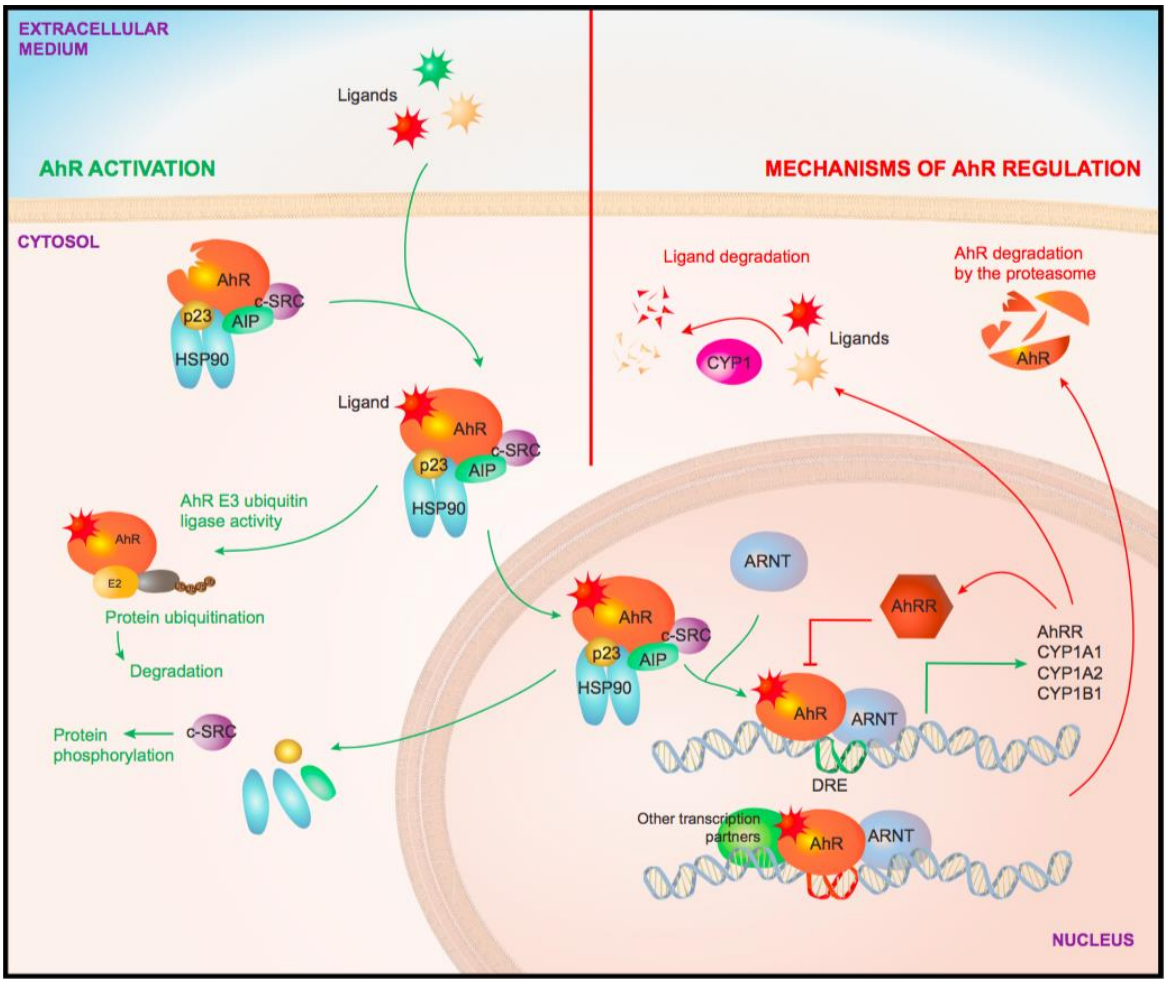

Figure 1.2: Visual representation of the AhR complex displaying translocation into the nucleus upon binding of a ligand as well as multiple downstream pathways adopted from a previous study (Gutierrez-Vazquez & Quintana, 2018).

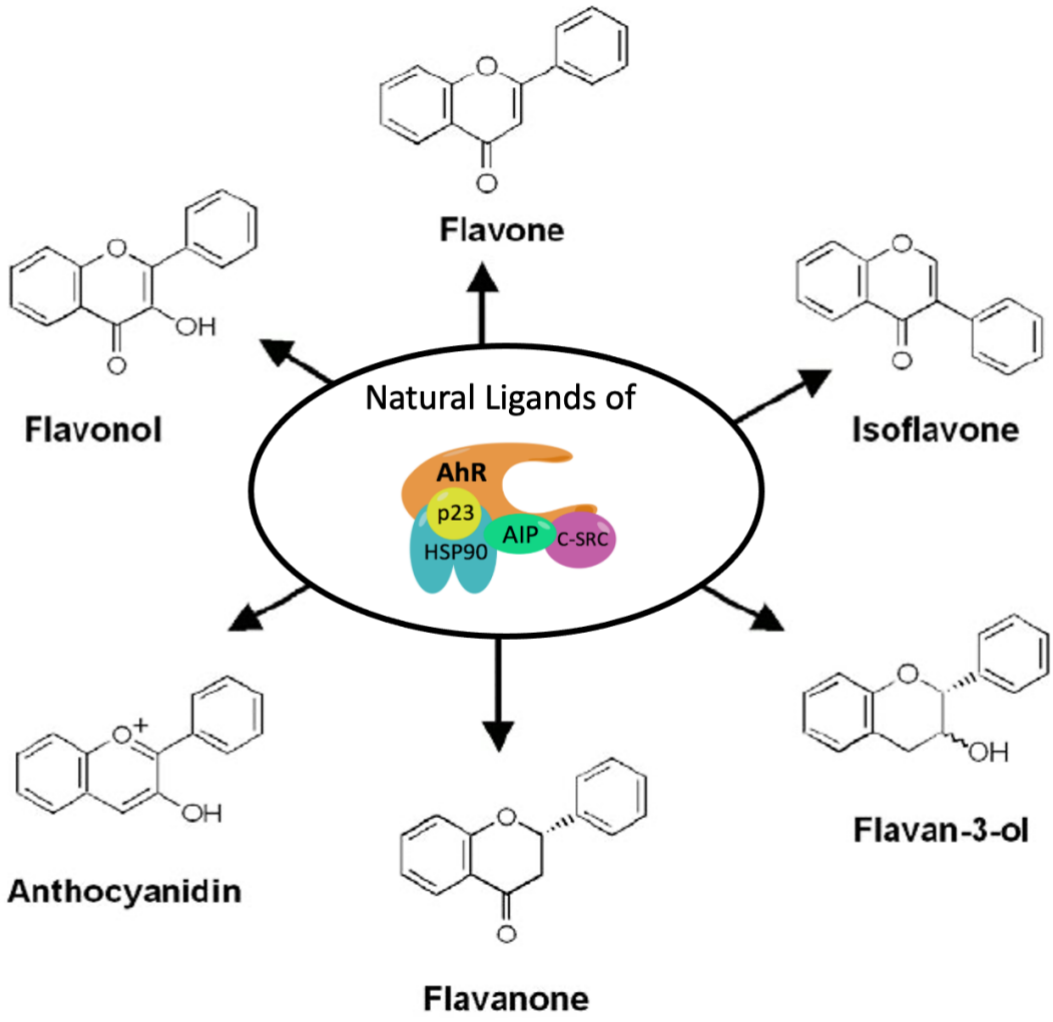

Figure 1.3: Visual representation of naturally found dietary ligands that activate the AhR. The diagram is adapted from a previous study (Nishiumi et al., 2011)

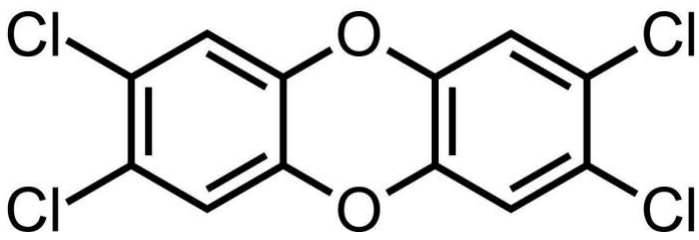

Figure 1.4: Chemical structure of 2,3,7,8-Tetrachlorodibenzodioxin (TCDD) which remains the most toxic dioxin and the most potent activator of AhR.

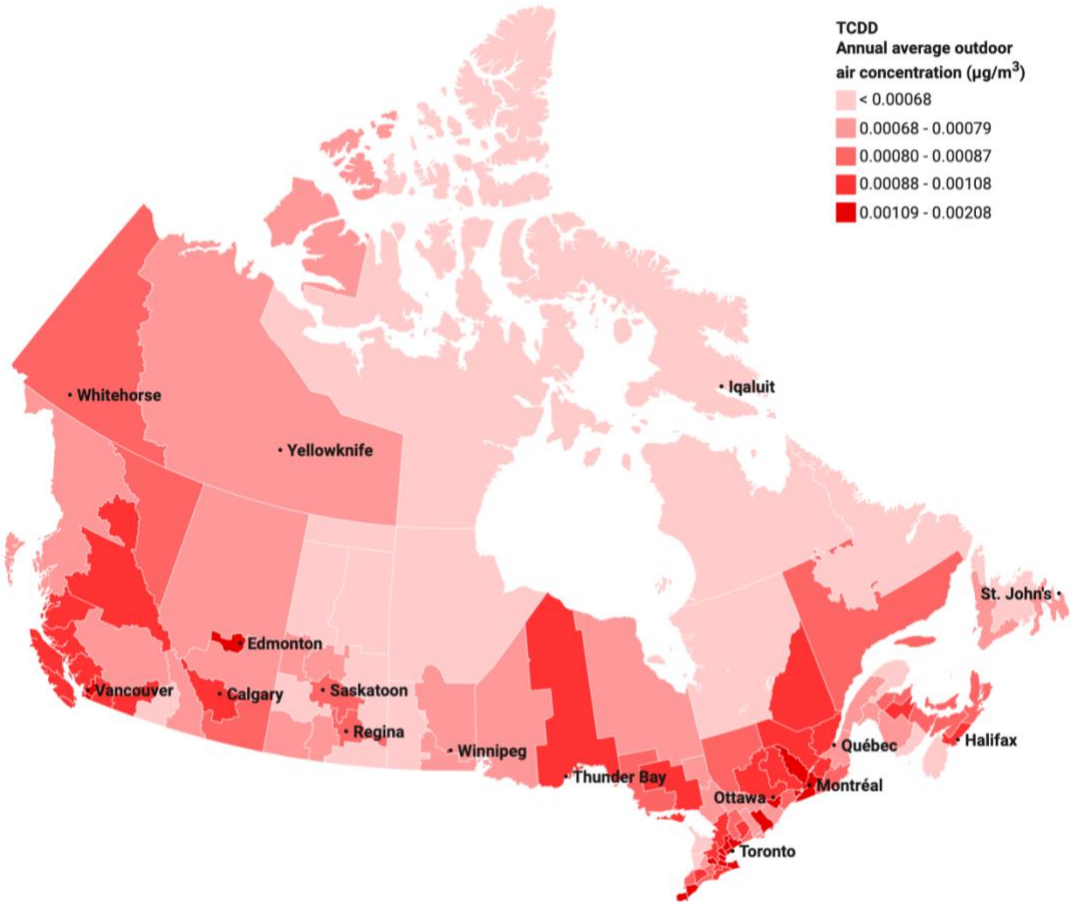

Figure 1.5: Map of Canada displaying predicted 2011 annual average TCDD concentrations of outdoor air at residential locations by health region based on data from Statistics Canada. Source: CAREX Canada ("2,3,7,8-Tetrachlorodibenzo-para-dioxin Environmental Exposures," 2021).

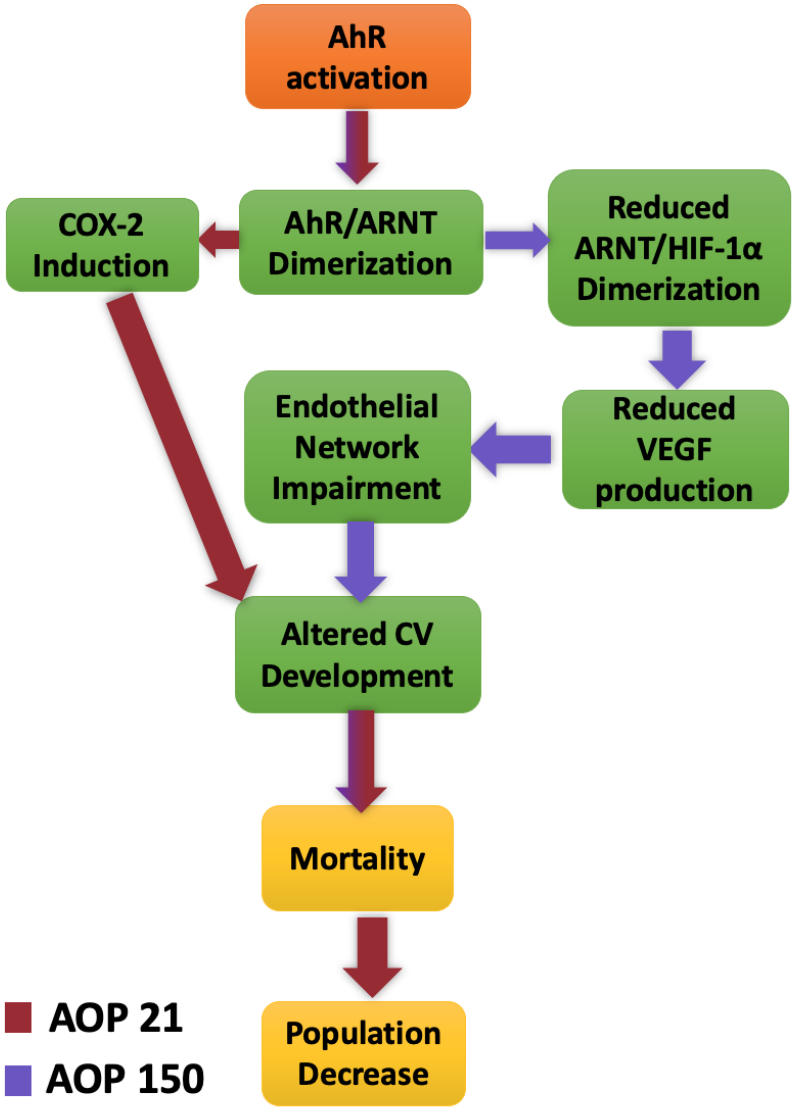

Figure 1.6: Existing AOPs 21 and 150 displaying effects of dioxin and dioxin-like chemicals on cardiovascular (CV) development. Altered CV development is seen as reduced blood flow, pericardial edema (PE), and impaired angiogenesis in Japanese medaka embryos (Oryzias latipes). The AOPs are differentiated by the red and purple arrows where red is AOP 21, and purple is AOP 150. The orange box indicates the molecular initiating event = AhR activation, the green boxes represent the key events and the yellow boxes indicate the adverse outcome.

Chapter 2. Methodology

2.1. Japanese Medaka

2.1.1 Medaka culturing and Embryo collection

Japanese Ricefish *(Oryzias latipes)*, also known as Japanese medaka, was used as the model organism for our study. Adult medaka are small (up to 1.4 inches) freshwater fish that are native to Asia. Advantages of using this species are that their entire genome has been sequenced, fertilized eggs are easy to obtain, embryos develop to full hatch in approximately nine days (Iwamatsu, 2011), and the wild-type strain is housed at the Aquatic Omics lab in Ontario Tech University.

The embryo's cardiovascular system development is easy to observe under a simple microscope. The stages of interest with respect to cardiovascular development are 2 days post fertilization (dpf) and 7 dpf and as described previously (Iwamatsu, 2011). At 2 dpf, the embryo develops a tubular heart and a blood island which eventually leads to a beating heart and onset of blood circulation. At 7 dpf, the cardiovascular and heart development is complete with a pericardial sac. The embryo can be observed using a simple microscope with a camera at these two stages, and also daily, to qualitatively capture organism development.

In the Aquatic Omics lab, fish are kept at a maximum density of 2.3 cm of fish length per liter of water at a ratio of one male for every two females. Adult fish of breeding age are kept at this ratio and pairs are spotted to collect as mating pairs after observation of

courtship behaviour. Typical courtship behaviour generally observed are a male following the female, repetitive quick-spin swimming underneath the female by the male and, finally, the male wrapping its anal fin around the female's body (when fertilization occurs). Individual pairs were kept in flow-through tanks and each tank was separated by a dark divider to avoid external disturbances. Water quality was maintained regularly by checking pH, nitrate, nitrite, ammonium, hardness of water, and temperature (maintained at 26 ºC). Water was cleaned by net and siphon daily to ensure no food was decaying or deposited eggs remained.

Consistent photoperiod is extremely important as a breeding condition with 14 hours of light and 10 hours of dark which creates a simulated spring season for optimal productivity. Fish began breeding immediately following the onset of light at 9:00 am until two hours after lighting. Medaka also breed spontaneously throughout the day. Due to increased energy expenditure during breeding, a surplus diet is also necessary. Therefore, fish were fed brine shrimp twice daily (morning and afternoon) and flakes once a day (evening).

2.1.2 Collection of eggs at 1-cell stage

For the collection of eggs of the same stage, eggs were collected 10 minutes after the lights came on each day. I was careful not to startle the fish in case of ongoing breeding simultaneously for all pairs while collecting eggs on ice. When eggs are kept on ice, the development stage of the embryos can be held at the 1-cell stage for up to 30 minutes (Kinoshita, Murata, Naruse, & Tanaka, 2009).

We found that nearly 300 eggs at the one-cell stage can be collected from nine pairs for a month using this method. However, the fertilization rate per pair needed to be tracked to ensure pairs reproduce consistently each day. Compatible pairs mate within 10 minutes of lighting and pairs that did not mate for more than two days consecutively were placed back in the population. Sometimes females would become stressed after some time and begin to reject males, and then take longer to mate. However, at this stage, the female produces more eggs than the average clutch.

Eggs can be retrieved by gently catching a female in a net and moving her closer to the surface of the water. The eggs can be directly pipetted off the abdomen of the female using a handheld aspirator and a 50 mL pipette while the female remains calm in the water. This method of egg collection causes less stress to the fish (and the humans!). Collected eggs are placed with a small amount of tank water directly in a fresh petri dish. They are naturally wrapped and held together by an attachment filament (which helps the clutch stick to the abdomen of the female), which we separate using sharp tweezers, viewing the eggs more closely using a stereomicroscope, so that individual embryos can be manipulated

one at a time (Kinoshita et al., 2009). The individual eggs are then rolled on P1200 sandpaper to remove microvilli (Kinoshita et al., 2009). This step must be performed with clean hands bare of gloves as friction from gloves may cause eggs to burst. Additionally, it is important to note that removal of microvilli improves heartbeat detection by the *Heartbeat* software (Gierten et al., 2020) which is why it was specially performed in this study. After removing the microvilli, the eggs were submerged in a rearing solution with methylene blue, which suppresses fungal outbreaks, and indicates non-viable embryos when it penetrates the chorion, turning the embryos a blue colour (Kinoshita et al., 2009). Rearing solution consists of methylene blue as well as NaCl, MgS04, CaCb, KCI and MilliQ (MQ) water (see Appendix A for details).

2.2 Pilot Tests

2.2.1 Dioxin pilot study in Japanese Ricefish (Oryzias latipes) embryos

A pilot study was conducted to ensure concentrations used for toxicity do not cause significant mortality but were sufficient to result in observable adverse outcomes. A concentration range between 0.001 and 10 ppb of TCDD, as a model dioxin, was used as previous studies indicate low mortality in this range (W. Dong et al., 2010; Elonen et al., 1998; Giesy et al., 2002). A serial dilution starting from 10 ppb to 0.001 ppb was performed using clean rearing medium (Appendix A) and a stock ampule of 10,000 ppb TCDD (Sigma-Aldrich, Oakville Ontario, product #48599). The embryos were exposed to the dioxin for 1 hour at the 4-hour post-fertilization mark and cardiovascular development was observed under the microscope daily. Mortality and hatching were recorded, and it was concluded that this range does not cause sufficient mortality in the wild-type strain and therefore all concentrations can be used for the purposes of this study. As well, during visual development observation, TCDD concentrations 0.01 ppb and up evidently displayed reduced blood flow, pericardial edema, and impaired angiogenesis (the adverse outcomes related to the AOPs being studied).

2.2.2 RNA extraction and qPCR optimization

RNA extraction was limited by the potential saturation of the column provided in the Qiagen RNeasy Micro Kit. Pilot RNA extractions were quantified using a Biodrop spectrophotometer and demonstrated that the purest and best quality extractions were obtained from three embryos per column with concentrations that ranged from 40 – 180 ng/ul depending on the life stage of the embryos.

As three embryos are a very small amount to work with, mortar and pestle methods (further described in 2.4.1) were chosen as ideal as it causes the least loss of the sample. Recommended homogenization with syringe and needle after generating a powder with mortar and pestle under liquid nitrogen was carried out as recommended in the Qiagen RNeasy Micro handbook.

Three target genes were chosen for qPCR: *ahR2a, hif-1α* and *cox-2,* which are associated with the key events in AOP 150 and 21. Primers were designed (Table 2.1) for *ahR2a* and *hif-1α* using Primer 3 software (Untergasser et al., 2012) and qPCR was stimulated in the software SnapGene® software (from Insightful Science; available at snapgene.com) to ensure adequate product designs. *cox-2* primers were found in a previous study (W. Dong et al., 2010). Medaka housekeeping gene *rpl7* was chosen to normalize the data as primers have been used successfully in our lab for years. It was found the ideal concentrations for *ahR2a, hif-1a*, *cox-2,* and *rpl7* primers were as follows: 0.35, 0.4, 0.4, and 0.3 mM, respectively. All primers were ordered from Invitrogen (Burlington, Ontario) and qPCR was performed using the iTaq Universal SYBR® Green One-Step Kit (Bio-rad, Mississauga, Ontario).

2.2.3 Optimization of Proteomics Protocol for medaka embryos

As embryos are extremely small, it was a difficult task to retrieve a sufficient amount of protein from a small number of embryos for the proteomics protocols. All protein levels were measured using the Protein Assay Kit by Qubit (Thermo Fisher Scientific, Whitby, Ontario). Protocols were changed to require half the amount of the protein normally used. To fulfill this, pilot studies found that at least fifty embryos are required per sample to

provide enough protein to perform proteomics using formic acid digestion, as performed in the Aquatic Omics Lab at Ontario Tech.

Homogenization was carried out in the same way as for the RNA extraction protocols using a pestle and then aspiration with a syringe and needle. However, liquid nitrogen was not necessary and instead the embryos were allowed to thaw on ice prior to homogenization. Further detail on the workflow is found in 2.4.2.

We optimized the laboratory's standard method for digestion of plasma to make sure that embryo proteins were digested adequately to give the best results. Various tests to optimize the protocol (Table 2.2) were tested with "Test 6" being the one chosen for sample preparation in the remainder of the study. Test 6 indicated that an increase in added iodoacetamide (IAA) from 200 mM to 400 mM, formic acid concentration remaining at 20%, and incubation on the heating block at 115 ºC for 45 minutes rather than 30 minutes increased the digestion efficiency.

2.2.4 Calibration of HeartBeat software

HeartBeat is an open-source software that was recently published (Gierten et al., 2020). This software automatically quantifies fish embryo heart rate using video capture as short as 10 seconds. It was previously applied in an automated microscopy setup; however, we adapted it to work with a low-cost setup. We utilized an economical microscope cell phone adapter and the camera from an iPhone 11 Pro Max that provided sufficient framerate to capture the medaka heartbeat. The setup was compared to manual heartbeat data collection, and it was found that there were no significant differences between the software and manual data collection. Therefore, we chose to use this setup and software for the final study to

save time and reduce the potential errors that come with fatigue when doing manual heartbeat measurements.

2.3. Study Design and Execution

A temperature control room set at 25ºC with 14 hours of light and 10 hours of dark was used to hold all eggs and fish during experimentation. To ensure reproducibility, the collection of data for all TCDD exposures occurred simultaneously and replicates were pooled from over fifteen repetition experiments that were conducted over five weeks. Exposures were performed in 24 well plates, with each column of three wells containing one exposure dose with three replicate wells, and exposure treatments of control (0ppb), 0.001, 0.01, 0.1, 1, to 10 ppb, across the plate. Each well contained twelve embryos which were exposed for 1 hour at 4 hpf to the designated dose. Embryos were washed in clean rearing medium solution three times before returning to clean rearing solution for the remainder of their development and for use in our study (See Appendix A). Non-viable embryos were identified (blue in colour), recorded, and removed daily. Rearing media was changed daily until the embryos reached 7 dpf. One embryo per replicate well, per dose, was collected for qPCR and three embryos per replicate well, per dose, were collected for proteomics on 2 dpf and 7 dpf from each experiment. On 7 dpf, all remaining embryos were moved to plates retaining replicates, such that all surviving embryos had their own well and media was no longer changed from this day forward, until collection and observation on the day of hatch. Individual heartbeat videos, thirty seconds long, were recorded for each embryo on 7 dpf. Hatch day for each embryo was recorded and each

embryo was euthanized in 10% formalin the day of hatching for subsequent malformation analysis.

2.4 Sample preparation and analyses

2.4.1 RNA extraction and qPCR

Embryos from six repetition experiments were pooled keeping the three replicates per dose within each experiment intact with the pooled replicate consisting of three embryos each. This was performed for each stage, 2 dpf and 7 dpf. RNA extraction for both stages was carried out simultaneously. To prevent contamination, gloves and a lab coat were used at all times and all benches and instruments were wiped with 70% ethanol and RNase away. Embryos were placed in liquid nitrogen for 2-3 seconds and quickly homogenized using a pestle directly in the collection tube turning the sample to a fine powder. 350 uL of buffer RLT, supplied in the RNeasy Micro Kit (Qiagen, Toronto, Ontario), was added to each sample and the homogenate was passed through a 0.9 mm syringe and needle ten times to ensure homogeneity. The mixture was centrifuged at full speed for three minutes at 4 ºC. The supernatant was transferred to a new Eppendorf tube and 1x the volume of 70% ethanol was added and mixed by pipetting. The sample mixture was transferred carefully to a column supplied in the RNeasy Micro Kit resting inside of an Eppendorf tube. The samples were allowed to rest for five minutes. The column inside of an Eppendorf tube is centrifuged at 10,000 rotations per minutes (rpm) for fifteen seconds; the flowthrough liquid was discarded and the Eppendorf tube was reused. 350 uL of RW1 supplied in the kit was added to each sample. The column inside of an Eppendorf tube is centrifuged at 10,000 rpm for fifteen seconds again; the flowthrough liquid was discarded and the

Eppendorf tube holding the column was reused. Optional DNase treatment supplied in the kit was also applied. DNase mixture was prepared using 10 uL of DNase I stock and 70 uL of supplied RDD for each sample in a separate tube. The total 80 uL of the prepared mixture was applied to each sample. The samples were allowed to rest at room temperature for fifteen minutes. 350 uL of RW1 supplied was added to each sample and centrifuged at 10,000 rpm for fifteen seconds and the flowthrough liquid as well as the Eppendorf tube containing the flowthrough was discarded. A new Eppendorf tube was used to collect the flowthrough and 500 uL of RPE supplied was added to each sample. The column inside of an Eppendorf tube is centrifuged at 10,000 rpm for fifteen seconds; the flowthrough liquid was discarded and the Eppendorf tube was reused. 500 uL of 80% ethanol was added to each column of sample inside of an Eppendorf tube and centrifuged at 10,000 rpm for fifteen seconds. The flowthrough and Eppendorf tube was discarded and the column was placed in a new collection tube (2 mL). The samples were centrifuged at full speed for five minutes. The flowthrough and collection tube was discarded again and the column was placed in a new collection tube (2 mL) for RNA collection. 14 uL of RNase free water was added to each column and allowed to rest for five minutes. The RNA was eluted from column into the tube by centrifuging at full speed for one minute. All RNA samples were stored at -80 ºC until qPCR.

For qPCR, each gene was tested in individual 96 well plates. To generate a standard curve, a concentration range by serial dilutions of pooled RNA was made. RNA was pooled from all samples (36 samples per stage, 2 dpf and 7 dpf) using 1 uL per sample. To the concentrated 36 uL of pooled RNA, 36 uL of RNase-free water (supplier) was added to

generate a pooled RNA concentrate diluted down by 50%. This was used as the first standard which was run in duplicate replication. Each plate consisted of six standards in total which were made by further diluting the pooled RNA using a 1:4 ratio of dilution for each standard which was run in duplicate replication. Each extracted RNA sample was diluted 40x using RNase-free water. Two wells were allocated for no reverse-transcriptase (NoRT) and two wells were allocated for water (NTC) as negative controls to monitor baseline contamination.

All plates for all genes were run the same day for each stage using the iTaq™ Universal SYBR® Green One-Step Kit and the Bio-rad CFX96 Touch Real-Time PCR Detection System thermocycler. The RT-qPCR annealing temperature was 58 ºC for all genes except for *cox-2* which was 56.8 ºC. The thermocycler settings were as follows: reverse Transcription reaction, 10 min at 50 °C; polymerase activation and DNA denaturation, 1 min at 95 °C; Amplification: denaturation at 95 °C, 10 sec; annealing/extension + plate read at gene dependent temperature, 10-30 sec; cycles, 45; melt-curve analysis, 65-95 °C with 0.5 °C increments 2-5 sec/step. Data were analyzed using the Bio-Rad CFX manager and excel, which is further described in 3.4 Statistical Analysis.

2.4.2. Proteomics

Fifty one individual embryos were pooled into a single centrifuge tube from all fifteen experiments, maintaining the three replicates per dose in each experiment. This was performed at both embryonic stages – 2 dpf and 7 dpf. Following this, 104.55 uL of 200 mM AB (Appendix B) was added to each tube and the embryos were homogenized using

a mortar and pestle followed by aspiration with a syringe and needle. The homogenates were centrifuged for 15 mins at 4 ºC and 14,000 xg, and the supernatant was transferred to a low retention tube. All samples were placed in the centrifugal evaporator (SpeedVac™ SPD 1030/2030) and then evaporated to 50 uL. 35 uL of AB was added to each sample followed by 2.65 uL of 100 mM Tris(2-carboxyethyl) phosphine hydrochloride (TECP) in 200 mM AB (Appendix B).

The samples were vortexed and placed at room temperature to incubate for 45 minutes. Following incubation, 2.8 uL of the 400mM iodoacetamide (IAA) in 200 mM AB (Appendix B) was added to each sample and they were vortexed and incubated in the dark for 45 minutes. Next, 50 uL of 20% formic acid (Appendix B) was added to each sample and vortexed. Lid locks were placed on each tube and samples were incubated on a dry heating block at 115 ℃ for 45 minutes.

The samples were evaporated down to near dryness in the centrifugal evaporator and then resuspended in 20 uL of dilution buffer (Appendix B). All samples were vortexed until the samples were completely resuspended. Samples were centrifuged at 14,000 g for 10 minutes and the supernatant was collected in a pre-labelled 2 mL screw thread HPLC vials containing a 250 uL polypropylene spring bottom insert. Vials were capped with 9 mm blue PTFE/silicone/PTFE screw caps (Figure 2.3). 2 µL of the digested protein samples were injected onto a reverse-phase liquid chromatography (RPLC) column (Zorbax, 300SB-C18, 1.0 × 50 mm 3.5 µm, Agilent Technologies Canada Inc., Mississauga, ON) and separated peptides were detected by an Agilent 6545 Accurate-Mass Quadrupole

Time-of-Flight (Q-TOF) mass spectrometer. Each sample was run with two iterations and a blank and an analytical standard of digested bovine serum albumin (BSA) peptides were injected every 10 samples during the runtime. All instrumental methods and settings are described further in detail in Appendix C.

2.4.3. Proteome Identification and Quantification

Spectral data were searched against the Japanese rice fish *(Oryzias latipes)* reference proteome (UP000001038) downloaded from Uniprot on February 26, 2021, using Spectrum Mill MS Proteomics Workbench (Rev B.06.00.201) software for protein identification. Skyline (Version 20.2) software was used to determine protein abundances using chromatographic peak area to fill in missing values. Protein quantification was performed using a cut-off score of 0.9, 5 maximum missed cleavages, and retention time window of 5 minutes for MS1 filtering using TOF transition settings and DDA acquisition method for MS/MS filtering. Mass Profiler Professional (MPP) (Version 15.1) software was used to import results from Skyline and then export the data into a comma separated format that included a list of all Uniprot accession numbers for proteins detected with protein abundance in total mean intensity for the peak areas of each protein-peptide group. The maximum values between the two iterative runs were taken and all abundances less than 5000 mean intensity counts were removed. The medaka accession numbers were used to BLAST search against the Human reference proteome (UP000005640) to find the nearest human protein orthologs. If there were any duplicate proteins, they were consolidated using the maximum function in excel.

2.4.4. HeartBeat Data Processing

Video was edited using iMovie editing software to remove dark spaces above and below the video, as well as to remove the first three seconds of video which contained focus adjustments. The contrast was also increased to make the heartbeat easier to detect with the *Heartbeat* (Version 2.1) software algorithm. The video was saved as an mp4 file format so that it could be imported into the *Heartbeat* open-source software, which includes a video to image converter. To use this converter, each video for each individual embryo replicate was placed in its own folder and converted to the software's proprietary format. Data was automatically detected in most cases where 30 seconds of stable video was used. However, when necessary, usually due to weak heartbeat or embryo movement, the threshold of detection was lowered in 0.5 increments to detect lower stimulus and the amount of video analyzed was decreased to a minimum of 10 seconds to improve automated heart rate detection and counting of the heartbeat.

2.4.5. Malformation Analysis

Observations of developmental malformations were performed under the Leica EZ4 stereomicroscope with a built-in camera. The images were retrieved using the Leica EZ Application Suite (Version 3.4.0) software. Each fry was placed with a little bit of formalin on a clear glass microscope slide using a 3 mL transfer pipette. Fry were imaged and assigned to a group by letter to avoid bias. Each group by letter was scored for severity of pericardial edema. Scoring was on a scale of 0 – 3 with descriptions and examples, which are displayed in Table 2.3. Once scoring was complete, groups of scored fry were placed back into data tables according to concentration groups.

2.5 Statistical Analyses

Data from qPCR were analyzed using Bio-Rad CFX Manager Version 3.1. For each gene, the relative quantity of RNA was determined using the Cq value, efficiency, and R2. Only an efficiency of greater than 90% and R2 greater than 0.95 was found acceptable. The data underwent square root transformation and relative fold change was generated for each dose with respect to control. Normalization of each gene was performed using the housekeeping gene *rpl7*.

All statistical tests were performed using GraphPad Prism (Mac Version 9.1.2) software with the exception of proteomics data, which was performed using Metaboanalyst 5.0. One-way ANOVAs with Dunnett's multiple comparisons post-hoc tests were performed on relative fold change data on each gene, hatching time, and heart rate data to reveal significant differences. A chi-square test was performed on pericardial edema scores to detect differences in malformations among exposure groups. Similar to a post-hoc test, the Kolmogorov-Smirnov test was performed to find differences between control and individual treatment groups.

Proteomics data was analyzed using Metaboanalyst 5.0 (Pang et al., 2021). Data was uploaded as a peak intensity table with samples in unpaired columns. Data was normalized by median and scaled using auto-scaling. Raw data from volcano plot results were exported with all proteins, associated fold change (relative to the control) and *p*-values. A false-discovery-rate (FDR) cut off of 0.2 was applied using the Benjamini–Hochberg procedure (Benjamini & Hochberg, 1995). Over-representation pathway analysis was performed on

the orthologous human gene symbols of significant proteins (p-value < 0.05) with FDR correction (< 0.2) that increased in abundance relative to the control (positive fold change) and decreased in abundance relative to the control (negative fold change) separately, for each dose using ConsensusPathDB-human (Herwig, Hardt, Lienhard, & Kamburov, 2016; Kamburov et al., 2011).

Tables

Table 2.1: Wild-type Japanese Ricefish (Oryzias latipes) qPCR primers

Target Gene	Forward primer sequence (5'–3')	Reverse primer sequence (5'–3')
ahR2a	GCTGGCTTTATTCGCCATCG	AACCACCTTTCCTCTGCCATC
hif-1α	CCTGGACAAAGCGTCAGTCA	TGTTTAGGCTCATCGGTGCC
cox-2	CCCTATGCGTCTTTTGAGGA	AACAATGTCGAAGCCTACGCT
rpl7	CCCCAACTTGAAGTCTGTGC	TGTTGGCAGGCTTGAAGTTC

Table 2.2: Optimization of the laboratory's standard method to ensure adequate digestion of proteins. Test 6 indicates the run that detected the most abundance of proteins.*

Variable	Test 1	Test 2	Test 3	Test 4	Test 5	Test 6 *	Test 7
Alkylation reagent (IAA) concentration	400 mM	200 mM	200 mM	400 mM	200 mM	400 mM	400 mM
Formic acid (FA) concentration	20%	30%	20%	30 %	30%	20%	30%
Digestion Time	30 minutes	30 minutes	45 minutes	30 minutes	45 minutes	45 minutes	45 minutes

Table 2.3: Scoring of pericardial edema surrounding the heart based on Blue Sac disease scoring of heart as previously mentioned (Rhodes, Farwell, Hewitt, Mackinnon, & Dixon, 2005). Pictures were taken in the Aquatic Omics lab using a Leica EZ4 microscope with a built-in camera and Leica EZ Application Suite (Version 3.4.0) software. The heart and surrounding cardiovascular development is indicated by the black box on each picture of a hatch.

0	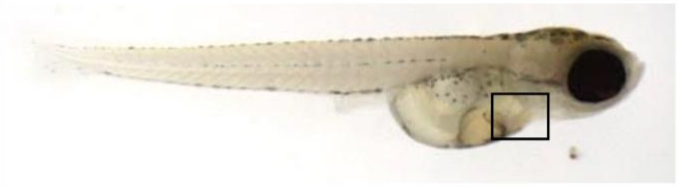	No abnormalities or malformation
1		Slight malformation of the heart including poor circulation
2		Moderate malformation including elongation of any/all heart chambers
3		Severe Tube Heart

Figures

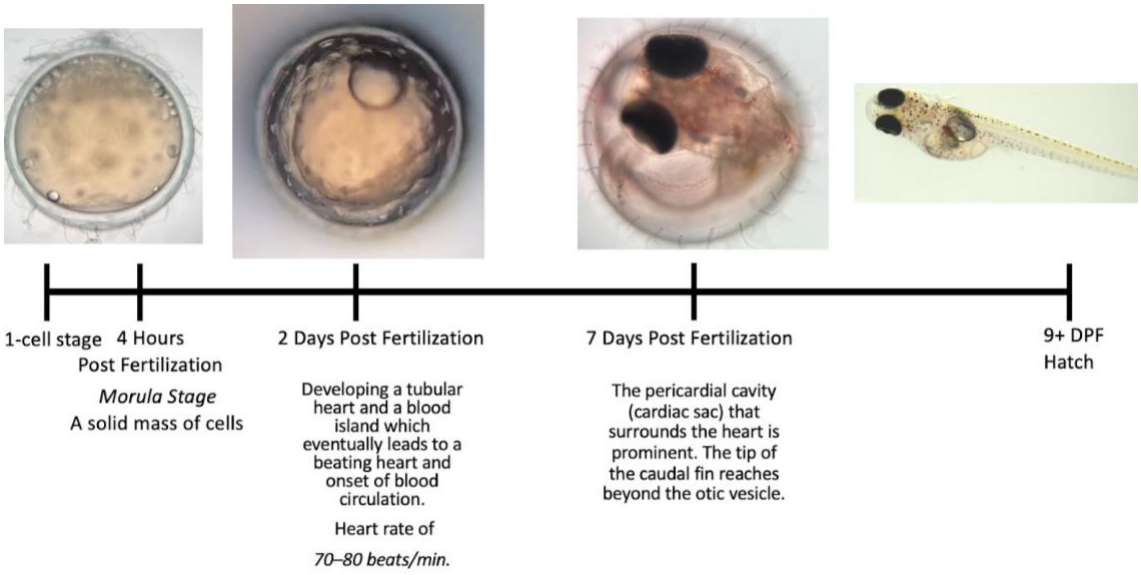

Figure 2.1: Stages of Japanese Ricefish (Oryzias latipes) cardiovascular development. Only 4 hours after fertilization, the embryo reaches division into a mass of cells known as a morula. 2 dpf marks the onset of blood circulation, and at 7 dpf cardiovascular development is complete. Fry normally hatch between 9 and 11 dpf.

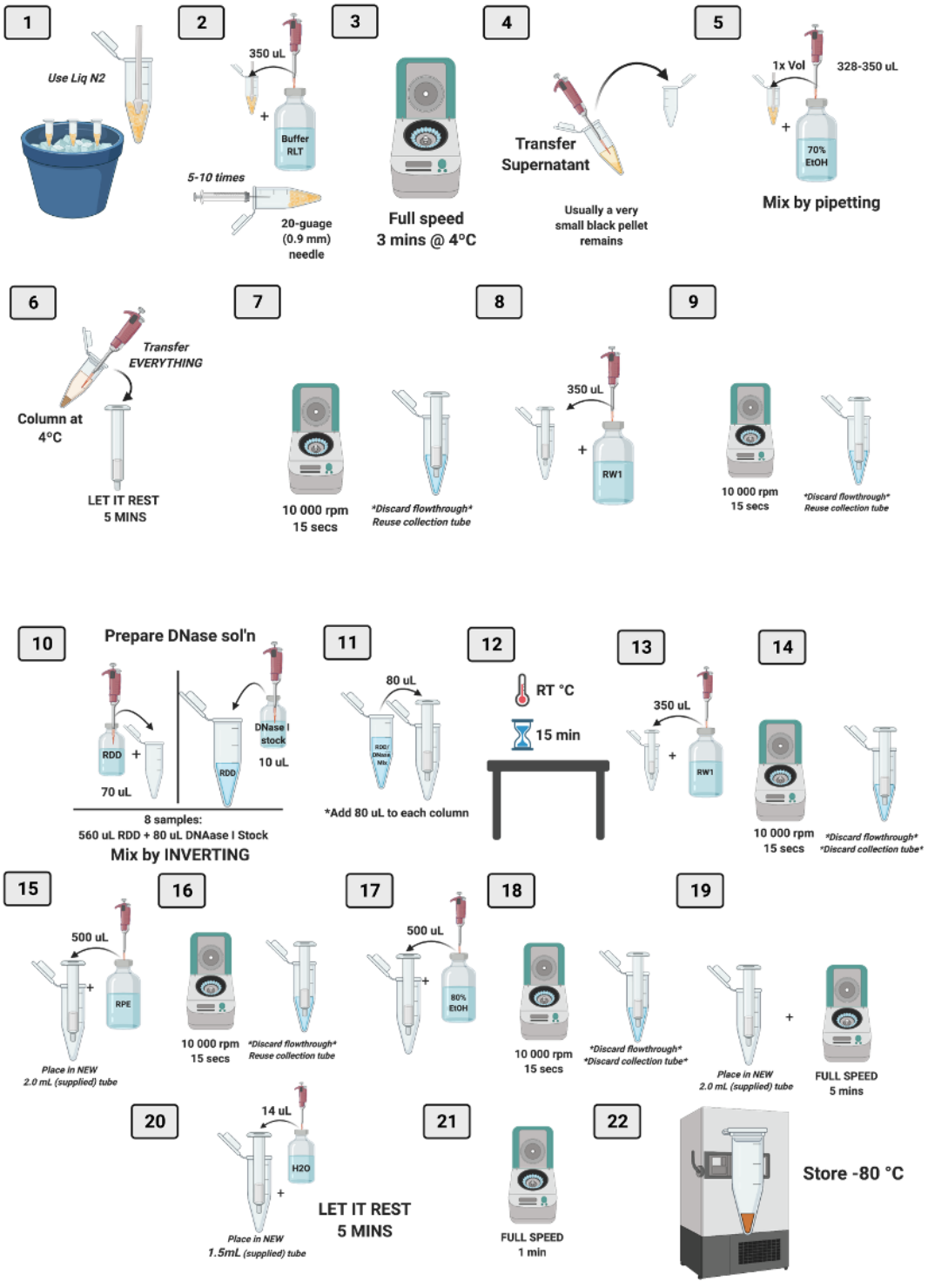

Figure 2.2: mRNA extraction workflow as outlined in the Qiagen RNeasy Micro handbook modified for extracting RNA from 3 Japanese Ricefish (Oryzias latipes) embryos per column.

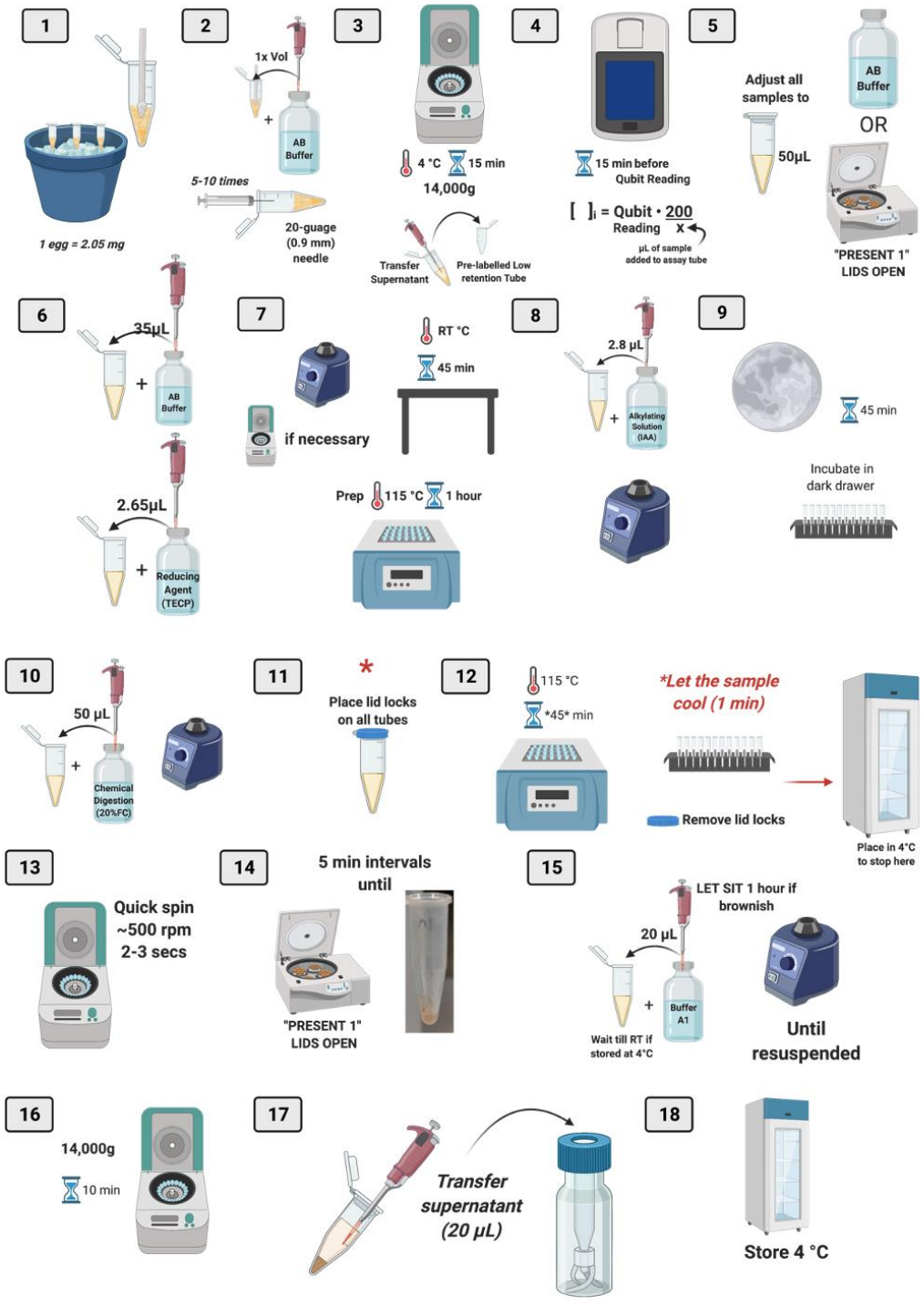

Figure 2.3: Proteomics sample preparation workflow until storage for running on LC-QTOF MS/MS.

Chapter 3. Results

3.1 Cardiovascular Development

All concentrations of TCDD tested (0.001 ppb - 10 ppb) caused impaired angiogenesis, examples of which can be seen in Figure 3.1. The number of mortalities among the different TCDD exposure concentrations were not significantly different. However, a one-way ANOVA with Dunnett's multiple comparisons post-hoc test identified significant delays in hatching time between control and the 1ppb (*p*-value = 0.0314), as well as between the control and the 10 ppb treatments (*p*-value = 0.0036) (Figure 3.2). The most severe pericardial edema was observed in the higher concentrations, especially in 10 ppb exposure (Figure 3.3) (*p*-value = 0.01, chi-square test). The median pericardial edema score increased 2-fold, from 1 to 2 in the 10-ppb group compared to the control (*p*-value = 0.01, non-parametric t-test) (Figure 3.4). There was a significant decrease in mean heart rate across all exposure groups compared to the control (Figure 3.5, one-way ANOVA with Dunnett's multiple comparisons post-hoc test, *p*-values: 0.0001, 0.0002, <0.0001, <0.0001, and 0.0319, in order from 0.001 ppb - 10 ppb, respectively).

3.2 Gene expression

Significant differences in gene expression were observed for *ahr* and *cox-2*, but not *hif-1a* (Figure 3.6). Where *ahr* is affected at both stages of development tested, *cox-2* is only affected in the later stage at 7 dpf. All significant differences occurred in only the highest exposure concentration (10 ppb TCDD) (Figure 3.6).

3.3 Embryo Proteins

Over-representation pathway analysis (Herwig et al., 2016; Kamburov et al., 2011) performed on the orthologous human gene symbols of all proteins detected in the control 2 dpf Japanese Ricefish *(Oryzias latipes)* embryos revealed activation of the following pathways (Figure 3.7) significantly ($p < 0.01$): cardiac conduction (Table 3.1), Cardiac muscle contraction - Homo sapiens (human) (Table 3.2), Retinoid metabolism and transport (Table 3.3), Retinoic acid receptors-mediated signaling (Table 3.4), and Melanogenesis - Homo sapiens (human) (Table 3.5).

Over-representation pathway analysis performed on orthologous human gene symbols of all proteins detected in the 10ppb 2 dpf Japanese Ricefish *(Oryzias latipes)* embryos revealed significant ($p < 0.01$) activation of several cardiomyopathy pathways, specifically for dilated, hypertrophic, and arrhythmogenic right ventricular cardiomyopathy (Figure 3.8; Table 3.6). Activation of the HIF-1α transcription factor network pathway was also observed (Table 3.7).

Overall, more proteins were detected in the 2 dpf samples (382 proteins; Appendix D) than the 7 dpf samples (99 proteins; Appendix E). As well, all proteins that were detected in the control samples were also detected in all samples treated with TCDD. Changes in protein abundance detected in the lower concentration groups: 0.001, 0.01, 0.1, and 1 ppb of TCDD were not significantly different compared to control in the 2 dpf samples, and none of concentrations significantly affected protein abundance in the 7 dpf samples. However, in the 2 dpf 10 ppb treatment group, a total of 196 proteins were decreased in abundance and 186 proteins were increased in abundance; of which 30 proteins were significantly decreased in abundance (Table 3.8) and 29 proteins were significantly increased (Table 3.9) in abundance compared to the control (volcano plot, $p < 0.05$ with Benjamini-Hochberg correction of < 0.20 FDR).

Proteins that decreased significantly in abundance were generally associated with Vegf signaling and a potential relationship between inflammation (Cox-2) and Egfr (Figure 3.9). Specifically, Hras and Kras decreased in the 10ppb group from the control significantly according to the Benjamini–Hochberg procedure (Figure 3.10). Over-representation pathway analysis (p-value < 0.01) of performed on orthologous human gene symbols of significantly decreased proteins revealed these two genes are associated with VEGFR2 mediated cell proliferation, Signaling by EGFRvIII in Cancer, Constitutive Signaling by Ligand-Responsive EGFR Cancer Variants, Signaling by Ligand-Responsive EGFR Variants in Cancer, and Signaling by EGFR in Cancer pathways in Reactome; and also the VEGF signaling pathway - Homo sapiens (human) pathway in KEGG (Figure 3.10). Additionally, Pik3cg was found to be significantly decreased in abundance in 10 ppb compared to control, and this gene, along with Hras and Kras, are found to be overlapping in the Relationship between inflammation, COX-2 and EGFR pathway (Wikipathways) upon over-representation pathway analysis (p-value < 0.01) of the orthologous human gene symbols (Figure 3.11). The proteins Hras, Kras, Pik3cg, in addition to, Krt8, Mvp, and Anxa1 were all decreased significantly in abundance from control, according to the Benjamini–Hochberg procedure, in the 10ppb TCDD treatment. Their orthologous human gene symbols were also found overlapping in the EGFR1 pathway discovered by over-representation pathway analysis ($p<0.01$) (Table 3.10).

Proteins that significantly increased in abundance were associated with a much shorter list of distinct pathways found by over-representation analysis ($p<0.01$) of their orthologous human gene symbols. These proteins were identified in pathways including Arf6 signaling events, RAC2 GTPase cycle, EPH-Ephrin signaling, RHO GTPases Activate WASPs and WAVEs, Regulation of actin cytoskeleton - Homo sapiens (human), and Endocytosis - Homo sapiens (human) (Figure 3.12). Git1, Actr3, Cyfip1, Psd4 and Kif13b were proteins involved in many of these pathways and were all significantly increased in abundance in the 10ppb compared to control in the 2 dpf embryos (Figure 3.13 and 3.14).

The subset of proteins detected in the 7 dpf samples were generally associated with pathways of stress detected by over-representation pathway analysis (*p-value* < 0.01) (Figure 3.15) performed on the orthologous human gene symbols which specifically showed activation of the Regulation of HSF1-mediated heat shock response (Table 3.11), Oxidative Stress Induced Senescence (Table 3.12), and Lipid and atherosclerosis - Homo sapiens (human) pathways (Table 3.13).

Tables

Table 3.1: Orthologous human gene symbols with associated Uniprot protein accession numbers that were detected in the 2 dpf Japanese Ricefish (Oryzias latipes) samples that overlap with the Cardiac conduction pathway found in Reactome with corresponding mean protein abundances (average of three technical replicates) shown per treatment. Lower abundances of protein are more yellow, while higher abundances are bluer.

Orthologous Human Gene Symbol	Medaka Accession #	Control	0.001 ppb	0.01 ppb	0.1 ppb	1 ppb	10 ppb
RYR1	H2L660	331460	284463	363641	320205	345533	325238
SLC8A2	H2L495	1747960	1557960	1890787	2133744	1916446	1962224
ABCC9	H2M3J2	784320	466727	759470	693925	721030	859581
ATP2B2	H2MYV2	221420	212698	132311	215009	227851	73141
KCNH2	H2LGS9	263099	138677	191081	247602	174319	322995
CACNA1C	H2MH40	837305	724582	830064	889343	840900	805252
ATP2B1	H2MYU7	442841	425395	264621	430017	455702	146282
ATP1A2	H2LBL9	460840	467406	564196	541638	488592	471059

Table 3.2: Orthologous human gene symbols with associated Uniprot protein accession numbers that were detected in the 2 dpf Japanese Ricefish (Oryzias latipes) samples that overlap with the Cardiac muscle contraction - Homo sapiens (human) pathway found in KEGG with corresponding mean protein abundances (average of three technical replicates) shown per treatment. . Lower abundances of protein are more yellow, while higher abundances are bluer.

Orthologous Human Gene Symbol	Medaka Accession #	Control	0.001 ppb	0.01 ppb	0.1 ppb	1 ppb	10 ppb
MYH7	H2MDC8	158412	126424	171537	155761	163607	143922
CACNA1C	H2MH40	837305	724582	830064	889343	840900	805252
CACNA1D	H2LBF8	1674610	1449164	1660128	1778687	1681801	1610504
CACNA1F	H2MR69	837305	724582	830064	889343	840900	805252
SLC8A2	H2L495	1747960	1557960	1890787	2133744	1916446	1962224
ATP1A2	H2LBL9	460840	467406	564196	541638	488592	471059
CACNA2D3	H2LY22	459013	382152	492304	506689	412771	470144

Table 3.3: Orthologous human gene symbols with associated Uniprot protein accession numbers that were detected in the 2 dpf Japanese Ricefish (Oryzias latipes) samples that overlap with the Retinoid metabolism and transport pathway found in Reactome with corresponding mean protein abundances (average of three technical replicates) shown per treatment. Lower abundances of protein are more yellow, while higher abundances are bluer.

Orthologous Human Gene Symbol	Medaka Accession #	Control	0.001 ppb	0.01 ppb	0.1 ppb	1 ppb	10 ppb
AGRN	H2L4F8	444242	365672	416929	584602	505760	422320
APOE	H2MG05	1509892	1219660	1599458	1647528	1639730	1464490
APOB	H2LQ37	970223	884494	1012176	964585	1061283	924759
HSPG2	H2MMH3	229089	220368	256039	253978	259439	227624
LRP2	H2MRQ6	369318	350549	419376	358137	361282	377845
LDLR	H2LFW4	1873151	1591719	1945678	1844745	1864853	1820245

Table 3.4: Orthologous human gene symbols with associated Uniprot protein accession numbers that were detected in the 2 dpf Japanese Ricefish (Oryzias latipes) samples that overlap with the Retinoic acid receptors-mediated signalling pathway found in PID with corresponding mean protein abundances (average of three technical replicates) shown per treatment. Lower abundances of protein are more yellow, while higher abundances are bluer.

Orthologous Human Gene Symbol	Medaka Accession #	Control	0.001 ppb	0.01 ppb	0.1 ppb	1 ppb	10 ppb
CREBBP	H2LWE6	492753	471621	503650	349850	355578	496858
EP300	H2MFZ7/H2LB35	985507	943242	1007300	699700	711156	993716
RARG	H2MKN6/H2LUS1	893141	825142	944472	1220152	1001835	947537
RARB	H2LX30	446570	412571	472236	610076	500918	473769
NCOR2	H2MG30/H2MG32	746336	750641	843605	942282	913722	764082

Table 3.5: Orthologous human gene symbols with associated Uniprot protein accession numbers that were detected in the 2 dpf Japanese Ricefish (Oryzias latipes) samples that overlap with the Melanogenesis - Homo sapiens (human) pathway found in KEGG with corresponding mean protein abundances (average of three technical replicates) shown per treatment. Lower abundances of protein are more yellow, while higher abundances are bluer.

Orthologous Human Gene Symbol	Medaka Accession #	Control	0.001 ppb	0.01 ppb	0.1 ppb	1 ppb	10 ppb
ADCY6	H2MAE8	281479	267310	321558	322678	286993	339007
ADCY9	H2LWC3/H2MJQ1	386241	391070	521579	483259	450465	419841
HRAS	H2M6R0/H2MXD7	150104	207914	138293	435130	297463	212440
KRAS	O42277/O57467	150104	207914	138293	435130	297463	212440
CAMK2D	H2N045	1399511	1157649	1450918	1418878	1342041	1387542
CREBBP	H2LWE6	492753	471621	503650	349850	355578	496858
EP300	H2MFZ7/H2LB35	985507	943242	1007300	699700	711156	993716

Table 3.6: Orthologous human gene symbols with associated Uniprot protein accession numbers that were detected in the 2 dpf Japanese Ricefish (Oryzias latipes) samples that overlap with the Dilated cardiomyopathy - Homo sapiens (human) indicated by Dilated CM, Hypertrophic cardiomyopathy - Homo sapiens (human) indicated by Hypertrophic CM, and Arrhythmogenic right ventricular cardiomyopathy - Homo sapiens (human) indicated by Arrhythmogenic RV CM. These pathways are found in the KEGG database and the corresponding mean protein abundances (average of three technical replicates) detected in the 2 dpf samples are shown per treatment. Lower abundances of protein are more yellow, while higher abundances are bluer.

Orthologous Human Gene Symbol	Medaka Accession #	Control	0.001 ppb	0.01 ppb	0.1 ppb	1 ppb	10 ppb	Dilated CM	Hypertrophic CM	Arrhythmogenic Right Ventricular CM
ADCY6	H2MAE8	281479	267310	321558	322678	286993	339007	✓		
ADCY9	H2LWC3/H2MJQ1	386241	391070	521579	483259	450465	419841	✓		
CACNA1C	H2MH40	837305	724582	830064	889343	840900	805252	✓	✓	✓
CACNA1D	H2LBF8/H2LE53	1674610	1449164	1660128	1778687	1681801	1610504	✓	✓	✓
CACNA1F	H2MR69	837305	724582	830064	889343	840900	805252	✓	✓	✓
CACNA2D3	H2LY22	459013	382152	492304	506689	412771	470144	✓	✓	✓
DES	H2L9W4	721335	442476	856876	560300	624333	588177	✓	✓	✓
DSP	H2MX47	214428	123524	185784	152155	156646	162427			✓
ITGA7	H2LJI2/H2LJI5/H2LJI0	3279193	2864179	3600219	3369172	3286750	3384615	✓	✓	✓
ITGB4	H2N2N3	276962	243250	335025	377782	350412	329567	✓	✓	✓
MYH7	H2MDC8	158412	126424	171537	155761	163607	143922	✓	✓	
PRKAG1	H2L825/H2L827	1422061	848144	1334953	1143696	1129166	1262461		✓	
SLC8A2	H2L495	1747960	1557960	1890787	2133744	1916446	1962224	✓	✓	✓

Table 3.7: Orthologous human gene symbols with associated Uniprot protein accession numbers that were detected in all Japanese Ricefish (Oryzias latipes) samples that overlap with the HIF-1α transcription factor network pathway found in the PID database with corresponding mean protein abundances (average of three technical replicates) detected in the 2 dpf samples are shown per treatment. Lower abundances of protein are more yellow, while higher abundances are bluer.

Orthologous Human Gene Symbol	Medaka Accession #	Control	0.001 ppb	0.01 ppb	0.1 ppb	1 ppb	10 ppb
ALDOA	H2LIU7	364511	275968	358544	407100	370583	368062
PGM1	H2M3I0	1130218	655252	991829	911593	1007084	1066435
TF	P79819/H2MPL0	555216	519950	595380	624919	517259	520386
CREBBP	H2LWE6	492753	471621	503650	349850	355578	496858
EP300	H2MFZ7/H2LB35	985507	943242	1007300	699700	711156	993716
SMAD4	H2LJX9/H2LU73	157585	64414	176042	198955	193075	170985

Table 3.8: Orthologous human gene symbols with associated Uniprot protein accession numbers that were detected in the 2 dpf 10 ppb Japanese Ricefish (Oryzias latipes) samples that were decreased in abundance relative to control with log fold change values retrieved from Metaboanalyst and FDR-corrected p-values using Benjamini Hochberg procedure.

Protein Name	Orthologous Human Gene Symbol	Medaka Uniprot Accession #	log2(FC)	Raw p-value	Benjamini-Hochberg Corrected p-value
annexin A1	ANXA1	H2MEL1	-2.2	0.0284	0.1976
KRAS proto-oncogene, GTPase	KRAS	O42277	-1.673	0.0264	0.1939
HRas proto-oncogene, GTPase	HRAS	H2M6R0	-1.673	0.0264	0.1939
recombination activating 1	RAG1	H2M914	-0.71258	0.0018	0.0502
phosphatidylinositol-4,5-bisphosphate 3-kinase catalytic subunit gamma	PIK3CG	H2M0C9	-0.69954	0.0008	0.0381
chromosome 12 open reading frame 56	C12orf56	H2MS66	-0.68379	0.0028	0.0603
ZXD family zinc finger C	ZXDC	H2M0J6	-0.68182	0.0018	0.0502
EH domain binding protein 1 like 1	EHBP1L1	H2M8L4	-0.6455	0.0006	0.0372
envoplakin	EVPL	H2MJN4	-0.6386	0.0005	0.0366
chromosome 18 open reading frame 25	C18orf25	H2LJX7	-0.63547	0.0003	0.0277
tripartite motif containing 71	TRIM71	H2LLW2	-0.59926	0.0003	0.0277
perilipin 3	PLIN3	H2MPB1	-0.56454	0.0243	0.1887
major vault protein	MVP	H2N0A4	-0.55336	0.0118	0.1523
leucine rich repeat, Ig-like and transmembrane domains 2	LRIT2	H2LRG7	-0.52278	0.016	0.1614
shieldin complex subunit 2	SHLD2	H2LCP2	-0.5107	0.0112	0.1522
agrin	AGRN	H2L4F8	-0.50934	0.0233	0.1887
nucleoporin 210	NUP210	H2M719	-0.48718	0.0071	0.1079
pentatricopeptide repeat domain 1	PTCD1	H2LZR2	-0.4608	0.0137	0.154
oxysterol binding protein like 3	OSBPL3	H2LUG4	-0.43816	0.0147	0.1606
drosha ribonuclease III	DROSHA	H2MEP2	-0.40562	0.0025	0.0593
calnexin	CANX	H2L9G7	-0.40225	0.0055	0.0876
adaptor related protein complex 1 subunit beta 1	AP1B1	H2LQQ4	-0.39101	0.0022	0.0567
arrestin 3	ARR3	H2L9D0	-0.31022	0.0164	0.1614
mortality factor 4 like 1	MORF4L1	H2LQS2	-0.30359	0.0124	0.1523
protein regulator of cytokinesis 1	PRC1	H2LM39	-0.28225	0.0247	0.1887
YEATS domain containing 4	YEATS4	H2MFM7	-0.26329	0.0197	0.1674
heat shock transcription factor 1	HSF1	H2MF92	-0.25739	0.0276	0.1976
RNA binding region (RNP1, RRM) containing 3	RNPC3	H2LM89	-0.23503	0.0011	0.0424
complement C7	C7	H2LGZ3	-0.16923	0.0308	0.1994
HECT and RLD domain containing E3 ubiquitin protein ligase 4	HERC4	H2M9V4	-0.11724	0.0173	0.1614

Table 3.9: Orthologous human gene symbols with associated Uniprot protein accession numbers that were detected in the 2 dpf 10 ppb Japanese Ricefish (Oryzias latipes) samples that were increased in abundance relative to control with log fold change values retrieved from Metaboanalyst and FDR-corrected p-values using Benjamini Hochberg procedure.

Protein Name	Orthologous Human Gene Symbol	Medaka Uniprot Accession #	log2(FC)	Raw *p*-value	Benjamini-Hochberg Corrected *p*-value
GIT ArfGAP 1	GIT1	H2MFK1	0.15708	0.0017	0.0502
kinesin family member 7	KIF7	H2LZU6	0.19788	0.0194	0.1674
terminal uridylyl transferase 4	TUT4	H2MD26	0.20843	0.0121	0.1523
ODZ1 protein	ODZ1	H2LWM7	0.25842	0.0043	0.0709
teneurin transmembrane protein 1	TENM1	H2LWN2	0.25842	0.0043	0.0709
extended synaptotagmin 3	ESYT3	H2MV11	0.25843	0.0039	0.0709
glial fibrillary acidic protein	GFAP	H2L6N1	0.25865	0.0088	0.1294
calcineurin like phosphoesterase domain containing 1	CPPED1	H2LCL6	0.2889	0.0285	0.1976
N-alpha-acetyltransferase 20, NatB catalytic subunit	NAA20	H2MS46	0.308	0.0155	0.1614
bromodomain and PHD finger containing 3	BRPF3	H2LFX6	0.31694	0.0173	0.1614
coiled-coil domain containing 85C	CCDC85C	H2MD86	0.3287	0.024	0.1887
coiled-coil domain containing 85A	CCDC85A	H2MD85	0.3287	0.024	0.1887
filamin C	FLNC	H2N036	0.37834	0.0304	0.1994
transient receptor potential cation channel subfamily C member 4 associated protein	TRPC4AP	H2MFJ2	0.38182	0.0291	0.1987
plexin B2	PLXNB2	H2MR98	0.39381	0.0027	0.0603
RB1 inducible coiled-coil 1	RB1CC1	H2MSZ9	0.40677	0.0016	0.0502
tubulin tyrosine ligase like 7	TTLL7	H2LPJ0	0.4429	0.0111	0.1522
ring finger protein 103	RNF103	H2N260	0.45893	0.0008	0.0381
dynein axonemal heavy chain 5	DNAH5	H2LEP5	0.50894	0.0009	0.0381
ubiquitin protein ligase E3C	UBE3C	H2M4A2	0.5206	0.0001	0.027
actin related protein 3	ACTR3	H2LVP0	0.55445	0.0033	0.0631
cytoplasmic FMR1 interacting protein 1	CYFIP1	H2MMS2	0.58834	0.0129	0.1537
pleckstrin and Sec7 domain containing 4	PSD4	H2LSI6	0.68414	0.0166	0.1614
zinc finger protein 106	ZNF106	H2MAH8	0.69956	0.0189	0.1674
transporter 2, ATP binding cassette subfamily B member	TAP2	H2LQG7	0.71036	0.0133	0.1537
cartilage intermediate layer protein	CILP	H2L507	0.7187	0.0302	0.1994
kinesin family member 13B	KIF13B	H2MHR9	0.7578	0.0186	0.1674
sterile alpha motif domain containing 1	SAMD1	H2LRV5	0.82542	0.003	0.0609
zinc finger protein 750	ZNF750	H2LSP7	1.3633	0.0002	0.0277

Table 3.10: Orthologous human gene symbols with associated Uniprot protein accession numbers that were detected in all Japanese Ricefish (Oryzias latipes) samples that overlap with the EGFR1 pathway found in the NetPath database with corresponding mean protein abundances (average of three technical replicates) detected in the 2 dpf samples are shown per treatment. Lower abundances of protein are more yellow, while higher abundances are bluer. Proteins in the 10ppb group are significantly decreased compared to control as found by the Benjamini–Hochberg procedure indicated by the asterisk.

Orthologous Human Gene Symbol	Medaka Accession #	Control	0.001 ppb	0.01 ppb	0.1 ppb	1 ppb	10 ppb*
HRAS	H2M6R0/H2MXD7	150104	207914	138293	435130	297463	212440
MVP	H2N0A4	426423	363252	406739	591600	386468	454345
PIK3CG	H2M0C9	643243	550596	595794	961110	683266	724475
KRAS	O42277/O57467	150104	207914	138293	435130	297463	212440
ANXA1	O57467	36621	26185	38582	171448	72361	96176

Table 3.11: Orthologous human gene symbols with associated Uniprot protein accession numbers that were detected in all the 7 dpf Japanese Ricefish (Oryzias latipes) samples that overlap with the Regulation of HSF1-mediated heat shock response pathway found in the Reactome database with corresponding mean protein abundances (average of three technical replicates) detected in the 7 dpf samples are shown per treatment. Lower abundances of protein are more yellow, while higher abundances are bluer.

Orthologous Human Gene Symbol	Medaka Accession #	Control	0.001 ppb	0.01 ppb	0.1 ppb	1 ppb	10 ppb
HSPA8	A5HL62/H2LKZ3/A5HL63	412953	442252	308347	162002	333040	383438
NUP54	H2LPZ3	1238211	969836	915567	795905	1129550	803858
NUP210	H2M719	80479	69124	84077	91837	115901	37922
HSPA1B	Q9I8F9/H2L3G7	275302	294835	205565	108001	222027	255625
SERPINH1	H2LF66	70928	27297	70468	8711	80692	60085

Table 3.12: Orthologous human gene symbols with associated Uniprot protein accession numbers that were detected in all the 7 dpf Japanese Ricefish (Oryzias latipes) samples that overlap with the Oxidative Stress Induced Senescence pathway found in the Reactome database with corresponding mean protein abundances (average of three technical replicates) detected in the 7 dpf samples are shown per treatment. Lower abundances of protein are more yellow, while higher abundances are bluer.

Orthologous Human Gene Symbol	Medaka Accession #	Control	0.001 ppb	0.01 ppb	0.1 ppb	1 ppb	10 ppb
H3-3A	H2LU55	460726	283649	189227	255113	370701	423497
H3C15	H2LD49/H2L744/ H2L375/H2M8F5/ H2L6K8	2303630	1418246	946136	1275565	1853507	2117486
H3-3B	H2L503	460726	283649	189227	255113	370701	423497
H4C1	H2L6I7/H2MZJ2/ H2L5J3/H2L743/ H2L727/H2L385	2775888	2147516	2085563	2002372	2578905	2161427

Table 3.13: Orthologous human gene symbols with associated Uniprot protein accession numbers that were detected in all the 7 dpf Japanese Ricefish (Oryzias latipes) samples that overlap with the Lipid and atherosclerosis - Homo sapiens (human) pathway found in the KEGG database with corresponding mean protein abundances (average of three technical replicates) detected in the 7 dpf samples are shown per treatment. Lower abundances of protein are more yellow, while higher abundances are bluer.

Orthologous Human Gene Symbol	Medaka Accession #	Control	0.001 ppb	0.01 ppb	0.1 ppb	1 ppb	10 ppb
MAPK12	H2MX42	216141	167217	160197	164725	163710	199669
HSPA1B	Q9I8F9/H2L3G7	275302	294835	205565	108001	222027	255625
HSPA8	A5HL62/H2LKZ3/A5HL63	412953	442252	308347	162002	333040	383438
APOA1	H2MLX9	146374	123052	110495	122550	108075	120775
APOB	H2LQ37	640562	559281	520246	423354	762875	312618
CAMK2D	H2N045	765011	614174	584466	554440	775389	457516

Figures

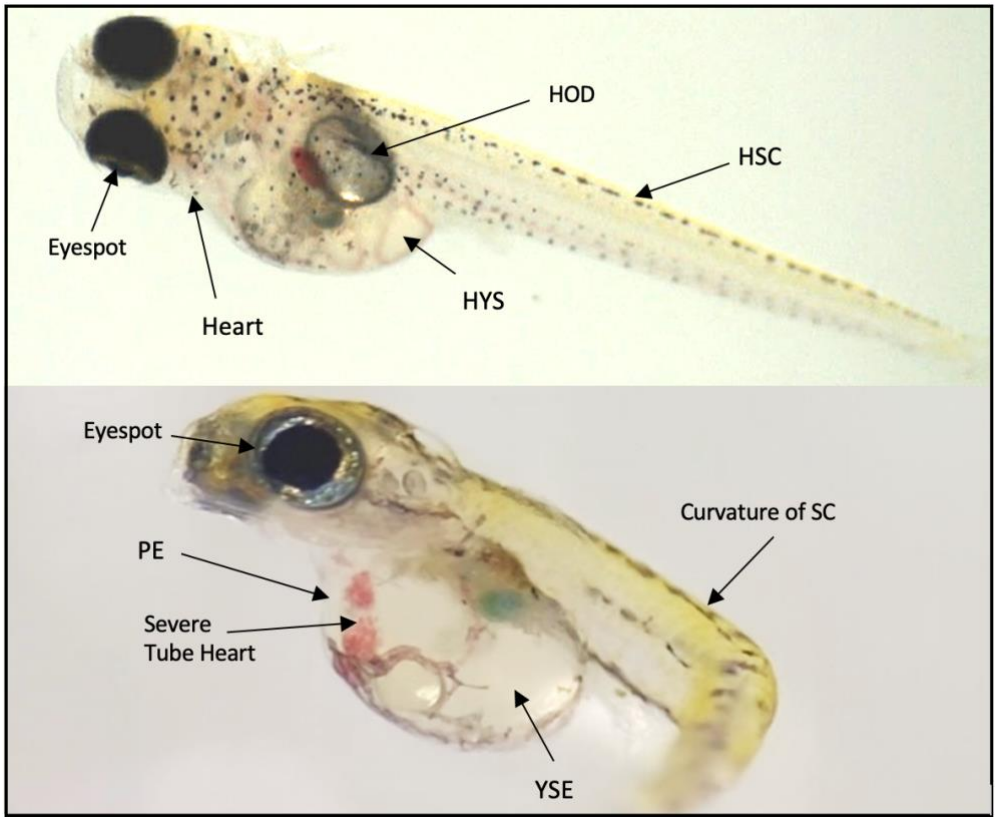

Figure 3.1: A normally developed newly hatched fry (upper image), and a malformed hatch exposed to 10 ppb of TCDD for 1 hour at the 4-hour-post-fertilization mark (lower image). The malformed fry has pericardial edema (PE), yolk sac edema (YSE), craniofacial and spinal cord (SC) malformations, and has a tube heart with coagulation. [HOD: Healthy oil droplet; HSC: Healthy Spinal Cord; HYS: Healthy Yolk Sac].

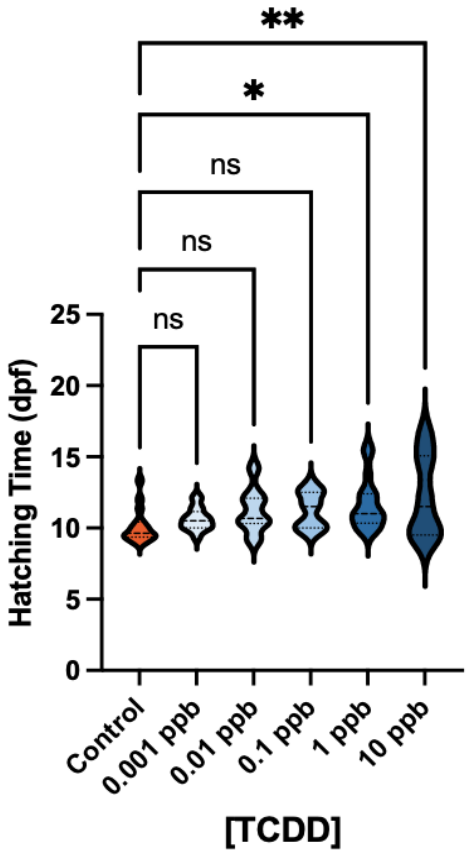

*Figure 3.2: Violin plot of hatching time between control embryos and embryos from each TCDD exposure group: 0.001, 0.01, 0.1, 1, and 10 ppb. Significant delay in hatching time are indicated with * p-value = 0.0314; ** p-value = 0.0036 (one-way ANOVA with Dunnett's multiple comparisons post-hoc test). Distribution of data is shown mirrored as a bell shape at each concentration. The median is shown by a darker dashed line and quartiles are represented by lighter dashed lines.*

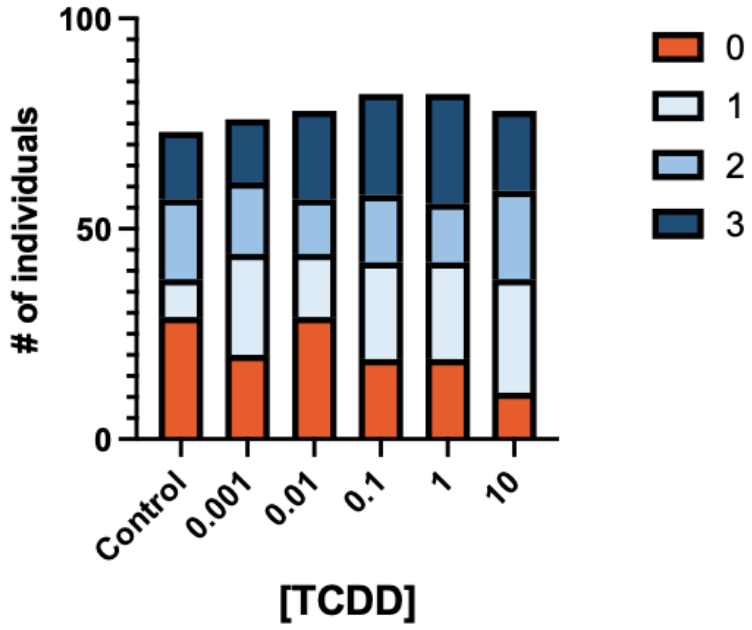

Figure 3.3: The number of embryos with malformations by severity score in each exposure group (p-value = 0.0127, Chi square test). Each dose consisted of fry categorized in one of four scoring categories based on Blue Sac disease heart scoring (see Table 2.3 for details).

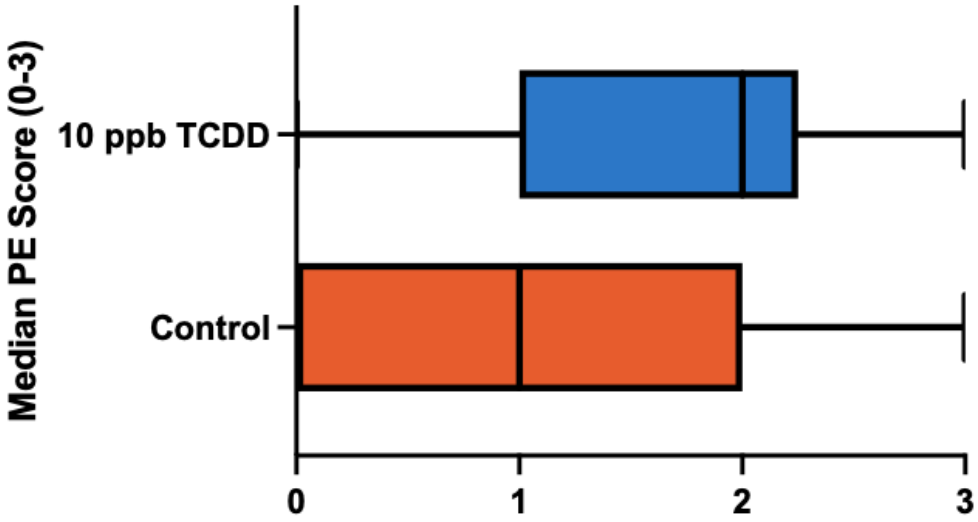

Figure 3.4: The median pericardial edema (PE) score for the control and 10 ppb exposure groups, (p-value = 0.0141, Kolmogorov-Smirnov test). Medians are shown as solid lines between the boxes with the boxes themselves indicating the range of scoring found in each group. The error bars represent the 0-3 scoring used for the groups (see Table 2.3 for details).

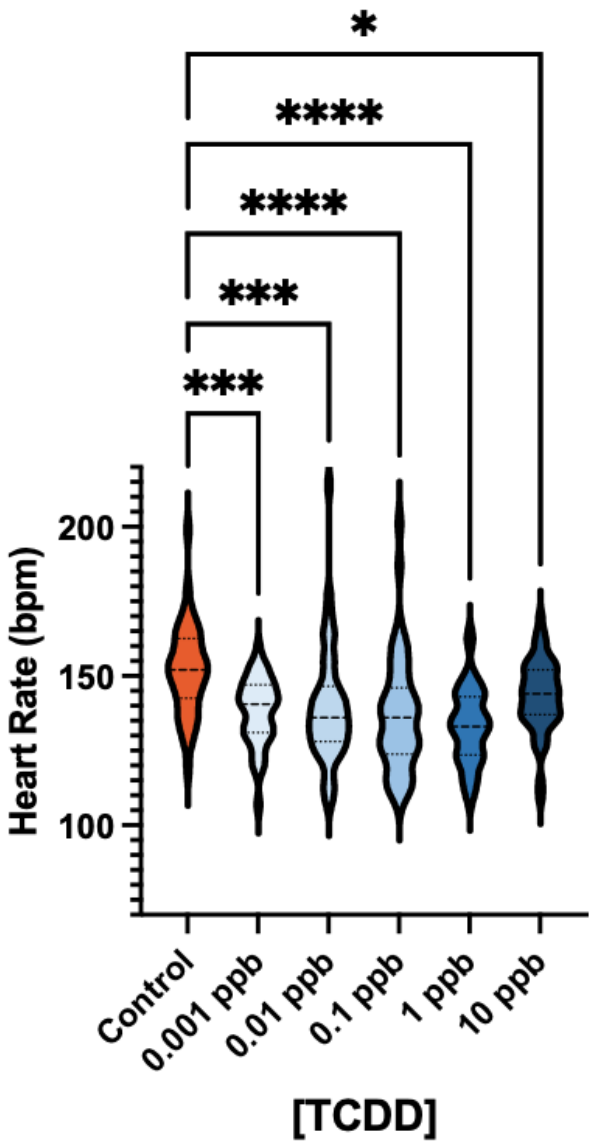

*Figure 3.5: Violin plot of Japanese rice fish (Oryzias latipes) heart rate at 7 dpf for each exposure group. Heart rate significantly declines in all treatment groups of TCDD (Dunnett's multiple comparisons post-hoc test) p-values: * = 0.0319; ***= <0.002, **** = < 0.0001. Distribution of data is shown mirrored as a bell shape at each concentration. The median is shown by a darker dashed line and quartiles are represented by lighter dashed lines.*

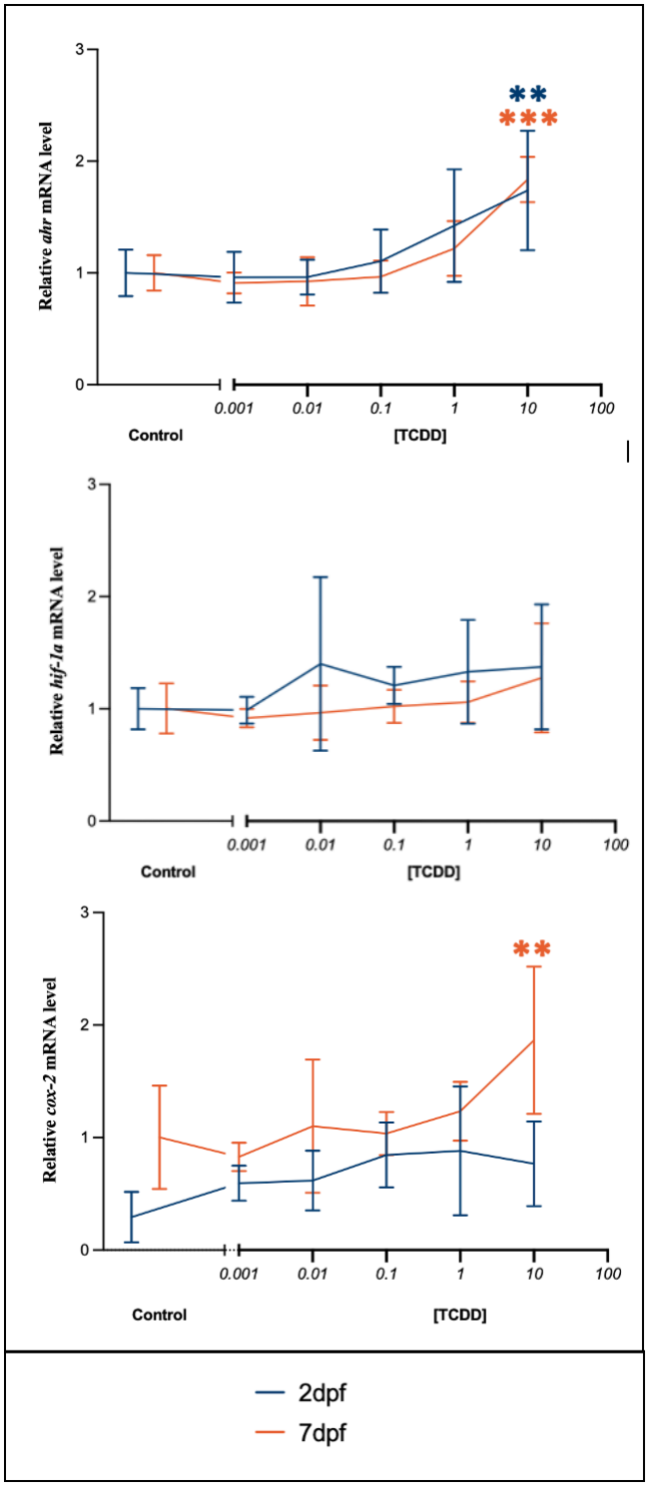
Relative ahr mRNA level
3
2
1
0
**
***
0.001
0.01
0.1
1
10
100
Control
[TCDD]
Relative hif-1a mRNA level
3
2
1
0
0.001
0.01
0.1
1
10
100
Control
[TCDD]
Relative cox-2 mRNA level
3
2
1
0
**
0.001
0.01
0.1
1
10
100
Control
[TCDD]
2dpf
7dpf

*Figure 3.6: Relative ahr, hif-1α, cox-2mRNA level normalized with rpl7 gene. (ahr = [** 2 dpf p-value = 0.1738 and *** 7 dpf p-value = <0.0001]; cox-2 = [** 7 dpf stage p-value = 0.002])*

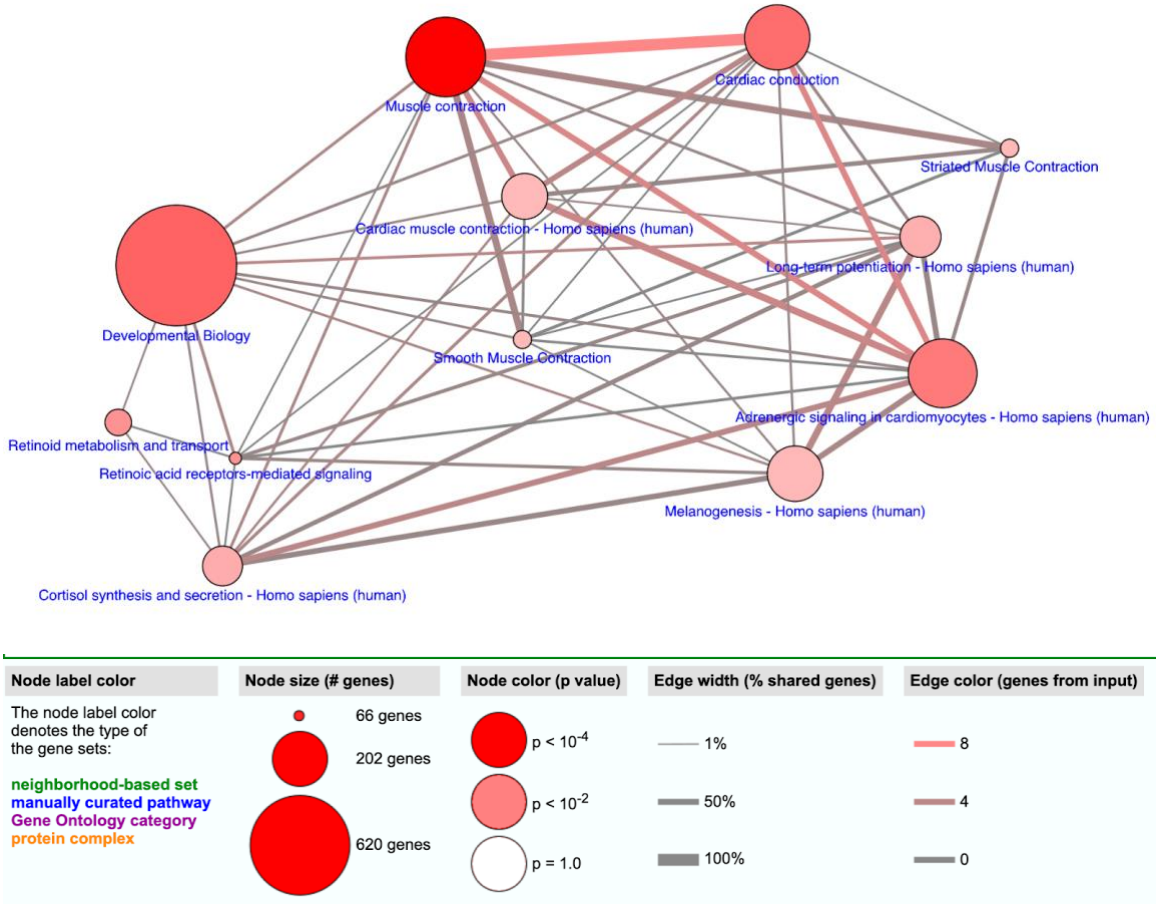

Figure 3.7: Over-representation pathway analysis (p <0.01) (Herwig et al., 2016; Kamburov et al., 2011) performed on orthologous human gene symbols of all proteins detected in the control 2 dpf Japanese Ricefish (Oryzias latipes) embryos.

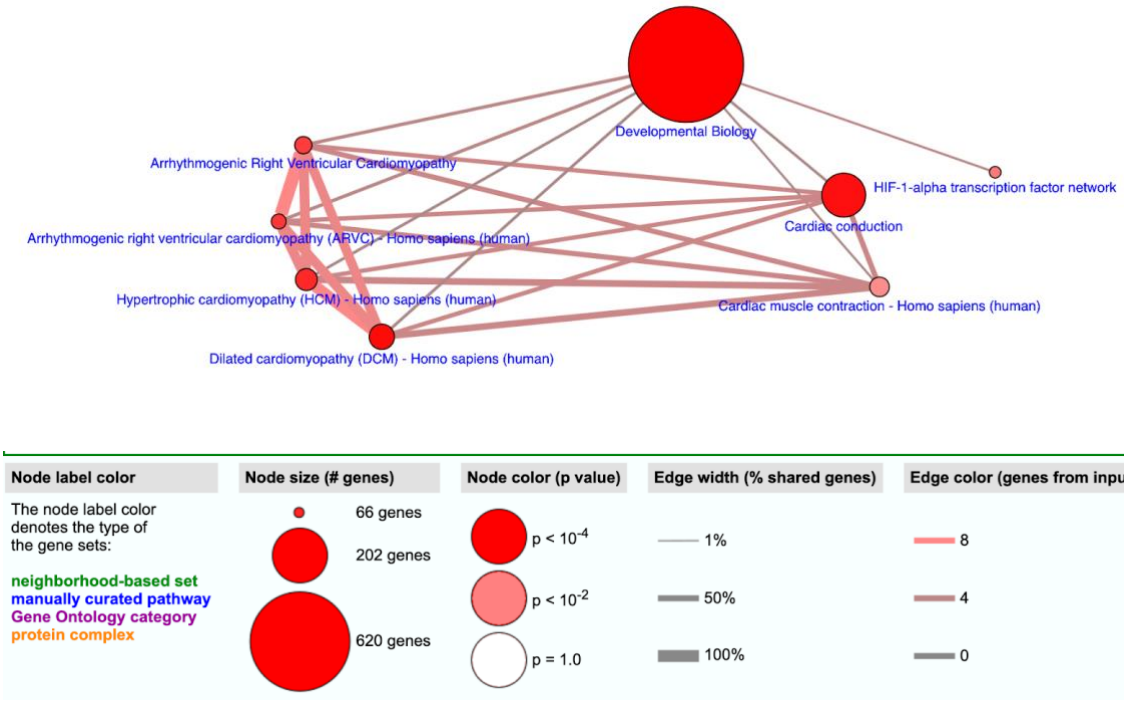

Figure 3.8: Over-representation pathway analysis (p <0.01) (Herwig et al., 2016; Kamburov et al., 2011) performed on orthologous human gene symbols of all proteins detected in the 2 dpf Japanese Ricefish (Oryzias latipes) embryos exposed to 10 ppb TCDD for 1 hour at the 4hpf.

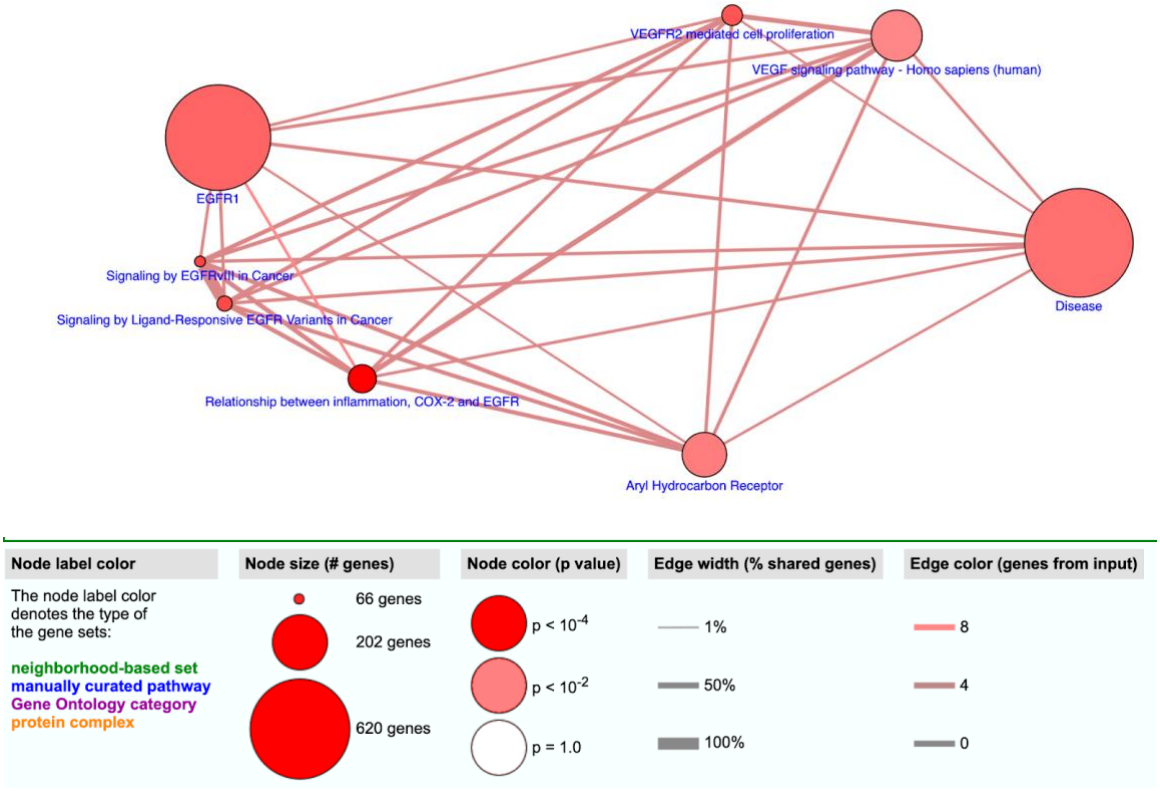

Figure 3.9: Over-representation pathway analysis ($p < 0.01$) (Herwig et al., 2016; Kamburov et al., 2011) of orthologous human gene symbols of all proteins significantly decreased in abundance found in the 10ppb group relative to control, also found in Table 3.8.

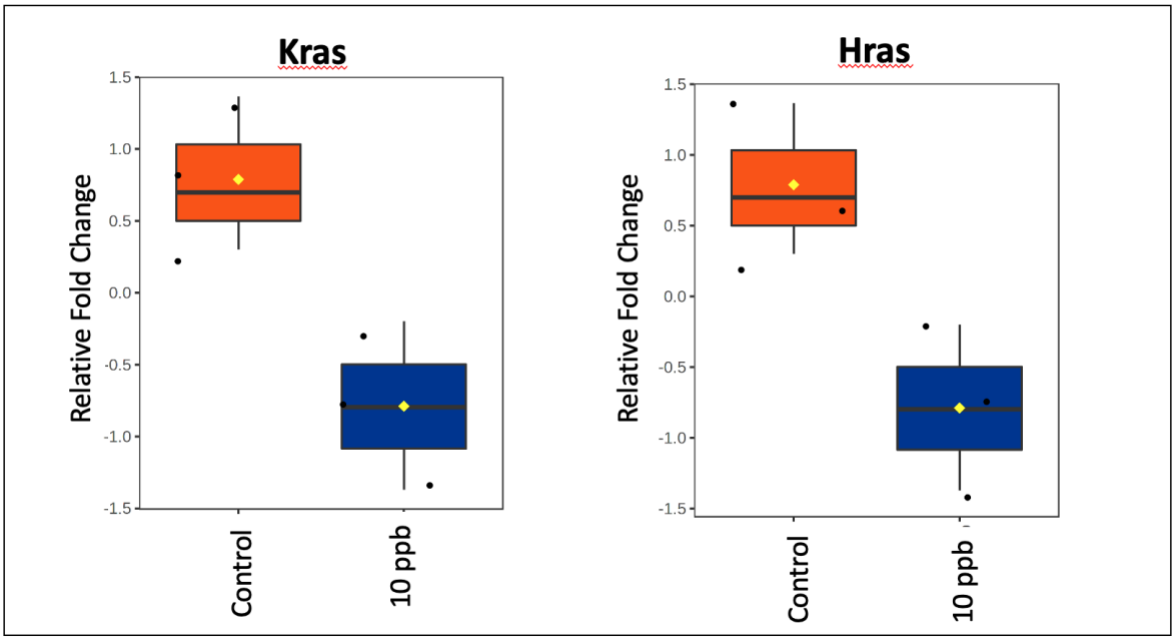

Figure 3.10: Boxplot of Kras and Hras normalized protein abundance generated by Metaboanalyst (Pang et al., 2021). The black dots indicate the three replicates, the line indicates the median and the yellow dot represents the mean. Both proteins decreased in abundance in the 10ppb compared to control (volcano plot, p-value <0.05, FDR-corrected <0.2). These genes are found in multiple pathways as detected by over-representation pathway analysis (p<0.01) such as VEGFR2 mediated cell proliferation, Signaling by EGFRvIII in Cancer, Constitutive Signaling by Ligand-Responsive EGFR Cancer Variants, Signaling by Ligand-Responsive EGFR Variants in Cancer, and Signaling by EGFR in Cancer pathways in Reactome; and also VEGF signaling pathway - Homo sapiens (human) pathway in KEGG (also seen in Figure 3.9).

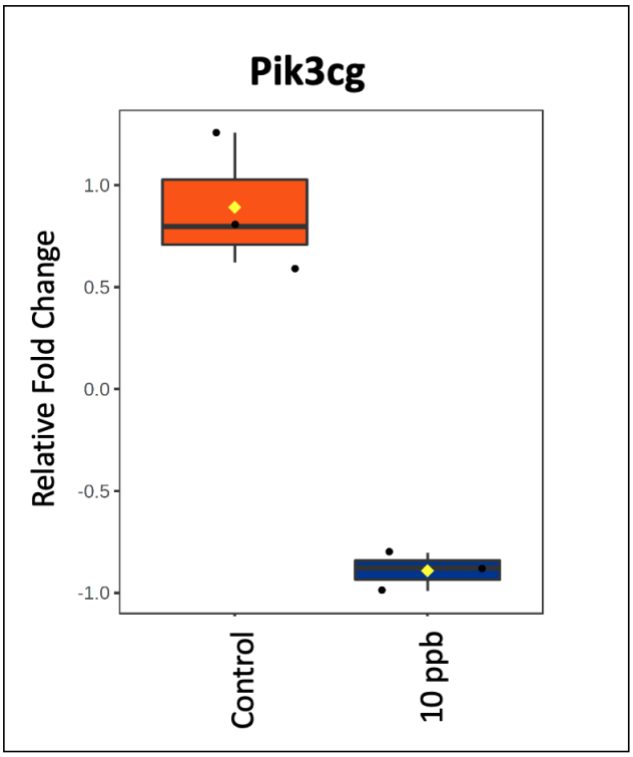

Figure 3.11: Boxplot of Pik3cg normalized protein abundance generated by Metaboanalyst (Pang et al., 2021) which decreased in abundance in the 10ppb compared to control (volcano plot, p-value <0.05, FDR-corrected <0.2). The black dots indicate the three replicates, the line indicates the median and the yellow dot represents the mean. This gene, along with Hras and Kras are found to be overlapping in the Relationship between inflammation, COX-2 and EGFR pathway found in Wikipathways upon over-representation pathway analysis (p<0.01)(Pang et al., 2021)(also seen in Figure 3.9).

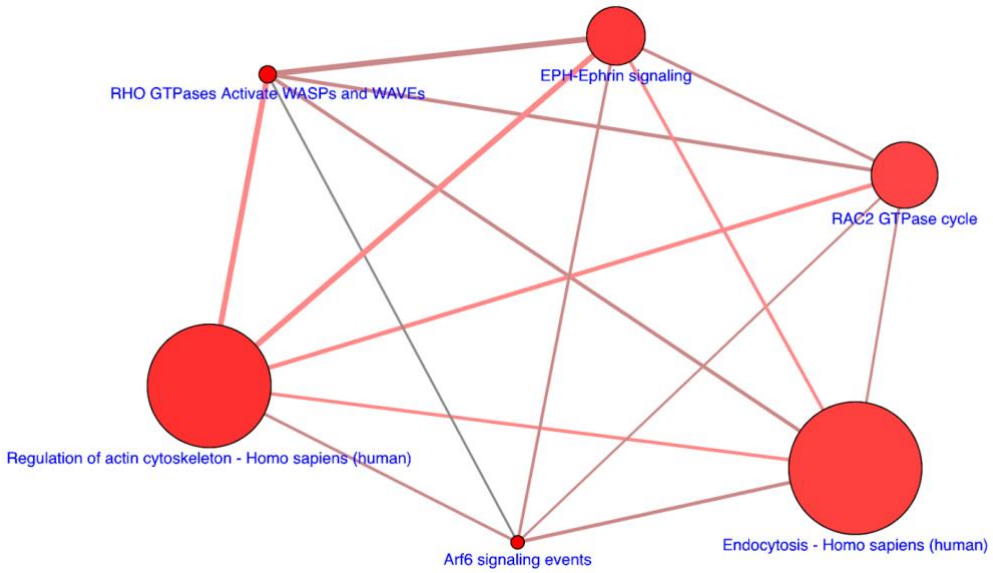

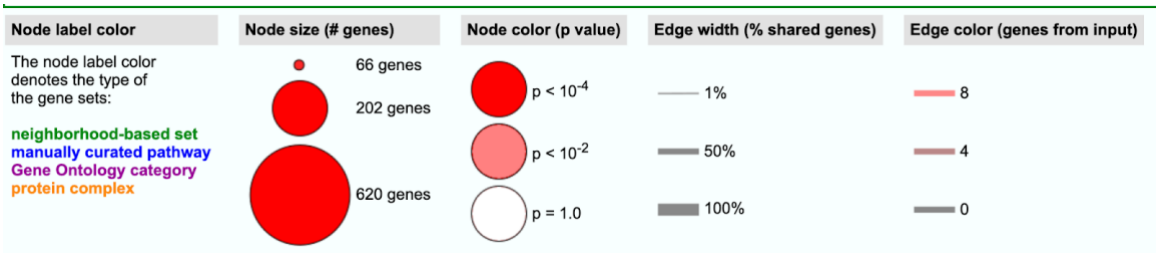

Figure 3.12: Over-representation pathway analysis ($p < 0.01$) (Herwig et al., 2016; Kamburov et al., 2011) of orthologous human gene symbols of all proteins significantly increased in abundance found in the 10ppb group relative to control, also found in Table 3.9.

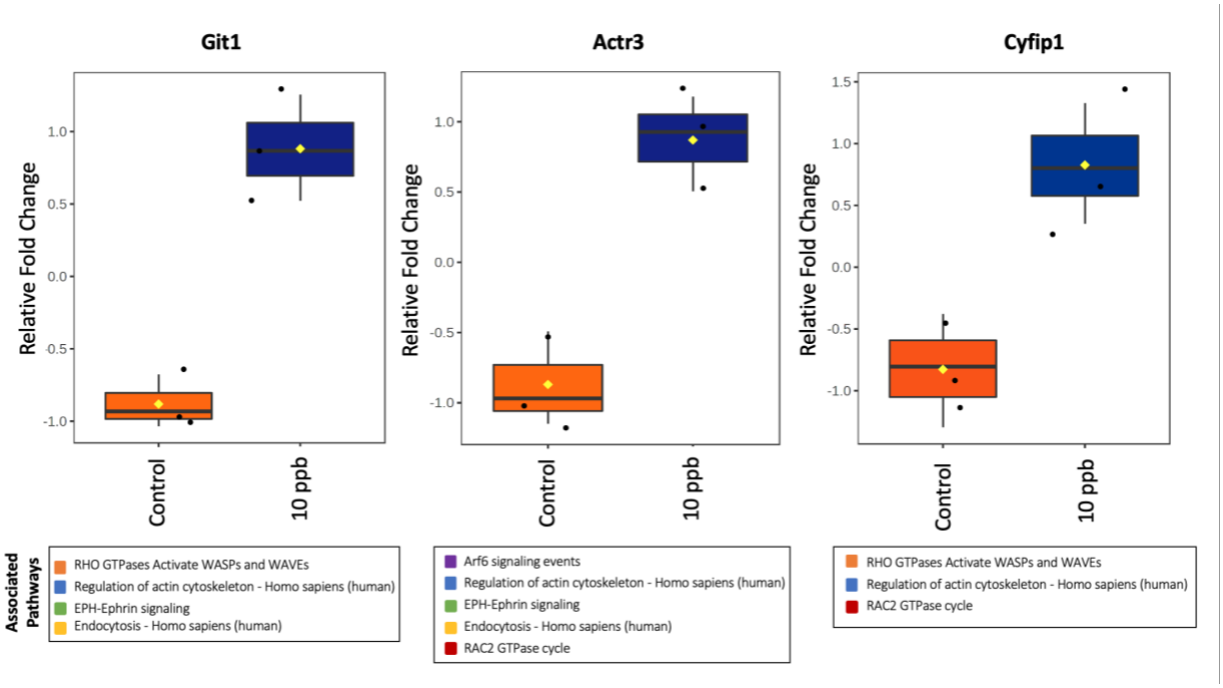

Figure 3.13: Boxplot of Git1, Actr3, and Cyfip1 normalized protein abundance generated by Metaboanalyst (Pang et al., 2021). The black dots indicate the three replicates, the line indicates the median and the yellow dot represents the mean. All proteins increased in abundance in the 10ppb compared to control (volcano plot, p-value <0.05, FDR-corrected <0.2). The orthologous human gene symbols of these proteins are found in multiple pathways as detected by over-representation pathway analysis (p<0.01) (Herwig et al., 2016; Kamburov et al., 2011) which are listed in the legend below each boxplot.

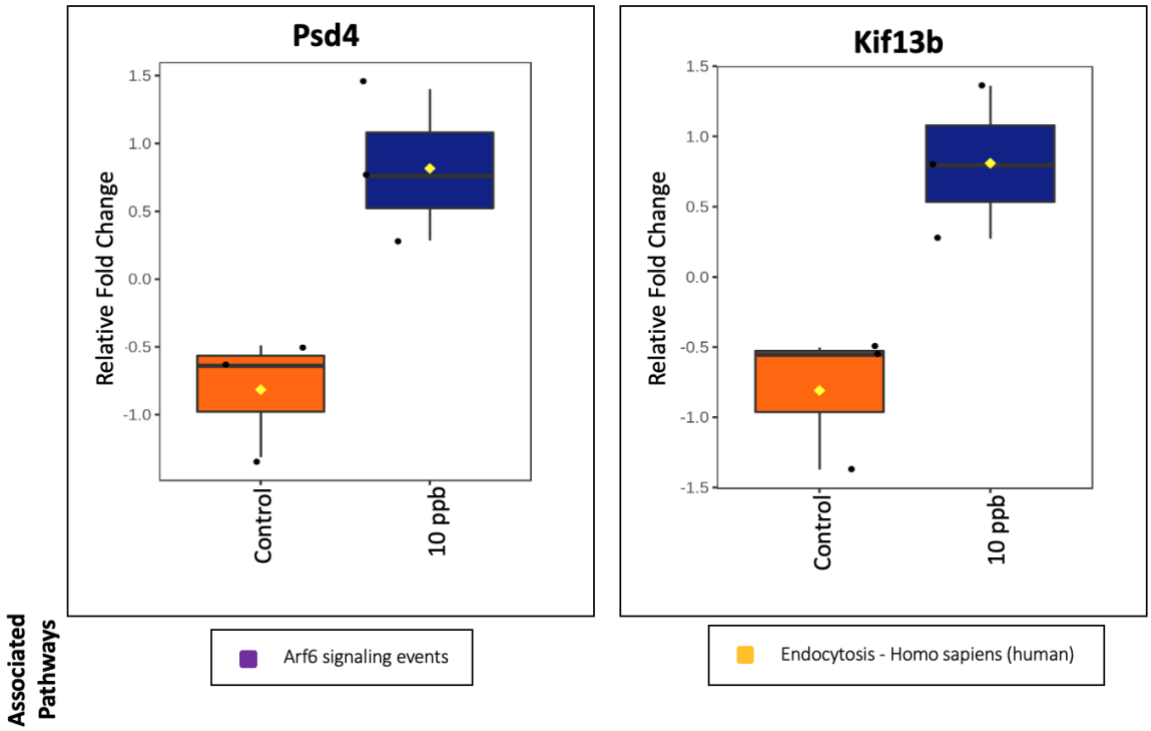

Figure 3.14: Boxplots of Psd4 and Kif13b normalized protein abundance generated by Metaboanalyst (Pang et al., 2021). The black dots indicate the three replicates, the line indicates the median and the yellow dot represents the mean. Both proteins had increased in abundance in the 10ppb compared to control (volcano plot, p-value <0.05, FDR-corrected <0.2). After over-representation pathway analysis (p<0.01) (Herwig et al., 2016; Kamburov et al., 2011), each was associated with the pathway indicated in the legend below each boxplot with the additional proteins associated with those pathways noted in Figure 3.13.

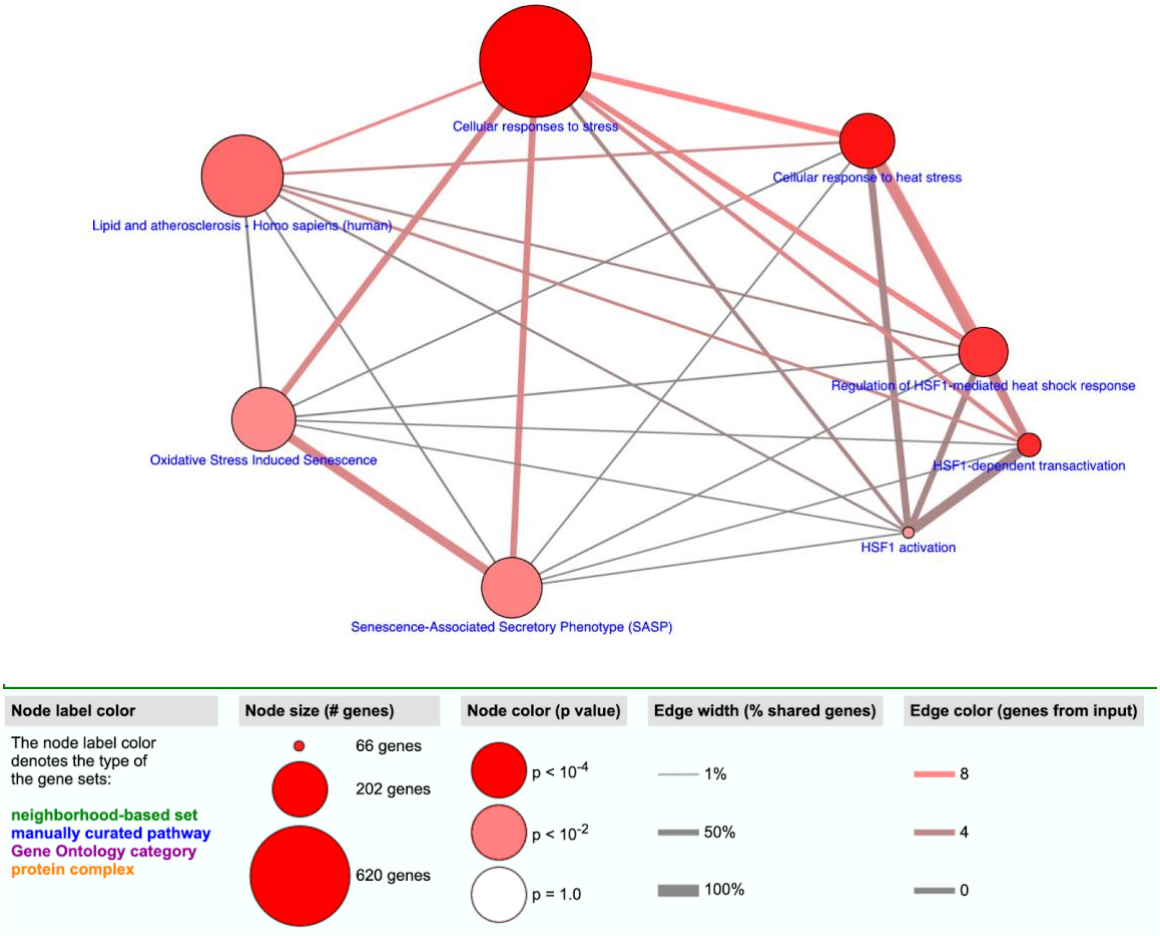

Figure 3.15: Over-representation pathway analysis ($p < 0.01$) (Herwig et al., 2016; Kamburov et al., 2011) of orthologous human gene symbols of all proteins detected in the 7 dpf samples revealed that many proteins were associated with cellular responses to stress.

Chapter 4. Discussion

Vasculogenesis, angiogenesis, and cardiogenesis are important processes which an embryo uses to form its cardiovascular system by developing new blood vessels, blood vessels from existing blood vessels and the heart itself, respectively (Drake, 2003). This study was designed to alter cardiovascular development in Japanese Ricefish *(Oryzias latipes)* embryos to understand the molecular differences that occur during development displaying this phenotype. The study design took advantage of a large body of existing knowledge found regarding altered cardiovascular development caused by chemicals in embryos (from AOPs 21 and 150) by analyzing each step of the predicted mechanism of effect (Bolt, 2017).

In comparison to a previous study (W. Dong et al., 2010), with similar exposure parameters of a 1-hour exposure of TCDD at the 4hpf stage with Japanese Ricefish *(Oryzias latipes)* embryos, molecular differences from control were not detected in lower concentrations of TCDD. In that study, a significant increase in pericardial edema and *cox-2* expression was observed at lower concentrations as low as 0.2 ppb (W. Dong et al., 2010); however, in the present study, the only concentration sufficient to cause statistically significant differences was the highest concentration of 10 ppb.

Nonetheless, a dose-response was observed across all qualitative observations under the microscope following the expected outcome of decreased heartbeat, delayed hatching, and increased pericardial edema (relative to control) which were indicative of altered cardiovascular development leading to mortality caused by TCDD (Hanno et al., 2010;

Kim & Cooper, 1999; Wisk & Cooper, 1990). On the molecular level, activation of the *ahr* is indicative of activation of both of the AOPs (J. H. Doering, Markus; Villeneuve, Dan; Zhang, Xiaowei, 2019; Farhat & Kennedy, 2019) which was observed at both stages analyzed, 2 dpf and 7 dpf. The findings of Ahr activation (MIE) and altered cardiovascular development (AO) make both the AOPs "strong" (Bolt, 2017; J. H. Doering, Markus; Villeneuve, Dan; Zhang, Xiaowei, 2019; Farhat & Kennedy, 2019), as per the AOP framework, with subsequent key events that require further refining.

On a molecular level, at 2 dpf, many genes detected (in the control samples) were associated with developmental biology, and in particular, pathways associated with the onset of the heartbeat (Iwamatsu, 2011) which is indicative of the cardiovascular development specifically occurring at that stage. Additionally, 2 dpf is immediately after the stage where melanophores appear and optic lenses are complete in development (Iwamatsu, 2011), likely explaining the proteins involved in melanogenesis and retinoic acid signalling, which plays a critical role in eye development (Iwamatsu, 2011). Additionally, in 2 dpf 10ppb samples, genes associated with several forms of cardiomyopathy were detected, specifically dilated, hypertrophic, and arrhythmogenic right ventricular cardiomyopathy. Cardiomyopathy is a disease of the heart muscle causing it to become enlarged, thick or rigid, making contractility very difficult (Wexler, Elton, Pleister, & Feldman, 2009)and these pathways indicate altered cardiovascular development based on previous studies of cardiomyopathy in mice and chicken used to develop the two AOPs (Carmeliet et al., 1999; Walker & Catron, 2000).

However, In the 7 dpf samples, only a small subset of proteins were identified, and they were generally associated with stress at all doses. It has been previously suggested that detection of proteins may be affected by extrinsic noise that is caused by unobserved variation between cells during "omics" approaches (Eling, Morgan, & Marioni, 2019). This noise may be causing the over representation of stress proteins preventing detection of other key protein abundances. It can also be difficult to differentiate specific processes occurring in a whole organism as a multitude of processes are occurring simultaneously in various organs and systems during development (Nikinmaa & Anttila, 2019). Noise can result due to having all these various systems behaving differently from control in a single sample, making the detection of specific pathways more difficult. To overcome this noise in the future, single cell techniques (Eling et al., 2019) may be better suited to differentiate the molecular changes occurring at later embryonic stages where more complex processes are occurring individually in each organism. Variability between individuals can be captured with these techniques improving accuracy of pathway detection.

To assess the differences between key events found in the two AOPs in-depth, gene expression of two genes was looked into in detail. Specifically, a change in *hif-1α* was not observed as suggested in AOP 150 at either of the stages and *cox-2* was increased relative to the control, but only in the later 7 dpf stage as suggested by AOP 21. These observations indicate AOP 21 appears to be followed when TCDD causes altered cardiovascular development.

However, an additional gene of importance to these two AOPs is Vegf, whose associated signalling genes were observed to be decreased in abundance in the 2 dpf samples relative to control. This observation follows that of AOP 150; however, the absence of *hif-1α* expression change from control implies that the change in Vegf signalling is independent of the Arnt/Hif-1α signalling pathways. Instead, the relationship between inflammation, Cox-2, and Egfr could directly affect Vegf signalling, as the Egfr and Vegf pathways are known to be interrelated (Lichtenberger et al., 2010; Tabernero, 2007). This finding may indicate that the two AOPs cannot be considered separately, as initially proposed. Also, it may indicate Egfr plays a more significant role in angiogenesis, and thus, could be more influential in AOP 21 and 150 than Vegf. Regulating and controlling the temporal expression of Cox-2 may be key to preventing the adverse outcome of altered cardiovascular development from occurring.

As the relationship between Cox-2 and Egfr was over-represented in the list of proteins significantly decreased in abundance from the control in the 10 ppb treatment group in this study, each gene and related pathways were investigated further by literature review. Previous studies in humans have shown that increased COX-2 expression leads to increased EGFR signalling which is further enhanced by a positive feedback loop that increases the expression of both genes (Le et al., 2021; Lichtenberger et al., 2010; Tabernero, 2007). COX-2 is an enzyme that is responsible for the production of prostaglandin-E2 (PGE-2) at sites of inflammation (Lo, Cao, Zhu, & Ali-Osman, 2010). Significant evidence has shown that the PGE2 derived from COX-2 can activate EGFR signalling which stimulates cell proliferation (Lo et al., 2010). Of additional interest, PGE2 can also bind to the receptor of

c-Src which is a protein functionally attached to and regulated by the Ahr. This may suggest that the Ahr may also play a key role in dysregulating more than one pathway associated with angiogenesis when activated by a chemical. In this study, EGFR signalling was decreased in abundance relative to control in the 10ppb and *cox-2* expression levels were not significantly different from control at any of the doses or stages, except specifically the 7 dpf 10 ppb treatment group. Previous studies have found increased expression levels of *cox-2 in* Japanese Ricefish *(Oryzias latipes)* embryos exposed to concentrations 0.2, 0.5, and 1 ppb TCDD for 1 hour at the 4hpf in embryos 6 days post exposure (W. Dong et al., 2010) which was different from the results found in this study where cox-2 was only significantly increased in the highest concentration, 10 ppb (in later stage tested, 7 dpf).

EGFR signalling was decreased in abundance relative to control in the 10ppb and so we will discuss its effects on angiogenesis further. EGFR is a transmembrane receptor that controls a multitude of proteins and pathways associated with cell migration, adhesion, and proliferation (Le et al., 2021). As well, EGFR is known to be overexpressed in a wide variety of malignancies (Le et al., 2021). In this study, the decrease in Egfr signalling may indicate the significance of temporal effects caused by Cox-2 as it controls angiogenesis through various genes. Cox-2 may directly regulate Egfr signalling, which would further affect Vegf signalling. These ideas are novel to those found in AOP 21 and 150 as this would propose interdependence of the two pathways on one another, in an independent manner from the ARNT/HIF-1α dimerization as suggested by AOP 150. Additionally, the importance of controlling the temporal effect of Cox-2 is highlighted, as it likely increases in abundance until 7 dpf, which our study design was not able to capture. This stage-

specific difference in expression levels also suggests that a regulatory switch may occur between 2 dpf and 7 dpf, where Cox-2 expression levels rise as a result of the chemical exposure, and thus, changes in development occur. Ultimately, the effects of altered cardiovascular development are caused by the varying expression levels of Cox-2. Our data suggests that varying Cox-2 expression levels are likely caused by varied regulation of EGFR through c-Src controlled by Ahr.

Downstream, EGFR is predicted to drive VEGF expression as EGFR mutant cell lines have shown up-regulation of the HIF-1α in a hypoxia-independent manner (Le et al., 2021). As well, when the EGFR pathway is inhibited, VEGF is downregulated (Le et al., 2021). This may be the case in this study where, at 2 dpf, in the 10ppb treatment group, proteins significantly decreased in abundance from control are associated with both EGFR and VEGF signalling. This would also explain why the effect on VEGF signaling is independent of the HIF-1α signalling pathway. Additionally, EGFR and VEGF have been specifically studied together for their synergistic effect on angiogenesis during tumour development. These two genes have been targeted for many therapeutic purposes and studies show that no tumours develop in the absence of EGFR and VEGF (Lichtenberger et al., 2010). Dual inhibition of both of these genes has shown to be a successful method in promoting anti-tumour activity (Lichtenberger et al., 2010). As well, inhibition of COX-2 has been shown to lead to decreased angiogenesis in a manner that is dependent on VEGF (Hu et al., 2017). In lieu, knockdown of *cox-2* in zebrafish by morpholino antisense oligonucleotides has shown to recover TCDD induced damage to mesencephalic circulation (Teraoka, Kubota, Kawai, & Hiraga, 2008). Thus, this finding again may

indicate that the decrease in Egfr, caused by Cox-2, and Vegf signalling at 2 dpf may be associated with the embryo's early coping mechanism to protect from damage caused by TCDD. This further implies a temporal molecular threshold that is reached which worsens the effects caused by TCDD especially on the cardiovascular system causing it to alter.

Another pathway affected at 2 dpf is Arf6 signalling whose proteins are increased in abundance relative to control significantly in the 10 ppb TCDD group. This agrees with the previous notion that increased Arf6 signalling blocks downstream Vegf processes necessary for angiogenesis (Ikeda et al., 2005). Furthermore, overexpression of ARF6 is known to be associated with an increase in capillary density in a mouse hindlimb ischemia model of angiogenesis (Hongu et al., 2016). As well, Arf6 plays a crucial role in tumour angiogenesis and is a therapeutic target for anti-cancer drugs (Hongu et al., 2016). It is possible that downregulation of Vegf signalling seen at 2 dpf is caused by multiple pathways conjunctively causing the decrease, such as Cox-2 affecting Egfr signalling, in addition to Arf6 signalling.

Tumour angiogenesis and embryonic angiogenesis involve similar but distinct proteins and pathways. The distinct proteins from normal angiogenesis allow for separation of the two processes as they could be occurring in conjunction during embryonic development after a short chemical exposure during early stages of development such as in this study. Rac2, for example, provides this differentiation as its expression is increased only in adaptive angiogenic responses involving wound healing or tumorigenesis and not during normal embryonic angiogenesis (Joshi et al., 2014). Additionally, it has been found that a homozygous knockout of RAC2 in mice does not display any defects in organ development

(Joshi et al., 2014). Increased Rac2 activation at 2 dpf, in this study, indicates the embryo's early responses to the acute chemical exposure that is distinct from normal development. This further reinforces the concept that additional proteins and pathways are involved in the altered cardiovascular development phenotype not captured by AOP 21 or 150.

RHO GTPases are a family of proteins that regulate various processes in the cell including growth, differentiation, apoptosis, cell cycle, gene transcription, cell migration and the actin cytoskeleton (El Baba et al., 2020). CDC42 and RAC1, are two such RHO GTPases, that promote cell motility by stimulating actin polymerization and cause changes in the membrane's shape by extending the cytoplasm in the direction of movement (El Baba et al., 2020). CDC42 and RAC1 cause these changes through their respective downstream effectors WAVE and WASP (Bryan & D'Amore, 2007; El Baba et al., 2020). Increased RHO signalling has been traditionally associated with cancer (Cardama, Gonzalez, Maggio, Menna, & Gomez, 2017) and, in this study, this pathway was found to be over-represented in the subset of genes significantly increased in abundance relative to control in the 10ppb treatment group.

Additionally, another pathway significantly increased in the 10ppb group from control in this study was EPH-Ephrin signalling. The large families of Eph receptor tyrosine kinases and their ephrin ligands transduce signals in a cell-to-cell contact-dependent fashion coordinating growth, differentiation, and patterning of almost every tissue (Coulthard et al., 2012). Eph–ephrin interactions can trigger a wide array of cellular responses, including cell adhesion, boundary formation, and repulsion. The exact mechanism of these interactions remains unclear but seem to be involved in differential signaling, proteolytic

cleavage of ephrins, and endocytosis of the ligand–receptor complex (Coulthard et al., 2012).

Generally, both RHO and EPH-Ephrin signalling pathways are associated with a synergistic increase in VEGF signaling which is unlike what was observed in this study. In previous studies, VEGF has been found to upregulate EphrinB2 with an association of down-regulation of EphB4 (Du, Li, He, Li, & He, 2020). Additionally, EphB4 and EphrinB2 expression levels are greater in haemorrhagic than non-hemorrhagic samples of brain arteriovenous malformation (BAVM), which is an intracranial high-flow vascular malformation (Du et al., 2020). Meanwhile, although RHO GTPases are considered essential downstream effectors of VEGF signaling in the angiogenic process (El Baba et al., 2020), knocking down of RhoC and RhoA in astrocytoma cells has shown to decrease the expression levels of VEGF by approximately 25% and 40%, respectively (El Baba et al., 2020) highlighting the dependence of VEGF expression on both RhoA and RhoC expression levels. In this study however, a decrease in VEGF signaling is observed at the same stage, 2 dpf, as an increase in both RHO and EPH-Ephrin signalling pathways. This may indicate involvement of other molecular mechanisms not yet explored regarding activation of RHO and EPH-Ephrin signalling independently of VEGF signaling during angiogenesis.

Conclusion

There are several molecular changes that occur after a chemical exposure in an organism. Multiple proteins follow pathways that work in conjunction and divergence of one another and understanding these routes will aid in the protection of the environment and human health. AOPs form a framework that captures the effect of a chemical from the molecular through to the ecosystem level. In this way, refining the molecular changes that occur in the organismal level will aid in protection of ecosystems. Additionally, AOPs capture events that occur in time and can be prevented from causing the ultimate adverse outcome, usually population decline. An AOP can be stopped by targeting it earlier in the pathway as such by genetic silencing techniques that inhibit key events, thus preventing the adverse outcome from occurring. This may be key to protecting a species at risk which may be temporally affected during a crucial embryonic stage by a chemical exposure in the natural environment. Refining the AOPs found in the framework allows for future formations of guidelines not only regarding the safe amount of contaminant, but also policies surrounding when contaminant release would be allowed temporally to protect species at sensitive embryonic stages (i.e., protecting fish during spawning season). In this research, two AOPs (21 and 150) were investigated with the goal of refinement. The findings of this study suggest that AOP 21 and not AOP 150 leads to the adverse outcome of altered cardiovascular development, but also that the two pathways may be more connected by downstream key events. This study encourages additional research to specifically refine AOPs which will strengthen the AOP framework; ultimately benefiting society by improving our ability to respond to chemical contaminants more effectively to prevent adverse outcomes in humans and their environment.

Appendices

Appendix A. *Japanese Medaka Embryo Rearing Solution*

Materials
Five 1L glass bottles
Milli-Q (MQ) water
NaCI, MgS04, CaCb, KCI, Methylene Blue
Graduated Cylinder
Disposable Plastic Weighing Boats
Balance

Method

1. Make the following stock solutions and store them in the refrigerator in a labelled bottle or flask:
    - 10% NaCl solution (10 g NaCl in 100 mL H2O)
    - 0.30% KCl solution (0.30 g KCl in 100 mL H2O)
    - 0.40% CaCl2•2H2O solution (0.40 g CaCl2•2H2O in 100 mL H2O)
    - 1.63% MgSO4•7H2O solution (1.63 g MgSO4•7H2O in 100 mL H2O)
    - 0.01% Methylene blue solution (0.01 g Methylene blue in 100 mL H2O)

2. 1 mL of each stock solution is added (total volume of 5 mL) to which 95 ml of Milli-Q water is added for a final volume of 100 mL.

3. Rearing solution is normally made up 10 to 20 liters at a time and kept aerated in the 25 degree climate controlled rearing room for immediate use.

4. The rearing solution **must be at 25°C before putting eggs into it**, extreme temperature differences can shock the embryos and alter phenotype or kill them.

Appendix B. *Proteomics Reagents*

Ammonium bicarbonate buffer (AB) working solution

200mM Ammonium bicarbonate buffer (AB) working solution was prepared by diluting 7.91 g of ammonium bicarbonate in 500 mL of MilliQ water.

400mM Iodoacetamide (IAA) in 200 mM AB

Iodoacetamide (IAA) is a solid (Sigma: I1149-5G) stored at 4ºC. This solution is made fresh and kept in the dark. It can be made in 15 ml polyethylene conical centrifuge tubes and wrapped in aluminum foil to minimize exposure to light. The IAA is removed from 4ºC to equilibrate to room temperature and 73.98 mg is weighed and placed into a 15 mL conical tube. A 1000 uL pipette to add 1 mL AB (200mM) to the IAA. The tube is mixed gently until all the IAA has dissolved. The tube is wrapped in aluminum foil and placed in 4ºC for storage.

100 mM Tris(2-carboxyethyl) phosphine hydrochloride (TECP) in 200 mM AB

100 mM Tris(2-carboxyethyl) phosphine hydrochloride (TECP) in 200 mM AB is prepared by removing Tris (2-carboxyethyl) phosphine hydrochloride (TECP) ampule from 4ºC fridge to equilibrate to room temperature. Breaking the ampule at the score line in an away motion, a glass pasteur pipette is used to transfer the ampule (1 mL) of 0.05M TECP to a newly labelled falcon tube (10 mL). The ampule is rinsed with a small volume (1 mL) of 200 mM AB 3 times and the rinse is transferred to the falcon tube to ensure all the TECP has been transferred. One more mL of 200 mM AB (for a total of 4 mL added including the rinses) to the falcon tube is added so that 5 mL of 100 mM TECP solution is prepared.

20% Formic Acid

A graduated cylinder is used to transfer 40 mL MilliQ water into a 50 mL polyethylene conical centrifuge tube. A 5-10 mL pipette is used to add 10 mL Formic acid to the water. The conical centrifuge tube is capped, vortexed, and kept for storage at 4ºC.

Dilution Buffer

Dilution buffer is prepared 1L at a time in a designated pre-labelled 1L volumetric flask. Approximately 700 mL HPLC grade water (Fisher Scientific; W5-4) is transferred to a volumetric flask. A 50 mL graduated cylinder is used to add 50 mL HPLC optima grade Acetonitrile (Fisher Scientific) to the flask and then a 1000 uL pipette is used to add 1 mL Formic acid (Sigma Aldrich: 06440) to the flask. The volume is brought to 1L with HPLC grade water, the stopper is placed on the flask and the flask is mixed by inversion 10x.

Appendix C. *Proteomics Acquisition Methods*

Devices
Multisampler
Binary Pump
Column Comp.
Q-TOF

Component Name	MS Q-TOF		
Component Model	G6545A		
Ion Source	Dual AJS ESI	**Stop Time (min)**	No Limit/As Pump
Can wait for temp.	Enable	**Fast Polarity**	FALSE
MS Abs. threshold	500	**MS Rel. threshold(%)**	0.01
MS/MS Abs. threshold	5	**MS/MS Rel. threshold(%)**	0.01

Time Segment #	Start Time (min)	Diverter Valve State	Storage Mode	Ion Mode
1	0	MS	Both	Dual AJS ESI

Acquisition Mode AutoMS2	
MS Min Range (m/z)	300
MS Max Range (m/z)	1700
MS Scan Rate (spectra/sec)	3.00
MS/MS Min Range (m/z)	50
MS/MS Max Range (m/z)	1700
MS/MS Scan Rate (spectra/sec)	2.00
Isolation Width MS/MS	Medium (~4 amu)
Decision Engine	Adv

Ramped Collision Energy		
Charge	**Slope**	**Offset**
All	4	2

Auto MS/MS Preferred/Exclude Table					
Mass	**Delta Mass (ppm)**	**Charge**	**Type**	**Retention Time (min)**	**Isolation Width**
921.9686	100	1	Exclude	0	Narrow (~1.3 amu)

Precursor Selection	
Max Precursors Per Cycle	10
Threshold (Abs)	500
Threshold (Rel)(%)	0.010
Precursor abundance based scan speed	Yes
Target (counts/spectrum)	25000.000
Use MS/MS accumulation time limit	Yes
Use dynamic precursor rejection	No
Purity Stringency (%)	100.000
Purity Cutoff (%)	30.000
Isotope Model	Peptides
Active exclusion enabled	Yes
Active exclusion excluded after (spectra)	2
Active exclusion released after (min)	0.20
Sort precursors	By abundance only

Static Exclusion Ranges	
StartMZ	**EndMZ**
25	300

Charge State Preference
2
3
>3

Instrument Parameters	
	Parameter
Gas Temp (°C)	325
Gas Flow (l/min)	8
Nebulizer (psig)	35
SheathGasTemp	350
SheathGasFlow	11

Scan Seg #	Ion Polarity
1	Positive

Scan Source Parameters	
	Parameter
VCap	4500
Nozzle Voltage (V)	1000
Fragmentor	180
Skimmer1	65
OctopoleRFPeak	750

Reference Masses	
Ref Mass Enabled	Disabled

Chromatograms			
Chrom Type	**Label**	**Offset**	**Y-Range**
TIC	TIC	15	10000000
TIC	TIC	15	10000000

Name: Multisampler	**Module:** G7167A
Sampling Speed	
Draw Speed	100.0 µL/min
Eject Speed	400.0 µL/min
Wait Time After Drawing	1.2 s
Injection	
Needle Wash Mode	Standard Wash
Injection Volume	2.00 µL
Standard Needle Wash	
Needle Wash Mode	Flush Port
Duration	10 s
High Throughput	
Injection Valve to Bypass for Delay Volume Reduction	No
Sample Flush-Out Factor	5.0
Overlapped Injection	
Overlap Injection Enabled	No
Needle Height Position	
Draw Position Offset	-1.0 mm
Use Vial/Well Bottom Sensing	No
Stop Time	
Stoptime Mode	No Limit
Post Time	
Posttime Mode	Off

Scan Source Parameters	
	Parameter
VCap	4500
Nozzle Voltage (V)	1000
Fragmentor	180
Skimmer1	65
OctopoleRFPeak	750

Reference Masses	
Ref Mass Enabled	Disabled

Chromatograms			
Chrom Type	**Label**	**Offset**	**Y-Range**
TIC	TIC	15	10000000
TIC	TIC	15	10000000

Name: Multisampler	**Module:** G7167A
Sampling Speed	
Draw Speed	100.0 µL/min
Eject Speed	400.0 µL/min
Wait Time After Drawing	1.2 s
Injection	
Needle Wash Mode	Standard Wash
Injection Volume	2.00 µL
Standard Needle Wash	
Needle Wash Mode	Flush Port
Duration	10 s
High Throughput	
Injection Valve to Bypass for Delay Volume Reduction	No
Sample Flush-Out Factor	5.0
Overlapped Injection	
Overlap Injection Enabled	No
Needle Height Position	
Draw Position Offset	-1.0 mm
Use Vial/Well Bottom Sensing	No
Stop Time	
Stoptime Mode	No Limit
Post Time	
Posttime Mode	Off

Name: Binary Pump	Module: G7112B
Flow	0.100 mL/min
Use Solvent Types	Yes
Low Pressure Limit	0.00 bar
High Pressure Limit	400.00 bar
Maximum Flow Gradient	100.000 mL/min²
Stroke A	
Automatic Stroke Calculation A	Yes
Stroke B	
Automatic Stroke Calculation B	Yes
Stop Time	
Stoptime Mode	Time set
Stoptime	50.00 min
Post Time	
Posttime Mode	Off

Solvent Composition

	Channel	Solvent 1	Solvent 2	Selected	Used	Percent (%)
1	A	H20	IPA	Ch. 1	Yes	98.0 %
2	B	premixed ACN(95%) - H2O(5%)	IPA	Ch. 1	Yes	2.0 %

Timetable

	Time (min)	A (%)	B (%)	Flow (mL/min)	Pressure (bar)
1	0.00 min	98.0 %	2.0 %	0.100 mL/min	400.00 bar
2	2.00 min	98.0 %	2.0 %	0.100 mL/min	400.00 bar
3	27.00 min	60.0 %	40.0 %	0.100 mL/min	400.00 bar
4	32.00 min	40.0 %	60.0 %	0.100 mL/min	400.00 bar
5	32.01 min	15.0 %	85.0 %	0.100 mL/min	400.00 bar
6	37.00 min	15.0 %	85.0 %	0.100 mL/min	400.00 bar
7	37.01 min	98.0 %	2.0 %	0.100 mL/min	400.00 bar

Name: Binary Pump	Module: G7112B
Flow	0.100 mL/min
Use Solvent Types	Yes
Low Pressure Limit	0.00 bar
High Pressure Limit	400.00 bar
Maximum Flow Gradient	100.000 mL/min²
Stroke A	
Automatic Stroke Calculation A	Yes
Stroke B	
Automatic Stroke Calculation B	Yes
Stop Time	
Stoptime Mode	Time set
Stoptime	50.00 min
Post Time	
Posttime Mode	Off

Solvent Composition

	Channel	Solvent 1	Solvent 2	Selected	Used	Percent (%)
1	A	H20	IPA	Ch. 1	Yes	98.0 %
2	B	premixed ACN(95%) - H2O(5%)	IPA	Ch. 1	Yes	2.0 %

Timetable

	Time (min)	A (%)	B (%)	Flow (mL/min)	Pressure (bar)
1	0.00 min	98.0 %	2.0 %	0.100 mL/min	400.00 bar
2	2.00 min	98.0 %	2.0 %	0.100 mL/min	400.00 bar
3	27.00 min	60.0 %	40.0 %	0.100 mL/min	400.00 bar
4	32.00 min	40.0 %	60.0 %	0.100 mL/min	400.00 bar
5	32.01 min	15.0 %	85.0 %	0.100 mL/min	400.00 bar
6	37.00 min	15.0 %	85.0 %	0.100 mL/min	400.00 bar
7	37.01 min	98.0 %	2.0 %	0.100 mL/min	400.00 bar

Name: Column Comp.	Module: G7116A
Left Temperature Control	
Temperature Control Mode	Temperature Set
Temperature	40.0 °C
Enable Analysis Left Temperature	
Enable Analysis Left Temperature On	Yes
Enable Analysis Left Temperature Value	1.0 °C
Left Temp. Equilibration Time	0.0 min
Right Temperature Control	
Right temperature Control Mode	Temperature Set
Right temperature	40.0 °C
Enable Analysis Right Temperature	
Enable Analysis Right Temperature On	Yes
Enable Analysis Right Temperature Value	0.8 °C
Right Temp. Equilibration Time	0.0 min
Enforce column for run	
Enforce column for run enabled	No
Stop Time	
Stoptime Mode	As pump/injector
Post Time	
Posttime Mode	Off
Timetable	
Valve Position	Position 2 (Port 1 -> 2)
Position Switch After Run	Do not switch

Appendix D. ***All Proteins detected in 2 dpf with Abundances averaged over 3 replicates***

Orthologous Human Gene Symbol	Medaka Accession #	Control	0.001 ppb	0.01 ppb	0.1 ppb	1 ppb	10 ppb
SPEF2	H2LDZ8	247813	282010	93820	110970	168420	254076
HES2	H2LH93	386325	247852	327699	283967	303022	184549
MALT1	H2L3S2	442005	524419	491315	513212	475302	307354
ST3GAL4	H2MIE5	187751	451712	247365	215123	209507	150531
ANKRD16	H2M9B3	298261	290007	96735	92362	181551	240613
FUT8	H2M846	107217	68082	70951	75530	72107	91277
RAD50	H2L8A9	203766	92521	25368	52089	41712	46822
RALGAPA2	H2MSR2	290151	333010	85013	72155	88469	203739
TRAF7	H2MPZ4	287570	280943	411923	609771	241720	267310
UGCG	H2MZF3	282018	360660	198172	193686	225237	394151
RPAP1	H2MKR8	178126	167935	144269	196634	122288	191385
SLC25A25	H2MC50	1141311	1548401	837353	858106	957931	1754061
ABCF3	H2MZQ6	298781	351960	260166	240564	202545	302668
RBMS3	H2LL63	1365633	1155056	680446	403830	795452	701483
UBR2	H2LE01	321990	314810	317859	309796	264448	349817
ZP4	H2M5C0	68000	67495	72322	211939	73210	41268
OTOG	H2MZH3	255386	132404	178065	210405	197257	99049
CNDP2	H2MY27	280326	237865	72278	62868	110362	200828
COL12A1	H2MS91	172861	192358	163790	160264	138592	149097
LNX1	H2L4B6	83109	52478	46499	39107	104300	68082
TPRXL	H2MWU7	767975	978144	799887	784551	676943	898086
DNAJC6	H2M269	221144	189803	86290	35213	75973	152603
GCNT3	H2LTQ1	46503	56798	29101	29061	14126	52557
MCM7	H2L4G5	131381	153752	53933	26583	38628	84381
ATP2B2	H2MYV2	215009	227851	73141	221420	212698	132311
ATP2B1	H2MYU7	430017	455702	146282	442841	425395	264621
GTDC1	H2N0T1	44781	41373	38352	16508	17533	37509
LRRN1	H2MI08	108993	117104	124028	139028	66973	128561
APC2	H2MDC3	301072	345969	215204	292795	207030	309833
POC1A	H2LJ29	61578	61771	54226	28828	58423	53907
CTPS1	H2LW86	185605	249353	221128	221698	168077	280161
MPG	H2LKG3	50436	73187	34858	33437	81525	116948
ANXA1	H2MEL1	171448	72361	96176	36621	26185	38582
RPS6	H2LPD8	627012	467068	294669	197561	104700	324090
DYSF	H2LE95	562052	701902	179871	202074	93929	555577
FMN1	H2MQX7	208980	225945	200236	187040	187305	205749
FMN2	H2LKR4	208980	225945	200236	187040	187305	205749
SQOR	H2LK25	74080	65169	77870	60145	44661	71745
FANCB	H2MU59	69471	64051	69717	72582	54757	74657
LPIN2	H2MU96	77714	63621	84780	77212	73006	84823
LPIN1	H2MQI8	77714	63621	84780	77212	73006	84823
SMAD4	H2LJX9	198955	193075	170985	157585	64414	176042

DNAJB13	H2LYY0	165338	214319	101639	92764	142553	185459
PPRC1	H2MAB8	141637	120528	146963	95170	128127	107575
ZNF106	H2MAH8	128747	142169	160403	155146	118642	208811
ZNF750	H2LSP7	130744	130027	96587	237432	114782	344197
HEXB	H2LDW8	239936	407330	185689	155012	169965	285574
PAQR6	H2MNM9	133004	153446	125724	126137	116509	180193
SIRT1	H2MEX8	165539	143106	172926	159327	97035	202588
RASA3	H2LJF3	114539	109703	114133	111115	100110	109846
PDK2	H2LHY3	265084	264378	115895	129027	114752	163516
CDK10	H2MK88	126102	90845	86605	86950	96783	106068
JAKMIP2	H2LPX7	116102	126601	119149	132616	105865	138685
ZRANB1	H2LM49	268688	276068	274421	304088	249040	299124
RFX1	H2M8H1	473245	562599	541093	408433	336599	388969
C3	H2MVB4	162309	119385	87967	171133	123673	261242
ZNF592	H2LVC9	216238	208807	174085	201350	180143	214655
ERC2	H2LY86	199031	173778	147824	164881	156037	165434
DDX42	H2LAR5	101164	126623	121621	93893	111750	144928
ADCY9	H2LWC3	483259	450465	419841	386241	391070	521579
MYH7	H2MDC8	155761	163607	143922	158412	126424	171537
NPTX1	H2M5T1	183340	150873	187192	199693	140322	150428
MYL12A	H2MU76	183433	157484	154586	110256	139904	129287
RARS2	H2M771	152771	184069	195118	115401	139783	146584
SERPINH1	H2LF66	167390	141009	158354	144927	132553	161153
HSPA8	A5HL62	234373	196336	197340	195671	154701	235274
IQSEC1	H2M744	301693	310629	330172	325736	233114	321248
LHX9	H2LXY7	233140	202654	170912	177618	157984	196836
MAP3K10	H2LQR0	179124	156286	184655	145701	156712	144032
UGP2	H2LCN4	514658	570102	345779	505007	415163	548946
WDR70	H2LUX9	268564	222646	200379	226950	194159	208663
KRAS	O42277	435130	297463	212440	150104	207914	138293
HRAS	H2M6R0	435130	297463	212440	150104	207914	138293
LACC1	H2MGQ6	138702	174995	160853	158795	140636	217174
BTN1A1	H2N130	173179	167637	151276	178436	157957	204291
MOG	H2MZS5	173179	167637	151276	178436	157957	204291
KCNH2	H2LGS9	247602	174319	322995	263099	138677	191081
NAP1L1	H2M9M4	725983	752927	624969	512606	538455	531819
JMJD7	H2M2Q8	166782	112516	169958	164488	150317	187941
PCNXL2	H2LDF9	152155	156646	162427	214428	123524	185784
DSP	H2MX47	152155	156646	162427	214428	123524	185784
C12orf71	H2LX90	304310	313291	324854	428856	247049	371568
UHMK1	H2MH83	182828	226909	201010	194507	181964	236838
ARHGEF7	H2M9L9	684961	702300	589539	564400	544536	635631
TRPM5	H2L6C4	120817	140190	154662	140457	124243	139007
COG4	H2LYD2	115337	207820	202100	128621	123625	150220
CCDC88A	H2MCX6	250368	306112	304313	268162	156923	257594
TJP2	H2ME98	197739	171543	182471	175685	164793	178074
CEP350	H2MSE4	218280	180496	188980	186696	195711	221190

PCDH8	H2M662	209517	234884	196550	188378	184591	202060
NEB	H2LDB3	2857725	2911771	2553166	2788078	2644539	3145819
TRAIP	H2MGY9	247512	312375	230638	257362	252071	298369
HSPG2	H2MMH3	253978	259439	227624	229089	220368	256039
TTLL7	H2LPJ0	174039	214898	185417	218652	199304	239762
PSMD3	H2N1D2	262175	220053	210010	258608	187593	264131
EPB41L4B	H2LYQ7	217659	206903	219608	211331	201843	250039
ASCC2	H2N026	170588	156895	182873	152168	102716	168829
YAF2	H2LDN9	261682	257597	153906	150348	89290	168148
MED13L	H2LST6	255497	256548	235691	240676	232461	261849
CANX	H2L9G7	364289	317928	276228	313083	246449	278866
VPS13A	H2LMC0	637220	622926	637275	621074	530446	699663
CNTNAP5	H2MVE4	619593	426877	567304	522325	541313	558779
RRM2B	H2MD47	251086	254764	235728	226805	231939	264275
PRKG1	H2LPG9	718223	665678	588430	587754	575334	603427
PCDH7	H2LJK1	329733	273728	322819	318226	272416	250685
MYO5A	H2LLF2	830600	765265	728950	749936	729844	823292
SRP68	H2L5G8	262943	306327	255379	296438	313472	293195
FOXL2	H2LLD5	260431	297719	299298	276526	175913	303202
POLR2B	H2N223	247481	235076	210414	239881	217637	270283
GSTZ1	H2MNW8	483976	534785	568257	526847	575788	720260
DNM2	H2LRA1	236627	270827	231147	244756	211805	245622
KCNH7	H2LE00	346290	539820	382604	329692	288143	305697
ADPGK	H2L8G1	299147	284526	250895	259552	243564	293460
C12orf56	H2MS66	324272	233199	226943	201148	185758	204017
ZDHHC13	H2L574	473071	413725	409640	410543	376475	454918
NUP210	H2M719	312021	253465	243079	224669	192621	223818
MAMDC2	H2MED5	281289	335266	241205	264837	243135	288956
MAPKBP1	H2M2N0	304179	269244	243583	250193	202122	229133
KIF20B	H2LF52	313052	301463	269822	308966	328704	294408
DNAJC16	H2LBF2	300317	289778	299969	292778	322556	358660
SEC11A	H2MAK2	185301	289008	220439	199175	218699	242427
AFG3L2	H2L599	386725	299599	376105	284253	240974	388673
ITGB4	H2N2N3	377782	350412	329567	276962	243250	335025
REXO2	H2LKA6	256299	251783	244065	216711	199164	217944
PCLO	H2M0N5	312952	238447	249703	232266	238699	247289
MORF4L1	H2LQS2	979804	786786	872577	784210	827757	797553
SETD1B	H2LWU9	350105	309010	295777	327967	195998	313535
HSF1	H2MF92	323060	279643	288808	264330	287926	272301
PSMD4	H2M0M9	334899	432145	302835	358634	258239	336761
SLC12A9	H2MPV9	935362	1148256	940858	818254	655413	1328013
FAM20C	H2LDP5	245081	272568	280224	288631	237081	292787
MYH4	H2N1T3	793837	736686	684633	572726	522958	683940
MYH1	H2LPD7	1587673	1473371	1369266	1145452	1045916	1367880
MYH2	H2L9I1	396918	368343	342317	286363	261479	341970
CAB39	H2MKT4	414211	420539	369179	342936	276242	421787

GBA2	H2LUF8	309085	370692	296698	277681	224773	286251
RTF1	H2M141	464671	645751	562063	657486	491888	779894
SIK2	H2LTE1	267421	247269	263578	266588	213638	291793
TF	P79819	624919	517259	520386	555216	519950	595380
DROSHA	H2MEP2	354907	298233	292418	292535	231863	270785
PLD1	H2LC50	294079	314124	255554	242971	270554	252949
ACTR3	H2LVP0	259671	315268	344662	297822	278675	384330
ST14	H2MVR8	291874	281527	241970	280306	205742	306722
RAPGEF6	H2L668	557062	546807	575010	488622	551937	550902
CAPZA2	H2MZH1	622760	906353	665852	725636	619665	792547
C18orf25	H2LJX7	369029	272034	271823	235317	240375	239483
IMP3	H2LI14	323140	318363	273135	312312	275778	305268
PCDH9	H2LHX6	280684	278054	289941	253231	300592	306890
LCTL	H2LR97	701642	705802	670812	656411	489156	688126
PPP1R10	H2M451	665930	725982	624768	609588	465905	1050074
ASTL	H2MYZ5	582954	574281	584312	603309	526671	668584
IRF5	H2N0P9	671359	725618	580443	491516	217846	904458
FBXO11	H2M319	261460	289892	265707	312509	233526	387321
COL1A1	H2M6N2	418867	361382	317455	386152	345747	384709
FREM1	H2LEI6	344758	370151	377111	341688	310047	352661
CYBB	H2L7D0	288620	294201	301485	276801	315390	337542
CLTA	H2N2T7	309442	372394	348032	326974	283762	309740
TMCO3	H2LIU7	299585	298688	284958	268834	186484	273865
ODZ1	H2LWM7	763561	878087	712940	753855	706236	923254
TENM1	H2LWN2	381780	439044	356470	376928	353118	461627
ESYT3	H2MV11	381808	443192	357340	379300	352417	461633
RYR1	H2L660	320205	345533	325238	331460	284463	363641
PLS3	H2LY91	264076	256566	264715	249903	217869	258244
CSNK1G2	H2LUU9	792141	658307	735181	755404	653196	706315
CSNK1G1	H2L7T9	396070	329153	367591	377702	326598	353157
PLIN3	H2MPB1	429825	281404	349126	322588	260801	292277
HIVEP1	H2LZQ1	321482	364002	354563	333656	296788	340538
ACSL1	H2LXK0	370362	397367	383697	374161	300366	394933
SPHKAP	H2M8D2	344860	323910	327778	344824	272806	333923
PLEKHA7	H2LQR1	338930	378356	356256	365693	404215	399408
DNAH5	H2LEP5	322730	385127	323548	365655	285515	466441
FAM135A	H2M402	865298	781901	700232	651454	651061	676036
DLG4	H2LRA2	654868	875137	822565	731401	781381	766372
MTHFD1L	H2MHJ8	644576	731684	683685	726017	614793	751785
OSBPL3	H2LUG4	433530	395764	348583	326589	328229	325451
EVPL	H2MJN4	494115	372765	348024	310691	291688	319473
DFNB31	H2MFV1	323465	334925	323570	296320	231123	320749
CAMTA1	H2MNZ8	340104	305574	292507	353811	176582	336460
GIPC3	H2LR62	328547	337617	324318	310045	237647	316396
AP1B1	H2LQQ4	568515	485283	458550	477078	411349	437887
VCP	H2LWZ6	401569	471164	352767	391733	400211	471333
MACC1	H2LSM9	438377	397557	369312	360493	354969	386235

ATP6AP2	H2M835	486763	643369	412214	413577	299501	745688
ADAM11	H2LEN1	379631	506599	377574	366391	304037	339770
PDE4D	H2LIL7	1726863	1817004	1591638	1564914	1591747	1885726
LATS2	H2MD89	810665	872705	802035	691428	561490	735858
PTCD1	H2LZR2	483079	395270	357657	328745	269067	352783
DDR1	H2MC95	443953	361009	390007	357367	309284	381104
PLXNA2	H2LU57	355073	462123	422243	340151	328830	400281
CACNA2D3	H2LY22	506689	412771	470144	459013	382152	492304
TRMO	H2LS45	437041	498645	418404	398789	332195	459773
LRIT2	H2LRG7	1054583	865212	775955	712204	604391	736401
SHLD2	H2LCP2	514792	418085	382974	346140	315670	362509
AHNAK	H2L8R1	456656	407052	393082	410675	380729	474621
CLPX	H2LM21	804569	843159	683355	624951	609486	681525
ROBO2	H2M2I2	396437	441830	386207	404840	399411	432328
EPX	H2LZT8	2789538	2549914	2562761	2424404	2273095	2420082
LTB4DH	H2LTU0	269135	328418	307649	307893	320429	371829
NCOR2	H2MG30	942282	913722	764082	746336	750641	843605
EHBP1	H2LBB9	322179	330897	318195	327601	280195	400517
ASB1	H2MV44	430985	401182	413488	457319	425520	460870
DPP4	H2LBZ8	555147	552484	631378	613176	470470	666914
DDX21	H2MNV1	362772	334833	356995	335747	269557	340785
FAM13B	H2L3D9	370827	337908	371471	359758	287656	371763
KRT8	H2MPS1	743772	672599	626367	669998	483458	646032
CYFIP1	H2MMS2	1076204	1204128	1195018	1360382	929675	1634492
CKAP5	H2MHR3	451053	534536	459738	395541	373457	448827
EPB41L1	H2LJM1	472935	552180	473804	533038	365340	572352
ALDOA	H2LPL6	407100	370583	368062	364511	275968	358544
WASHC2C	H2LTR3	535050	442736	466015	451617	415942	509795
FAT4	H2N1Z4	555033	526763	416251	444464	341873	513756
FAT1	H2LVT4	399552	378094	394372	360108	341705	461801
HIPK2	H2MN28	468931	453943	445132	456942	417209	541337
ATP1A2	H2LBL9	541638	488592	471059	460840	467406	564196
GNA13	H2MX49	444783	488825	449884	540835	450539	504252
GIT1	H2MFK1	502157	591924	466247	493652	476175	564805
MVP	H2N0A4	591600	386468	454345	426423	363252	406739
ADCY6	H2MAE8	322678	286993	339007	281479	267310	321558
RGS6	H2MQH9	907066	906665	864321	914094	846665	1067537
GLDC	H2L7W3	611267	535870	415740	382552	414932	478085
FREM2	H2LEL3	883747	836301	968522	879954	693960	852431
USP9X	H2M4X8	353100	426700	405606	404085	353185	397650
CDH18	H2MFA8	480105	545065	454050	533605	308670	505052
RNF103	H2N260	478834	568094	488140	534215	516276	666063
KIAA1549	H2MN24	726637	822919	618213	441892	71557	1138113
GLS	H2MJZ5	499002	567886	514434	509515	365792	564105
MEPCE	H2LRR8	563005	420510	543439	476197	439547	456980
CDK4	H2MK52	485568	499576	444284	442968	412645	455355

COL6A2	H2MPB7	469627	465322	488133	499768	440473	500129
UBE3C	H2M4A2	344202	428953	424579	433842	400888	499672
CPSF1	H2MEH3	503231	461735	503029	463436	426287	438129
HCFC1	H2MG37	327791	392582	408648	415947	369208	402722
CUL5	H2L9J9	927953	951055	925107	973617	886274	1008973
RPL7A	H2LG61	440669	419773	413801	396954	312313	407114
ERAP2	H2LXS6	881819	845340	826805	791693	605354	815402
RCBTB2	H2LCV9	668588	561560	550398	559065	481819	567200
EPHB1	H2MMP9	1151106	1126320	912628	1007764	646336	1108831
PTPN12	H2MEM3	575836	535636	527502	514157	459894	485521
TNNI2	H2L4N2	314002	413449	401934	400913	347553	421120
TRIP4	H2L8F4	370620	400398	417322	411426	344528	397066
TRAPPC9	H2MDE5	370620	400371	421388	402579	344529	397744
ASCC3	H2LH33	435431	482808	406448	450352	432508	488944
LRP2	H2MRQ6	358137	361282	377845	369318	350549	419376
SACS	H2MCP6	457276	445493	461285	474354	379644	464122
NR1B2	H2LHL6	610076	500918	473769	446570	412571	472236
RARG	H2MKN6	1220152	1001835	947537	893141	825142	944472
RARB	H2LX30	610076	500918	473769	446570	412571	472236
NR1B3	H2LUS0	610076	500918	473769	446570	412571	472236
CILK1	H2M1B3	429121	462425	461273	475701	407645	512852
NAA20	H2MS46	530904	648283	527572	537742	529232	664029
AK8	H2MPY9	504490	591333	514324	561313	446162	581574
PRPF40A	H2MQ40	459808	511015	422476	458444	440835	533045
CPPED1	H2LCL6	1100766	1259718	1069411	1172253	1150210	1361703
MAGI1	H2LVK0	449930	507439	428528	458890	452581	518826
SLITRK5	H2LIJ7	1368814	1533458	1290322	1393806	1339998	1563887
RAP1GDS1	H2MY45	530374	570640	548108	557874	439735	595903
AGO3	H2MJH5	1333024	1475957	1265663	1311502	1207017	1345705
SERPINB1	H2LKS8	2201070	1989097	2224438	2101548	1822720	2113200
GFAP	H2L6N1	487729	613056	491821	512163	495405	591394
TUT4	H2MD26	498081	613732	497608	510960	485487	582445
TRPC4AP	H2MFJ2	877643	1132376	1039056	1092266	1040973	1147292
AGRN	H2L4F8	584602	505760	422320	444242	365672	416929
CPXM2	H2M0U4	706492	581393	577579	546434	580700	625975
NR2A1	H2MP51	687589	731072	604122	644034	498884	667724
RIMS1	H2LAU0	542190	645382	498882	553044	502118	659084
RIMS2	H2LAT9	542190	645382	498882	553044	502118	659084
CREBBP	H2LWE6	349850	355578	496858	492753	471621	503650
EP300	H2MFZ7	699700	711156	993716	985507	943242	1007300
DHX29	H2LL52	573121	515876	586050	589666	468810	566575
RAP1GAP	H2MG11	567999	598219	593695	546279	461013	591606
CCDC85C	H2MD86	528325	660915	589105	649047	557078	669624
CCDC85A	H2MD85	528325	660915	589105	649047	557078	669624
PRC1	H2LM39	1394884	1119672	1126659	1187729	1038456	1151538
GGT7	H2MFL5	468482	419083	476679	454802	396814	473655
KLHDC7A	H2MRP8	668017	649442	553878	591674	486300	563629

CHRNB2	H2MH58	674157	469690	581771	529056	513231	482803
UTY	H2MQU8	629580	579126	557468	533502	445562	592416
ANKRD54	H2MKJ9	617806	597457	570722	613862	443938	599560
STAG1	H2M9J7	1015061	991482	1016697	1026990	868678	1098835
PRKAG1	H2L825	1143696	1129166	1262461	1422061	848144	1334953
VPS13D	H2N093	665415	594141	561404	600255	461587	629313
MTMR14	H2M2R8	656429	488353	558239	541991	486132	628954
RAP1GAP2	H2MEY5	544900	547383	606049	615513	501046	597087
MYOM3	H2MJ04	622131	634428	636644	592710	513408	579658
SAMD1	H2LRV5	435779	590117	574590	527353	450867	776647
DOCK7	H2M3V7	640814	513016	561414	513624	439041	574690
GPATCH1	H2MWV6	681578	691012	651116	678529	582555	697872
IFT88	H2MCM7	587035	573182	579250	618296	527238	602001
RAG1	H2M914	1805753	1287260	1237500	1095932	1043706	1111927
TRIM71	H2LLW2	848301	646937	609780	544919	482303	563801
ZXDC	H2M0J6	904417	637833	624433	557453	327455	568158
ITIH5	H2MR21	620083	636164	726829	763581	443563	656651
FMOD	H2MLT1	1290880	1208180	1129166	1091002	937737	1159885
GPSM2	H2MLM7	590443	654611	581632	621492	497416	645992
ARMC2	H2ME88	755083	781176	766871	799218	652045	785222
INPP5F	H2MFL9	1530357	1630178	1560228	1615821	1383843	1672969
SMARCD1	H2LRD5	1126982	1150794	1238648	1206660	1055806	1279082
SMARCD3	H2M8D1	563491	575397	619324	603330	527903	639541
VCL	H2LX46	1287249	1261686	1340237	1500357	1101232	1469161
ELFN2	H2M529	1784124	1922304	1918459	2064069	1277423	1940427
GIMAP2	H2LFF1	661290	502404	655122	548443	520708	525618
DES	H2L9W4	560300	624333	588177	721335	442476	856876
PIK3CG	H2M0C9	961110	683266	724475	643243	550596	595794
WDR75	H2MK77	859042	759289	741055	736739	639424	762216
XRCC5	H2MP70	1464908	1647683	1389055	1459466	1396794	1732841
COPE	H2MST3	1331593	1252347	1087148	887466	769229	1044313
FLNC	H2N036	724034	889766	813670	833569	818250	957348
CACNA1F	H2MR69	889343	840900	805252	837305	724582	830064
CACNA1C	H2MH40	889343	840900	805252	837305	724582	830064
CACNA1D	H2LBF8	1778687	1681801	1610504	1674610	1449164	1660128
HERC4	H2M9V4	832416	799786	785271	765837	655203	777085
CREG2	H2MA28	1372184	1175911	1182856	1249226	1038276	1452420
KIF13B	H2MHR9	680805	752322	584377	866142	706081	1171217
ATP13A1	H2LQA2	786640	575843	712552	615024	645288	599130
APOB	H2LQ37	964585	1061283	924759	970223	884494	1012176
EHBP1L1	H2M8L4	1055943	788333	737158	656508	597507	680721
ENGASE	H2MS53	1246693	1315287	1327135	1349223	1196224	1422341
TLE3	H2LQR6	777881	753832	749169	724376	664698	789787
ARR3	H2L9D0	1898869	1547395	1548058	1474850	1335613	1549914
ABCC9	H2MRJ2	693925	721030	859581	784320	466727	759470
SESTD1	H2M415	1585030	1534887	1535547	1545139	1329524	1611357

KIF7	H2LZU6	779275	827715	813792	798051	702802	900830
IFIT1	H2LWE2	944156	893768	853764	978167	825210	933888
PSD4	H2LSI6	709445	781901	643300	975397	775984	1155936
ASMTL	H2M5E3	971289	987254	968250	1035601	886777	1023096
GABBR1	H2MMW3	872901	1023495	823575	982209	911862	1098413
CYP51A1	H2N0C8	953362	902127	842699	866087	704599	854702
PIM2	H2MBT0	959801	1002518	792116	906245	855361	1013900
SUPT6H	H2LD63	986301	920755	916255	944533	821388	1009370
LDLR	H2LFW4	1844745	1864853	1820245	1873151	1591719	1945678
CILP	H2L507	510970	766419	724303	666137	533908	854266
TAP2	H2LQG7	1336957	1596530	1292500	1806371	818440	2228384
RNF146	H2LME7	1484732	1782809	1382231	271055	1495766	2047567
RNPC3	H2LM89	1286210	1071374	1025296	1041638	1008935	1103223
CHID1	H2LQ72	999260	1084705	853600	929034	904238	1094160
PCK2	H2LPB1	3885005	2689610	3277929	3115648	2561830	3274850
PRTG	H2LL58	1429950	1606454	1735815	1652430	1492559	1806365
SEMA3A	H2MJK3	2966262	2926296	2926110	2852866	2500471	3159755
PGM1	H2M3I0	911593	1007084	1066435	1130218	655252	991829
LARS1	H2L846	735133	825833	888019	854406	735742	928179
CELSR2	H2MXM7	998811	977685	985454	957073	763241	985250
PLRG1	H2LWD5	2126167	2576303	2401401	2352777	2242992	2457951
PRMT8	H2MJ49	2800382	2926808	2593396	2768514	2543762	2937690
FAT2	H2M6P1	1024395	999392	1032908	1014230	894891	1103118
SGSM2	H2LWS2	1024645	1018633	1030148	1028514	911205	1104895
ASL	H2LB38	1209284	1077687	1081782	1078150	889833	1143204
UBE2D4	H2LKV0	1286115	1123349	1137628	1160627	1042439	1259955
MNX1	H2M463	1292786	1164680	1069617	1052023	910007	1076565
IDH3B	H2LWT7	2245563	2410390	2252966	2288365	2071831	2628075
C7	H2LGZ3	1358949	1265641	1230614	1221535	1117476	1220702
DENND4C	H2LK69	1244278	1272126	1236403	1262312	1100969	1357935
ITGA7	H2LJI2	3369172	3286750	3384615	3279193	2864179	3600219
TMEM131	H2MLY1	1189999	1237776	1118064	1181298	956739	1278563
ADGRV1	H2M3Y4	1476307	1354651	1289976	1231716	1166432	1368842
CHD1L	H2LF53	1291431	1280215	1223274	1292883	1061571	1370238
LLGL1	H2MDD6	1265002	1378768	1262535	1263271	1139398	1312442
CAMK2D	H2N045	1418878	1342041	1387542	1399511	1157649	1450918
CMSS1	H2N1B7	1417602	1251211	1233189	1235635	1085984	1295041
TMEM132D	H2MES6	1808811	1930424	1555861	1633378	1591364	1856989
BRPF3	H2LFX6	1750238	2005868	1633315	1774348	1745538	2203933
PLXNB2	H2MR98	1688883	2029300	1647590	1779849	1671773	2247600
HGSNAT	H2LJD3	3365339	3257731	3222273	3071749	2725216	3245840
APOE	H2MG05	1647528	1639730	1464490	1509892	1219660	1599458
NUFIP2	H2M133	1609962	1440456	1405574	1423533	1247226	1515244
GOLGB1	H2L2V4	1871820	1686569	1561759	1597759	1301412	1613378
RALGDS	H2N2A2	2376962	3062614	2925598	2918819	2791931	3508955
CEMIP2	H2M515	2333617	2077568	1842822	1914478	1822719	1970624
RASSF9	H2MVQ7	1782284	1632073	1505990	1571320	1250854	1691140

AJM1	H2MDF9	1910202	1732492	1902373	1796882	1671055	1732702
SLC8A2	H2L495	2133744	1916446	1962224	1747960	1557960	1890787
DNM3	H2M283	2014270	1940502	1913875	1889014	1536967	2003914
PDIA2	H2LX92	2793781	2112615	2107842	2209979	1857205	2267800
RB1CC1	H2MSZ9	2344773	2741868	2533863	2628529	2376006	3152359
YEATS4	H2MFM7	3330436	2962038	2658016	2748493	2208765	2803864
CTDNEP1	H2LP01	2841188	2622972	2533901	2565208	2005087	2730914
BTBD11	H2MPA6	2901492	2670902	2636314	2632885	2050960	2813799
KIAA2013	H2MYW0	5696159	5384961	5226716	5286173	4293128	5623707
VPS41	H2M7Z3	5695718	5311897	5134210	5154006	4169909	5566088
GAREM2	H2MTQ3	4117749	4303727	4027032	4099714	4212712	4287580
TENT4B	H2MG09	3650251	4441185	3929565	4204336	3771232	4319287
HIC2	H2L9V1	4967614	4365518	4711070	4521765	3850047	4597159
METRNL	H2LSS7	22052773	19374191	20833733	20207322	17057266	20719261

Appendix E. ***All Proteins detected in 7 dpf with Abundances averaged over 3 replicates***

Orthologous Human Gene Symbol	Medaka Accession #	Control	0.001 ppb	0.01 ppb	0.1 ppb	1 ppb	10 ppb
OXSR1	H2M8I5	554424	190250	356232	141454	585691	61572
MTX3	H2LYM8	291686	125348	177643	138419	235019	63046
EPB41L1	H2LJM1	202906	179100	188764	132097	277714	72451
SIK2	H2LTE1	180378	134183	145614	103692	158964	104000
HDHD2	H2M8S0	817818	150359	154381	358973	737408	208589
CHRNB2	H2MCZ7	49852	12523	15093	26134	42331	0
CHRNB4	H2MCZ9	49852	12523	15093	26134	42331	0
RBMS2	H2LUK8	2312291	556026	1603210	988633	1823751	366951
ESYT3	H2MV11	639284	113236	474885	439880	678720	167749
CTDNEP1	H2LP01	743897	301594	300660	338295	579855	111010
CYRIA	H2MMN5	386902	89144	182677	202013	355387	68728
UBAP2	H2LMV0	47741	26277	21095	15297	17121	12464
TRIB2	H2M2D0	703660	326033	396369	567042	661739	162430
TEF	H2MGJ8	407493	137076	159205	170060	230977	15377
EIF4A3	H2MW23	238142	87297	190780	207503	281853	6897
MYO6	H2MJD1	73879	53598	90070	42207	146221	13653
AMPD2	H2L476	332575	289005	237904	167980	426894	115192
MMP11	H2MXC2	277616	142521	104899	81449	171307	59556
DSE	H2MUP5	185600	73497	106608	100629	143993	39087
TIAM2	H2MSF4	207918	91700	59395	105009	146942	23305
GLS	H2MJZ5	169896	121522	89605	131104	193348	50806
PCLO	H2M0N5	104197	96273	108550	97435	53816	93120
SMARCD3	H2M8D1	153408	109038	85631	63634	146364	61656
PRDM1	H2M2D4	156168	162807	77311	126263	165045	53953
CPSF2	H2M7W9	292104	257495	147238	105951	272474	25790
HSPA8	A5HL62	412953	442252	308347	162002	333040	383438
HSPA1B	Q9I8F9	275302	294835	205565	108001	222027	255625
NUP210	H2M719	80479	69124	84077	91837	115901	37922
TANGO2	H2MK22	213253	185704	237683	246116	287970	117570
LRP2	H2MRQ6	306414	173683	194457	163735	211790	129719
SERPINH1	H2LF66	70928	27297	70468	8711	80692	60085
SYNPO2	H2LIS5	90425	74213	62333	48642	68224	66922
P2RY2	H2MEG1	153111	83279	79628	43799	94182	50387
MINDY3	H2LWJ9	280355	185935	183061	117292	339167	139858
GLG1	H2L578	144332	123071	100708	73516	107946	72379
POLR1A	H2LXY4	168759	76219	86130	56344	128522	83382
CAPN5	H2LRH5	87599	92991	105563	109183	97693	98045
TPRXL	H2LP13	426331	385118	359699	341448	487800	269920
ENO1	H2LLZ8	172271	138927	134538	118144	184163	84635
ZUP1	H2LB59	214027	232715	242852	206143	282388	165463
BTBD10	H2LT06	1360073	854713	1168425	740357	267018	435735
SLC6A19	H2MFH4	269819	190329	219066	227560	282719	105235

MAGOH	H2MEV8	307353	141511	152543	198478	290749	81761
APOA1	H2MLX9	146374	123052	110495	122550	108075	120775
NAB1	H2L365	247758	113056	166805	122639	275405	75012
MAP3K12	H2LKD4	209260	107848	175972	190555	215195	76926
APOL3	H2L7J0	203189	127004	111872	101593	139273	86677
EPHA7	H2MUM5	301509	239416	151292	155931	310451	162342
EXOSC2	H2LTB1	302844	160470	147700	241168	254060	88558
NCAPH	H2MMY0	147809	183916	131759	163802	156301	110991
VPS13D	H2N093	408015	154386	212915	298526	383685	97312
HES2	H2LH93	270996	161406	197478	121041	169073	198231
ACLY	H2LF97	380023	345288	366844	369987	417944	312293
ARFGEF1	H2LWJ4	441481	345358	237152	215445	378405	137792
TENT4A	H2LKJ0	442103	346101	260170	184648	407204	133622
RYR1	H2L660	181062	156072	178548	183948	199441	147637
SEZ6L	H2L6M4	596658	367002	207610	96936	264422	352814
PCDH11X	H2LD13	444509	271897	241013	211747	327525	171377
EIF5A	H2LCJ3	239960	120512	138429	13587	142967	194926
ASMTL	H2M5E3	214411	180402	196120	258340	291001	121767
MAPK12	H2MX42	216141	167217	160197	164725	163710	199669
DNAJC13	H2MAF9	360633	235832	218391	157161	279847	167512
HGSNAT	H2LJD3	917357	463309	588533	773074	1208178	364576
KIAA1549	H2MN24	745622	260987	253546	391802	591856	149578
MEPCE	H2LRR8	355641	275340	312843	291486	232079	270700
MAGI1	H2M4B5	933205	603022	546600	492858	945106	279494
TTC17	H2L634	290621	231360	254810	219642	168700	265890
SUCO	H2L8X7	358835	175707	97571	88784	281703	178339
ZP3	H2M2R4	878959	616858	570127	509214	730366	466833
TRAPPC9	H2MDE5	227438	273845	290156	183599	306777	225185
ALDH3A2	H2LB69	1721340	1243048	1702609	1117039	705201	990309
CILK1	H2M1B3	309402	282984	299711	287669	336200	253854
TPST1	H2MJK0	491049	444068	433960	452290	657111	347121
ZHX1	H2L626	371500	391902	295343	267780	453750	223095
HCN2	H2LHE7	359561	308994	329185	313863	380515	234893
GPATCH1	H2MWV6	308896	333413	329617	301416	403215	230593
MAPRE1	H2N103	285379	301694	284118	314045	350962	250164
PRMT8	H2MJ49	1077066	627856	969553	862566	1275066	524419
BBS5	H2MRS1	434052	447011	434425	458465	531907	371016
GNA14	H2LM72	818721	492073	424499	589853	668744	237714
CUX2	H2MMP6	708688	497735	563656	427733	796510	281579
H3-3A	H2LU55	460726	283649	189227	255113	370701	423497
H3-3B	H2L503	460726	283649	189227	255113	370701	423497
H3C15	H2LD49	2303630	1418246	946136	1275565	1853507	2117486
H4C1	H2L6I7	2775888	2147516	2085563	2002372	2578905	2161427
ZP4	H2M5C0	3943705	2745544	2701159	2698442	2796150	3409037
SUPT6H	H2LD63	520394	466023	458434	470170	546922	427425
IDH3B	H2LWT7	1403005	775985	780739	731104	1308468	584555

SGSM2	H2LWS2	513458	466398	455371	381194	505660	431260
FAT2	H2M6P1	506984	467015	459777	362662	558391	370681
APOB	H2LQ37	640562	559281	520246	423354	762875	312618
CAMK2D	H2N045	765011	614174	584466	554440	775389	457516
KCTD16	H2L7Z2	946406	599943	711547	1026350	1248267	375945
CELSR2	H2MXM7	788683	663688	663182	634047	823669	527495
NUP54	H2LPZ3	1238211	969836	915567	795905	1129550	803858
AAK1	H2LYD9	1196378	887090	859771	889958	876431	1049855
BTBD11	H2MPA6	1703517	1120359	1269626	1295281	2181256	643833
GAREM2	H2MTQ3	2620618	1451264	1347827	1259678	2059180	848737
TENT4B	H2MG09	2161927	1891640	1850042	1489921	2550346	892812

References

2,3,7,8-Tetrachlorodibenzo-para-dioxin Environmental Exposures. (2021, 2011). Retrieved from https://www.carexcanada.ca/profile/tcdd-environmental-exposures/

Benjamini, Y., & Hochberg, Y. (1995). Controlling the false discovery rate: a practical and powerful approach to multiple testing. *Journal of the Royal statistical society: series B (Methodological), 57*(1), 289-300.

Bolt, H. M. (2017). Adverse outcome pathways. *Arch Toxicol, 91*(12), 4023-4024. doi:10.1007/s00204-017-2123-6

Bryan, B. A., & D'Amore, P. A. (2007). What tangled webs they weave: Rho-GTPase control of angiogenesis. *Cell Mol Life Sci, 64*(16), 2053-2065. doi:10.1007/s00018-007-7008-z

Cardama, G. A., Gonzalez, N., Maggio, J., Menna, P. L., & Gomez, D. E. (2017). Rho GTPases as therapeutic targets in cancer (Review). *Int J Oncol, 51*(4), 1025-1034. doi:10.3892/ijo.2017.4093

Carmeliet, P., Ferreira, V., Breier, G., Pollefeyt, S., Kieckens, L., Gertsenstein, M., . . . Eberhardt, C. (1996). Abnormal blood vessel development and lethality in embryos lacking a single VEGF allele. *Nature, 380*(6573), 435-439.

Carmeliet, P., Ng, Y.-S., Nuyens, D., Theilmeier, G., Brusselmans, K., Cornelissen, I., . . . Mattot, V. (1999). Impaired myocardial angiogenesis and ischemic cardiomyopathy in mice lacking the vascular endothelial growth factor isoforms VEGF 164 and VEGF 188. *Nature medicine, 5*(5), 495-502.

Coulthard, M. G., Morgan, M., Woodruff, T. M., Arumugam, T. V., Taylor, S. M., Carpenter, T. C., . . . Boyd, A. W. (2012). Eph/Ephrin signaling in injury and inflammation. *Am J Pathol, 181*(5), 1493-1503. doi:10.1016/j.ajpath.2012.06.043

Denison, M. S., & Nagy, S. R. (2003). Activation of the aryl hydrocarbon receptor by structurally diverse exogenous and endogenous chemicals. *Annu Rev Pharmacol Toxicol, 43*, 309-334. doi:10.1146/annurev.pharmtox.43.100901.135828

Doering, J. A., Giesy, J. P., Wiseman, S., & Hecker, M. (2013). Predicting the sensitivity of fishes to dioxin-like compounds: possible role of the aryl hydrocarbon receptor (AhR) ligand binding domain. *Environ Sci Pollut Res Int, 20*(3), 1219-1224. doi:10.1007/s11356-012-1203-7

Doering, J. A., Wiseman, S., Beitel, S. C., Giesy, J. P., & Hecker, M. (2014). Identification and expression of aryl hydrocarbon receptors (AhR1 and AhR2) provide insight in an evolutionary context regarding sensitivity of white sturgeon (Acipenser transmontanus) to dioxin-like compounds. *Aquat Toxicol, 150*, 27-35. doi:10.1016/j.aquatox.2014.02.009

Doering, J. H., Markus; Villeneuve, Dan; Zhang, Xiaowei. (2019). Aop: 21 (Aryl hydrocarbon receptor activation leading to early life stage mortality, via increased COX-2). Retrieved from https://aopwiki.org/aops/21

Dong, B., Cheng, W., Li, W., Zheng, J., Wu, D., Matsumura, F., & Vogel, C. F. (2011). FRET analysis of protein tyrosine kinase c-Src activation mediated via aryl hydrocarbon receptor. *Biochim Biophys Acta, 1810*(4), 427-431. doi:10.1016/j.bbagen.2010.11.007

Dong, W., Matsumura, F., & Kullman, S. W. (2010). TCDD induced pericardial edema and relative COX-2 expression in medaka (Oryzias Latipes) embryos. *Toxicol Sci, 118*(1), 213-223. doi:10.1093/toxsci/kfq254

Drake, C. J. (2003). Embryonic and adult vasculogenesis. *Birth Defects Res C Embryo Today, 69*(1), 73-82. doi:10.1002/bdrc.10003

Du, E., Li, X., He, S., Li, X., & He, S. (2020). The critical role of the interplays of EphrinB2/EphB4 and VEGF in the induction of angiogenesis. *Mol Biol Rep, 47*(6), 4681-4690. doi:10.1007/s11033-020-05470-y

El Baba, N., Farran, M., Khalil, E. A., Jaafar, L., Fakhoury, I., & El-Sibai, M. (2020). The Role of Rho GTPases in VEGF Signaling in Cancer Cells. *Anal Cell Pathol (Amst), 2020*, 2097214. doi:10.1155/2020/2097214

Eling, N., Morgan, M. D., & Marioni, J. C. (2019). Challenges in measuring and understanding biological noise. *Nat Rev Genet, 20*(9), 536-548. doi:10.1038/s41576-019-0130-6

Elonen, G. E., Spehar, R. L., Holcombe, G. W., Johnson, R. D., Fernandez, J. D., Erickson, R. J., . . . Cook, P. M. (1998). Comparative toxicity of 2, 3, 7, 8-tetrachlorodibenzo-p-dioxin to seven freshwater fish species during early life-stage development. *Environmental Toxicology and Chemistry: An International Journal, 17*(3), 472-483.

Farhat, A., & Kennedy, S. W. (2019). Adverse Outcome Pathway on Aryl hydrocarbon receptor activation leading to early life stage mortality, via reduced VEGF.

Ferrara, N., Carver-Moore, K., Chen, H., Dowd, M., Lu, L., O'Shea, K. S., . . . Moore, M. W. (1996). Heterozygous embryonic lethality induced by targeted inactivation of the VEGF gene. *Nature, 380*(6573), 439-442.

Gabriely, G., Wheeler, M. A., Takenaka, M. C., & Quintana, F. J. (2017). Role of AHR and HIF-1alpha in Glioblastoma Metabolism. *Trends Endocrinol Metab, 28*(6), 428-436. doi:10.1016/j.tem.2017.02.009

Gierten, J., Pylatiuk, C., Hammouda, O. T., Schock, C., Stegmaier, J., Wittbrodt, J., . . . Loosli, F. (2020). Automated high-throughput heartbeat quantification in medaka and zebrafish embryos under physiological conditions. *Sci Rep, 10*(1), 2046. doi:10.1038/s41598-020-58563-w

Giesy, J. P., Jones, P. D., Kannan, K., Newsted, J. L., Tillitt, D. E., & Williams, L. L. (2002). Effects of chronic dietary exposure to environmentally relevant concentrations to 2, 3, 7, 8-tetrachlorodibenzo-p-dioxin on survival, growth, reproduction and biochemical responses of female rainbow trout (Oncorhynchus mykiss). *Aquatic toxicology, 59*(1-2), 35-53.

Goodale, B. C., La Du, J. K., Bisson, W. H., Janszen, D. B., Waters, K. M., & Tanguay, R. L. (2012). AHR2 mutant reveals functional diversity of aryl hydrocarbon receptors in zebrafish. *PLoS One, 7*(1), e29346. doi:10.1371/journal.pone.0029346

Grenert, J. P., Sullivan, W. P., Fadden, P., Haystead, T. A., Clark, J., Mimnaugh, E., . . . Sausville, E. (1997). The amino-terminal domain of heat shock protein 90 (hsp90) that binds geldanamycin is an ATP/ADP switch domain that regulates hsp90 conformation. *Journal of Biological Chemistry, 272*(38), 23843-23850. Retrieved from https://www.jbc.org/content/272/38/23843.full.pdf

Gutierrez-Vazquez, C., & Quintana, F. J. (2018). Regulation of the Immune Response by the Aryl Hydrocarbon Receptor. *Immunity, 48*(1), 19-33. doi:10.1016/j.immuni.2017.12.012

Hanno, K., Oda, S., & Mitani, H. (2010). Effects of dioxin isomers on induction of AhRs and CYP1A1 in early developmental stage embryos of medaka (Oryzias latipes). *Chemosphere, 78*(7), 830-839. doi:10.1016/j.chemosphere.2009.11.043

Herwig, R., Hardt, C., Lienhard, M., & Kamburov, A. (2016). Analyzing and interpreting genome data at the network level with ConsensusPathDB. *Nat Protoc, 11*(10), 1889-1907. doi:10.1038/nprot.2016.117

Hongu, T., Yamauchi, Y., Funakoshi, Y., Katagiri, N., Ohbayashi, N., & Kanaho, Y. (2016). Pathological functions of the small GTPase Arf6 in cancer progression: Tumor angiogenesis and metastasis. *Small GTPases, 7*(2), 47-53. doi:10.1080/21541248.2016.1154640

Hu, H., Han, T., Zhuo, M., Wu, L. L., Yuan, C., Wu, L., . . . Wang, L. W. (2017). Elevated COX-2 Expression Promotes Angiogenesis Through EGFR/p38-MAPK/Sp1-Dependent Signalling in Pancreatic Cancer. *Sci Rep, 7*(1), 470. doi:10.1038/s41598-017-00288-4

Huang, C. C., Chen, P. C., Huang, C. W., & Yu, J. (2007). Aristolochic Acid induces heart failure in zebrafish embryos that is mediated by inflammation. *Toxicol Sci, 100*(2), 486-494. doi:10.1093/toxsci/kfm235

Ikeda, S., Ushio-Fukai, M., Zuo, L., Tojo, T., Dikalov, S., Patrushev, N. A., & Alexander, R. W. (2005). Novel role of ARF6 in vascular endothelial growth factor-induced signaling and angiogenesis. *Circ Res, 96*(4), 467-475. doi:10.1161/01.RES.0000158286.51045.16

Ivnitski-Steele, I. D., Friggens, M., Chavez, M., & Walker, M. K. (2005). 2,3,7,8-tetrachlorodibenzo-p-dioxin (TCDD) inhibition of coronary vasculogenesis is mediated, in part, by reduced responsiveness to endogenous angiogenic stimuli, including vascular endothelial growth factor A (VEGF-A). *Birth Defects Res A Clin Mol Teratol, 73*(6), 440-446. doi:10.1002/bdra.20137

Ivnitski-Steele, I. D., & Walker, M. K. (2003). Vascular endothelial growth factor rescues 2, 3, 7, 8-tetrachlorodibenzo-p-dioxin inhibition of coronary vasculogenesis. *Birth Defects Research Part A: Clinical and Molecular Teratology, 67*(7), 496-503.

Iwamatsu, T. (2011). Developmental stages in the wild medaka, Oryzias latipes. *Bulletin of Aichi Univ. of Education, 60*, 71-81.

Jeong, J., & Choi, J. (2017). Use of adverse outcome pathways in chemical toxicity testing: potential advantages and limitations. *Environ Health Toxicol, 33*(1), e2018002. doi:10.5620/eht.e2018002

Joshi, S., Singh, A. R., Zulcic, M., Bao, L., Messer, K., Ideker, T., . . . Durden, D. L. (2014). Rac2 controls tumor growth, metastasis and M1-M2 macrophage differentiation in vivo. *PLoS One, 9*(4), e95893. doi:10.1371/journal.pone.0095893

Kamburov, A., Pentchev, K., Galicka, H., Wierling, C., Lehrach, H., & Herwig, R. (2011). ConsensusPathDB: toward a more complete picture of cell biology. *Nucleic Acids Res, 39*(Database issue), D712-717. doi:10.1093/nar/gkq1156

Kawajiri, K. F.-K., Yoshiaki. (2017). The aryl hydrocarbon receptor: a multifunctional chemical sensor for host defense and homeostatic maintenance. *Experimental Animals, 66*(2), 75-89. doi:10.1538/expanim.16-0092

Kim, Y., & Cooper, K. R. (1999). Toxicity of 2, 3, 7, 8-tetrachlorodibenzo-p-dioxin (TCDD) and polychlorinated biphenyls (PCBs) in the embryos and newly hatched larvae of the Japanese medaka (Oryzias latipes). *Chemosphere, 39*(3), 527-538.

Kinoshita, M., Murata, K., Naruse, K., & Tanaka, M. (2009). *Medaka: biology, management, and experimental protocols*: John Wiley & Sons.

Kozak, K. R., Abbott, B., & Hankinson, O. (1997). ARNT-deficient mice and placental differentiation. *Developmental biology, 191*(2), 297-305.

Lanham, K. A., Plavicki, J., Peterson, R. E., & Heideman, W. (2014). Cardiac myocyte-specific AHR activation phenocopies TCDD-induced toxicity in zebrafish. *Toxicol Sci, 141*(1), 141-154. doi:10.1093/toxsci/kfu111

Le, X., Nilsson, M., Goldman, J., Reck, M., Nakagawa, K., Kato, T., . . . Garon, E. B. (2021). Dual EGFR-VEGF Pathway Inhibition: A Promising Strategy for Patients With EGFR-Mutant NSCLC. *J Thorac Oncol, 16*(2), 205-215. doi:10.1016/j.jtho.2020.10.006

Lichtenberger, B. M., Tan, P. K., Niederleithner, H., Ferrara, N., Petzelbauer, P., & Sibilia, M. (2010). Autocrine VEGF signaling synergizes with EGFR in tumor cells to promote epithelial cancer development. *Cell, 140*(2), 268-279. doi:10.1016/j.cell.2009.12.046

Lo, H. W., Cao, X., Zhu, H., & Ali-Osman, F. (2010). Cyclooxygenase-2 is a novel transcriptional target of the nuclear EGFR-STAT3 and EGFRvIII-STAT3 signaling axes. *Mol Cancer Res, 8*(2), 232-245. doi:10.1158/1541-7786.MCR-09-0391

Maltepe, E., Schmidt, J. V., Baunoch, D., Bradfield, C. A., & Simon, M. C. (1997). Abnormal angiogenesis and responses to glucose and oxygen deprivation in mice lacking the protein ARNT. *Nature, 386*(6623), 403-407.

Nikinmaa, M., & Anttila, K. (2019). Individual variation in aquatic toxicology: Not only unwanted noise. *Aquat Toxicol, 207*, 29-33. doi:10.1016/j.aquatox.2018.11.021

Nishiumi, S., Miyamoto, S., Kawabata, K., Ohnishi, K., Mukai, R., Murakami, A., . . . Terao, J. (2011). Dietary flavonoids as cancer-preventive and therapeutic biofactors. *Front Biosci, 3*(3), 1332-1362.

Ordonez-Moran, P., & Munoz, A. (2009). Nuclear receptors: genomic and non-genomic effects converge. *Cell Cycle, 8*(11), 1675-1680. doi:10.4161/cc.8.11.8579

Pang, Z., Chong, J., Zhou, G., de Lima Morais, D. A., Chang, L., Barrette, M., . . . Xia, J. (2021). MetaboAnalyst 5.0: narrowing the gap between raw spectra and functional insights. *Nucleic Acids Res, 49*(W1), W388-W396. doi:10.1093/nar/gkab382

Pillai, R., & W, J. (2012). Distinct Role for ARNT/HIF-1β in Pancreatic Beta-Cell Function, Insulin Secretion and Type 2 Diabetes. In *Biochemistry*.

Plavicki, J., Hofsteen, P., Peterson, R. E., & Heideman, W. (2013). Dioxin inhibits zebrafish epicardium and proepicardium development. *Toxicol Sci, 131*(2), 558-567. doi:10.1093/toxsci/kfs301

Prasch, A. L., Tanguay, R. L., Mehta, V., Heideman, W., & Peterson, R. E. (2006). Identification of zebrafish ARNT1 homologs: 2,3,7,8-tetrachlorodibenzo-p-dioxin

toxicity in the developing zebrafish requires ARNT1. *Mol Pharmacol, 69*(3), 776-787. doi:10.1124/mol.105.016873

Rhodes, S., Farwell, A., Hewitt, L. M., Mackinnon, M., & Dixon, D. G. (2005). The effects of dimethylated and alkylated polycyclic aromatic hydrocarbons on the embryonic development of the Japanese medaka. *Ecotoxicol Environ Saf, 60*(3), 247-258. doi:10.1016/j.ecoenv.2004.08.002

Roman, A. C., Carvajal-Gonzalez, J. M., Rico-Leo, E. M., & Fernandez-Salguero, P. M. (2009). Dioxin receptor deficiency impairs angiogenesis by a mechanism involving VEGF-A depletion in the endothelium and transforming growth factor-β overexpression in the stroma. *Journal of Biological Chemistry, 284*(37), 25135-25148.

Rowlands, J. C., & Gustafsson, J. A. (1997). Aryl hydrocarbon receptor-mediated signal transduction. *Crit Rev Toxicol, 27*(2), 109-134. doi:10.3109/10408449709021615

Ryan, H. E., Lo, J., & Johnson, R. S. (1998). HIF-1α is required for solid tumor formation and embryonic vascularization. *The EMBO journal, 17*(11), 3005-3015.

Tabernero, J. (2007). The role of VEGF and EGFR inhibition: implications for combining anti-VEGF and anti-EGFR agents. *Mol Cancer Res, 5*(3), 203-220. doi:10.1158/1541-7786.MCR-06-0404

Teraoka, H., Kubota, A., Kawai, Y., & Hiraga, T. (2008). Prostanoid signaling mediates circulation failure caused by TCDD in developing zebrafish. *Interdis. Studies Environ. Chem. Biol. Resp. Chem. Pollut*, 61-80.

Thompson, L. A., & Darwish, W. S. (2019). Environmental Chemical Contaminants in Food: Review of a Global Problem. *J Toxicol, 2019*, 2345283. doi:10.1155/2019/2345283

Tuomisto, J. (2019). Dioxins and dioxin-like compounds: toxicity in humans and animals, sources, and behaviour in the environment. *WikiJournal of Medicine, 6*(1). doi:10.15347/wjm/2019.008

Untergasser, A., Cutcutache, I., Koressaar, T., Ye, J., Faircloth, B. C., Remm, M., & Rozen, S. G. (2012). Primer3--new capabilities and interfaces. *Nucleic Acids Res, 40*(15), e115. doi:10.1093/nar/gks596

Vorrink, S. U., & Domann, F. E. (2014). Regulatory crosstalk and interference between the xenobiotic and hypoxia sensing pathways at the AhR-ARNT-HIF1alpha signaling node. *Chem Biol Interact, 218*, 82-88. doi:10.1016/j.cbi.2014.05.001

Walker, M. K., & Catron, T. F. (2000). Characterization of cardiotoxicity induced by 2,3,7, 8-tetrachlorodibenzo-p-dioxin and related chemicals during early chick embryo development. *Toxicol Appl Pharmacol, 167*(3), 210-221. doi:10.1006/taap.2000.8992

Wexler, R., Elton, T., Pleister, A., & Feldman, D. (2009). Cardiomyopathy: an overview. *American family physician, 79*(9), 778.

Wisk, J. D., & Cooper, K. R. (1990). The stage specific toxicity of 2, 3, 7, 8-tetrachlorodibenzo-p-dioxin in embryos of the Japanese medaka (Oryzias latipes). *Environmental Toxicology and Chemistry: An International Journal, 9*(9), 1159-1169.

Xie, G., Peng, Z., & Raufman, J. P. (2012). Src-mediated aryl hydrocarbon and epidermal growth factor receptor cross talk stimulates colon cancer cell proliferation. *Am J*

Physiol Gastrointest Liver Physiol, *302*(9), G1006-1015. doi:10.1152/ajpgi.00427.2011

Young, J. C., & Hartl, F. U. (2000). Polypeptide release by Hsp90 involves ATP hydrolysis and is enhanced by the co-chaperone p23. *The EMBO journal*, *19*(21), 5930-5940.